Aus dem Institut für Physik der Universität Potsdam

STRUCTURE-FUNCTION RELATIONSHIP IN HIERARCHICAL MODEL OF BRAIN NETWORKS

Dissertation

zur Erlangung des akademischen Grades
"doctor rerum naturalium"
(Dr. rer. nat.)
in der Wissenschaftsdisziplin Nichtlineare Dynamik

eingereicht an der
Mathematisch–Naturwissenschaftlichen Fakultät
der Universität Potsdam

von
Lucia Zemanová

Potsdam, den 1. November 2007

Online published at the
Publikationsserver der Universität Potsdam:
http://opus.kobv.de/ubp/volltexte/2008/1840/
urn:nbn:de:kobv:517-opus-18400
[http://nbn-resolving.de/urn:nbn:de:kobv:517-opus-18400]

Abstract

The mammalian brain is, with its numerous neural elements and structured complex connectivity, one of the most complex systems in nature. Recently, large-scale corticocortical connectivities, both structural and functional, have received a great deal of research attention, especially using the approach of complex networks. Understanding the relationship between structural and functional connectivities is of crucial importance in neuroscience. Here, we try to shed some light on this relationship by studying synchronization dynamics in a realistic anatomical network of cat cortical connectivity. We model the nodes (cortical areas) by a subnetwork of interacting excitable neurons (multilevel model) and by a neural mass model (population model). With weak couplings, the multilevel model displays biologically plausible dynamics and the synchronization patterns reveal a hierarchical cluster organization in the network structure. We can identify a group of brain areas involved in multifunctional tasks by comparing the dynamical clusters to the topological communities of the network. The relationship between structural connectivity and functional connectivity at different levels of synchronization is explored. With strong couplings of multilevel model and by using neural mass model, the dynamics are characterized by well-defined oscillations. The synchronization patterns are mainly determined by the node intensity (total input strengths of a node); the detailed network topology is of secondary importance. The structure of the dynamical clusters significantly differs from the anatomical clusters. The improved multilevel model, e.g., with biologically more relevant chemical coupling and detailed intra-areal communication, exhibits similar dynamical patterns in the two regimes. Thus, the study of synchronization in a multilevel complex network model of cortex can provide insights into the relationship between network topology and functional organization of complex brain networks.

Zusammenfassung

Das Gehirn von Säugetieren stellt mit seinen zahlreichen, hochgradig vernetzten Neuronen ein natürliches Netzwerk von immenser Komplexität dar. In der jüngsten Vergangenheit sind die großflächige kortikale Konnektivitäten, sowohl unter strukturellen wie auch funktionalen Gesichtspunkten, in den Fokus der Forschung getreten. Die Verwendung von komplexe Netzwerke spielt hierbei eine entscheidende Rolle. Es ist für die Neurowissenschaften von tragender Bedeutung das Verhältnis von struktureller und funktionaler Konnektivität zu verstehen. In der vorliegenden Dissertation versuchen wir, dieses Verhältnis durch Untersuchung der Synchronisationsdynamik anhand eines realistischen Modells der Konnektivität im Kortex einer Katze näher zu beleuchten. Wir modellieren die Knoten (Kortexareale) durch ein Subnetzwerk interagierender, erregbarer Neuronen (*multilevel model*) und durch ein Modell von Neuronenensembles (*population model*). Bei schwacher Kopplung zeigt das *multilevel model* eine biologisch plausible Dynamik und die Synchronisationsmuster lassen eine hierarchische Organisation der Netzwerkstruktur erkennen. Indem wir die dynamischen Cluster mit den topologischen Einheiten des Netzwerks vergleichen, sind wir in der Lage die Hirnareale, die an der Bewältigung komplexer Aufgaben beteiligt sind, zu identifizieren. Desweiteren wird das Verhältnis von struktureller und funktionaler Konnektivität auf verschiedenen Stufen der Synchronisation näher untersucht. Bei starker Kopplung im *multilevel model* und unter Verwendung des Ensemblemodells weist die Dynamik klare Oszillationen auf. Die Synchronisationsmuster werden hauptsächlich durch die Eingangsstärke an den einzelnen Knoten bestimmt, während die genaue Netzwerktopologie zweitrangig ist. Die Struktur der dynamischen Cluster unterscheidet sich signifikant von der der anatomischen Cluster. Eine Erweiterung des Modells auf andere biologisch relevante Faktoren, wie der exakten Modellierung chemischer Synapsen und der interarealen Kommunikation, bestätigt die vorherigen Ergebnisse. Die Untersuchung der Synchronisation in einem *multilevel model* des Kortex ermöglicht daher tiefere Einblicke in die Zusammenhänge zwischen Netzwerktopologie und funktionaler Organisation in komplexen Hirn-Netzwerken.

List of Abbreviations and Annotations

AC	anatomical connectivity
FC	functional connectivity
EC	effective connectivity
V	visual system
A	auditory system
SM	somato-motor system
FL	fronto-limbic system
RN	random network
SWN	small-world network
SFN	scale-free network
EEG	electroencephalography/electroencephalogram
MEG	magnetoencephalography
fMRI	functional magnetic resonance imaging
DTI	diffusor tensor imaging
TI	tracer injections
LFP	local field potential
FHN	FitzHugh-Nagumo model
ML	Morris-Lecar model
NMM	Neural mass model
AP	action potential

x, V	potential
$\bar{x}$	mean field signal of a single area
X	mean field signal of the whole network
$A(i,j)$	adjacency matrix
$W(i,j)$	weighted matrix
k_i	degree of node i
S_i	intensity of node i
w_{IJ}	reciprocal strength
MI	matching index
H	Hamming distance
M^C	anatomical matrix of cat cortex
M^L	local matrix of connections within a single area
M^A	anatomical network
M^F	functional network
C	dynamical cluster
C^S	effective cluster
$r(i,j)$	Pearson correlation matrix
R	average correlation coefficient of $r(i,j)$
r_X	correlation between local mean field $\bar{x}$ and global mean field X
r_C	correlation between dynamical and effective clusters
Q^A	modularity of M^C
Q^C	modularity of $r(i,j)$
Q^4	modularity of M^C for partition V, A, SM, FL systems
Q^F	modularity of $r(i,j)$ for partition V, A, SM, FL systems
P0	non-connections in M^C
P1	uni-directional connections in M^C
P2	reciprocal connections in M^C

Contents

Chapter 1

Introduction

The mammalian brain is a complex system par excellence. This body organ is a unique mixture of various kinds of cells, linked by numerous synapses to form columns, circuits and areas. Brain anatomy, function, ongoing neurochemical processes, cognition and information transmission, all of them tightly interrelated, have already been the subject of investigation for centuries. An innumerable amount of information about brain anatomy and function has been collected [21, 64], different methods to analyze its structure and function have been applied, and various plausible interpretations of neuronal properties have been proposed.

One part of the research has concentrated on the topological properties of the cortex. Cortical *anatomical connectivity* has been described as a hierarchy of interacting elements of different functions and different interconnections. There are at least three basic levels in this hierarchy: i) the microscopic level of interacting neurons, ii) the mesoscopic level of minicolumns and local neural circuits, and iii) the macroscopic level of large-scale organization of the brain areas linked with nerve fiber projections [21, 95, 100, 111]. While details at the first two levels are still largely missing, extensive information has been collected about the last level in the brain of animals such as cats [99, 100] and macaque monkeys [41].

In parallel, investigation of brain activity has also placed significant emphasis on the function of individual brain areas and the functional interactions between them. Modern brain imaging techniques, e.g., functional magnetic resonance imaging (fMRI), allow researchers to explore this *functional connectivity* during special tasks. The recorded neural dynamics are studied by numerous linear and nonlinear time series analysis methods [11]. Functional correlations are manifested by interdependence and synchronization of the dynamical activities of different areas over a wide range of spatial and temporal scales [11, 73, 108].

The brain activity reflects a hierarchical organization of the dynamics which most likely arises from a hierarchy within the complex cortical networks [111]. For example, in an anesthetized state, the activity patterns reflect the functional architecture of the underlying anatomy [39]. Similarly, the coordination of the internal brain states in the form of inter-areal correlation gives origin to highly specific patterns corresponding to the functional networks. Detailed analysis of the properties of both the anatomical and the functional brain networks is then further required.

The graph theory approach is widely employed to explore the organization and features of complex networks such as the brain networks. This universal approach relies in representing the topological structures as graphs [5, 19, 20]. Special attention is paid to global properties of complex networks, such as scale-free and small-world features [119, 126, 127]. The network analysis of the anatomical connectivity of the mammalian cortex [108] and the functional connectivity of the human brain [11] have shown that both share typical features of many real complex networks. Neural anatomical network structures on various levels, especially the large-scale cortical networks, display characteristics of small-world networks, e.g., high clustering and short pathlength. This might allow the system to perform both specialized and integrated processes. Additionally, the robustness of cortical networks against node lesion manifests properties similar to those of scale-free networks [63]. The organization of the functional connectivity based on large-scale measurement of brain activities like fMRI [38, 98] also exhibits basic properties of small-world and scale-free networks [11].

Considering all these observations and parallelism, it is of fundamental importance to understand the interrelationship between topological structures and the dynamics of the brain. Hence, questions treated in this dissertation are: What is a meaningful approach to study such a complex system as the brain? What kind of model should be used? What is the relationship between the anatomical and functional connectivities? How will the underlying anatomical connectivity affect the dynamics of the brain?

To comprehend better the principles underlying brain dynamics, various models of neuronal activity have been studied for a long time. In physics, most of the studies have concentrated on the dynamics of the network, using generic oscillators (periodic or chaotic) as the nodes of typical network models like small-world and scale-free networks, globally or sparsely connected with random architectures [15, 23, 70]. The ability of the network to achieve rather idealized complete synchronization or coherent collective oscillations and the dynamical regimes, such as asynchronous on-going activity with balancing between excitation and inhibition [23, 125] were examined. However, neural networks display several levels of topological organization that are not well-accounted for by such typical network models [105]. In addition, the oscillatory dynamics of neurons cannot be sufficiently described by low-dimensional oscillators, and synchronization behavior is often far from the ideal situation [45, 97, 103].

On the other hand, in neuroscience, a wide spectrum of neuronal models realistically capturing processes ranging from the behavior of a single cell to large-scale neuronal population activity has been presented. However, concentration on an individual neural element and investigation of its activity cannot shed much light on the dynamics of the whole system. The interactions between the neurons cannot be considered to be only the perturbation of the process going on within the cells. The effects of neural communication are large and in the approach to study the neural dynamics we should examine the system globally [65]. Thus, 'bottom-up' modeling of the large cortical networks and investigating their synchronization behavior should provide meaningful insight into the problem. In this approach, the system consists of basic dynamical and topological units, e.g., single neurons, linked in the specific complex topology [22, 59, 77, 96, 130]. The topological model can represent a local neuronal ensemble of a cortical area

or the hierarchically organized architecture of the brain, reflecting for example the anatomical cortical connectivity of cat or monkey [41, 100].

The idea to use well-known cortical networks in the modelling of the neural dynamics and investigating its relation to the underlying topology has already been considered in the literature. One of the first models was proposed by Kötter and Sommer [69]. The dynamics of areas in a cat cortical network were modeled by a simple threshold activation function and the activity propagation was compared with experimental results, see also [118]. The same model was used later for modeling of the activity in the thalamo-cortical network of the cat [102]. Sporns et al. [110] chose a different approach, where the main goal was to compare functional patterns of network activity to anatomical structure. Areas linked by excitatory connections and self-inhibitory links were driven by a constant input in the form of uncorrelated noise. Later, Kiss [66] used a model of the cat cortex as a basis for the simulation of population activity on the mesoscopic level. He concentrated on the dynamics of the network after area lesions and information processing in the large-scale model. There have been also several works simulating cortical activity and adopting a two-level hierarchy (level of neurons and level of areas), but either simplifying the network architecture [67] or the dynamics of single units [120]. Recently, the very ambitious Blue Brain Project [77] has aimed to build a detailed and large-scale computer model of mammalian brain using realistic morphological properties of neurons and neuronal connectivity. Currently, a single cortical column has been reconstructed.

The above-mentioned studies were the main motivation for our modeling. We wanted to build a more complex and more realistic model of a neural network with improved dynamical properties. We have constructed a complex large-scale brain network using the 'bottom-up' approach. The cortical network is simulated by a multilevel model, *a network of networks*, where each cortical area is modeled by a subnetwork of interacting excitable neurons. We focus on the systems level of the connectivity formed by long-range projections among cortical areas. The dynamics of the nodes (cortical areas) in the networks is simulated with various models. These subnetworks have typical small-world topology which accounts for the basic features of realistic neuronal connectivity at the cellular level [26]. Such a general model should be able to capture and mimic various dynamical processes, as well as the wide spectrum of possible neuronal topologies. Our central task is to use this hierarchical neural model to study the impact of the known anatomical topology on dynamical processes.

The presented dissertation is organized into seven chapters. In Chapter 2, we introduce different types of neural connectivity together with their examples and methods how to extract them. The general concept of the connectome is sketched. In parallel, the basics of graph theory and its application in neural networks are discussed. Chapter 3 details the network of cat cortex and we design a two-level hierarchical model of the neural network topology. Structural details are presented and all network parameters are summarized. In Chapter 4, we deal with the dynamical characteristics of neurons representing an elementary unit in our model. The basic neuronal properties are listed and their specific roles in the neuronal dynamics are explained. Results of the simulations of the multilevel model are presented in Chapter 5, where we show different regimes of synchronization in the hierarchical networks. The analysis concentrates on the clustering behavior of the simulated neural activity and the study of their relationship

with the underlying anatomical structures of the network. The dynamics of the cat cortical network are compared to the dynamics of randomized networks and we demonstrate different mechanisms of synchronization organization. Chapter 6 is devoted to the dynamics of the set of the neural mass model modeled on the cat cortical network (for comparison with dynamics of the multilevel model). In the last chapter, Chapter 7, we conclude the work and discuss possible improvements and extensions of the model.

Chapter 2

Connectivity of brain networks

To discover the relationship between neural topology and neural dynamics requires, one requires a detailed knowledge about the structure of both of them. In this chapter, we describe different types of neural connectivity and show examples. The graph theory approach, widely applied to complex networks such as neural networks, is introduced to allow us to define the properties of brain anatomical and functional network topologies. We present the concept of a connectome, which is the parcellation of the brain into small components and basic units, linked and organized at various levels and hierarchies. The next section concerns the establishment of the connections and interactions between them. We discuss possible ways to extract functional networks.

2.1 Types of neural connectivity

The connections (links) between individual elements (neurons, areas) of brain can be identified in many ways. We can distinguish realistic anatomical links between cortical areas or estimate the correlation of their activity or the influence of one area over another one. Here, we introduce brief definitions of three types of neural connectivities [73, 108], which can be applied to every level of brain anatomical or functional hierarchy.

Anatomical connectivity (AC) can be defined as the set of all physical (structural) connections between neural units, cell assemblies or brain areas at a given time [108]. Anatomical links between neurons or cortical areas can be identified from the similar morphology (anatomy) or function of the neuron or area. These links, e.g. connections between the cortical areas of cat visual system [41], play an important role in communication and thus are a major determinant of functional properties [110]. The connections are relatively static at short time scales (seconds to minutes), but exhibit plasticity at longer time scales (due to development or learning).

Functional connectivity (FC) describes temporal correlations between neurophysiological events (spatially neighboring or distant) based on their correlation/covariance, spectral

coherence or phase-locking [46, 108]. Generally, this type of connectivity depends on the method of evaluation of the relationship (different methods lead to different estimates) and on the time (changes occurring in tens to hundreds of milliseconds). It can contribute to changes in the anatomical connections (spike-timing-dependent synaptic plasticity). FC mainly describes the pattern of the neural activity — *what* the brain does [73]. An example of FC is a correlation between voxels of fMRI measurements of brain activity [38].

Effective connectivity (EC) represents the set of causal effects of one neural system on another one, mediated directly or indirectly [73, 108]. For instance, at the synaptic level EC corresponds to a connectivity matrix of effective synaptic weights [46]. In comparison to FC (patterns of the activity), the EC offers the explanation of the origin of these patterns — *how* the brain does what it does [73]. The proper combination of the FC and of a selected causality model, specifying the links between units, is the key in the estimation of EC.

In our work, we have mainly concentrated on the first two types of connectivity — the anatomical connectivity drawn from known corticocortical fiber connections and the functional connectivity estimated from simulations of a large-scale model of cortex. As a model of anatomical connectivity and basis for our simulations, we chose cat cortex; its size, connectivity and topological properties have already been described in detail [99, 100, 108]. The main task is to find the intriguing relationship between these connectivities by comparing the corresponding anatomical and functional networks. Before we start to describe the properties of the individual connectivities in detail, we introduce the basics of graph theory analysis, the data analysis method to study the network topology.

2.2 Basics of graph theory analysis

Neural networks, along with other complex systems like metabolic pathways or the World Wide Web, are composed of sets of interacting elements with non-trivial topology. Such systems can be represented as a *graph* – basic elements as nodes (e.g, neurons or areas) and interactions between these individual elements as links (e.g., synapses and fibers) connecting particular nodes. The strength of the connection between two nodes corresponds to the strength of the interaction between them.

Each graph (network) can be characterized by the *adjacency matrix* describing the connections between the elements. For n neurons, we obtain an $n \times n$ matrix $A(i, j)$ with all-zero main diagonal and connections between neurons i and j being specified as:

$$A(i,j) = \begin{cases} 1 & \text{if } \exists \text{ connection between } i,j \text{ and } i \neq j; \\ 0 & \text{if } \nexists \text{ connection between } i,j. \end{cases}$$

We talk about *a undirected graph*, if the direction of interactions is not specified, i.e., $A(i, j) = A(j,i)$. In *a directed graph*, the connections $A(i, j)$ and $A(j,i)$ are strictly distinguished. Additionally, a *weight* $w(i, j)$ (strength) of the connections can be specified, where $W(i, j)$ is the *weight matrix* combining topology and weights, $W(i, j) = w(i, j)A(i, j)$.

The graph theory approach allows us to represent cortical areas of the cat brain and connections between them in the form of the network shown in Fig. 2.1. The cat cortical network is a directed network with numerous reciprocal links; additionally, a weight from the range 0 to 3 is assigned to each link. The entire matrix will be described in detail in Chapter 3.

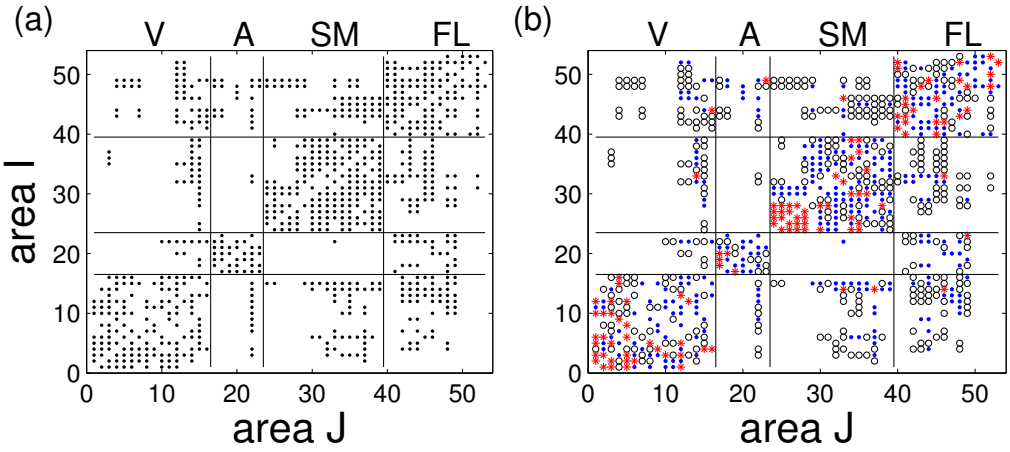

Figure 2.1: The representation of cat cortex in the form of the network: (a) binary matrix with unspecified weights, (b) weighted matrix, where the different symbols represent different connection weights: 1 (black ∘ sparse), 2 (blue • intermediate) and 3 (red ∗ dense). The organization of the system into four topological communities (functional subsystems, V, A, SM, FL) is indicated by the solid lines. See Chapter 3 for detailed description of the systems.

To characterize the structure and type of this network, we interprete and evaluate the main topological properties relevant for our later analysis, taking a cortical area as a basic unit of a network.

- The most basic node characteristic is its *degree* k. For an area i, k_i is the number of connections of the area i to the other areas in the network, i.e.,

$$k_i = \sum_j A(i,j).$$

  Incoming degree k_{in} (afferent connections) and outgoing degree k_{out} (efferent connections) of an area can be differentiated.

- The *intensity* of a node S_i, expresses the total strength of connections of the node (incoming S_{in} and outgoing S_{out}). It is the complete sum of the strength of all cortical fibers of the area:

$$S_i = \sum_j W(i,j).$$

- Additionally, we also define *reciprocity strength* as the average weight of the links between two nodes:

$$w_{ij} \equiv (W(i,j) + W(j,i))/(2w_{max}).$$

$2w_{max}$ is the maximal bidirectional weight, e.g., in the case of the cat cortical network [99], the maximal weight is $w_{max} = 3$.

- The *Matching Index MI* between two nodes quantifies the number of their common neighbors. For comparative reasons it is convenient to normalize it by the the number of non-overlapping connections of these two nodes:

$$MI(i,j) = \frac{\sum_{l=1}^{n} A(i,l)A(j,l)}{k_i + k_j - \sum_{l=1}^{n} A(i,l)A(j,l)}.$$

  Then $MI(i,j) = 1$ only if areas i and j receive input entirely from the same areas, and $MI(i,j) = 0$ if all inputs to i and j come from completely different areas. MI can be regarded as an estimation of the "functional similarity" of the nodes [51].

Based on the topology of the network and the structural properties, we distinguish four common types of networks — *regular networks, small-world networks (SW), scale-free networks (SF)* and *random networks*, see Fig. 2.2.

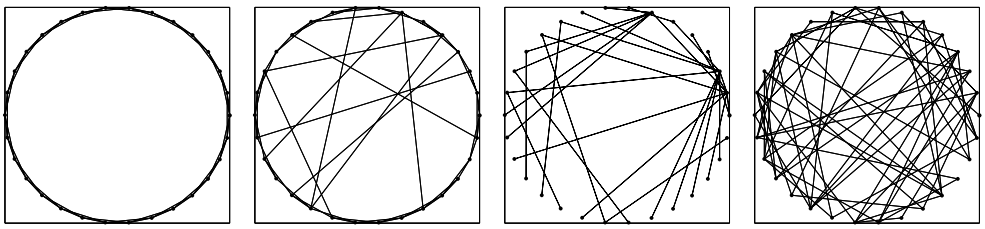

Figure 2.2: Different kinds of networks: (a) regular, (b) small-world, (c) scale-free and (d) random.

Roughly speaking, in regular networks, nodes usually have connections to a constant number of nearest neighbors (Fig. 2.2(a)), whereas in random networks, the number and topology of connections between nodes are entirely random (Fig. 2.2(d)). Small-world (SW) topology represents an intermediate structure between the random and regular one (Fig. 2.2(b)). Scale-free (SF) networks are characterized by the presence of a few hubs, i.e., nodes with a very high number of connections (Fig. 2.2(c)). Several authors have presented a general overview of these different kinds of networks, their network properties and the influence of such properties on the network dynamics [19, 20, 84, 137].

SF and SW networks have especially been at the center of interest because of their common occurrence in nature, e.g., SF networks in functional brain networks [38] and SW networks in cortical networks [108, 110], in the neuronal network of *Caenorhabiditis elegans* [127] and also in the functional networks [11]. We will pay special attention to the SW type of networks, originally proposed by Watts and Strogatz [127]. At the beginning, each unit of the network connects to a number k_a of the nearest neighbors, alternatively specified by a connection density parameter $p_{ring} = k_a/n$. Later, links are rewired with a probability p_{rew} to a randomly selected node, which introduces some long-range connections ('shortcuts'). The parameters p_{ring} and p_{rew} are crucial for the selection of specific network character (regular, small-world or random), see [127].

Taking a neural network as an example of SW topology, the high *average clustering coefficient*, expressing the large number of densely interconnected nodes, points out the existence of clusters of neurons. The presence of a few shortcuts decreases the *path length*, i.e., the distance between two nodes i and j. The efficiency of neural communication within and between cell assemblies is increased in networks with such properties. The spreading of the signal often leads to synchronization of the dynamics of neurons [71, 72, 79, 47]. Such enhanced synchronization has also been confirmed by analytical studies [9, 88]. It has been argued that the evolution of systems into networks with small-world topology probably attempts to maximize the dynamical complexity while minimizing wiring costs, i.e., cost-effective information processing [11].

The use of graph theory methods has revealed many basic characteristics of brain networks. Now, we introduce the general anatomical connectivity of the brain at different levels and its topological properties.

2.3 Anatomical connectivity

Mammalian brain consists of a vast number of neurons that are interconnected in complex ways [111]. In recent years, the network of anatomical links connecting various neural elements, the *connectome*, has been the subject of intensive investigation. From numerous neurohistological studies, information about the morphology, location and connections of different types of neuronal cells, microcircuits and anatomical areas has been collected and sorted. This data plays an important role in creating a global image of the brain. The implementation of such topological information in a large-scale neuronal model might help us to understand the mechanisms of temporal and spatial spreading of brain activity.

2.3.1 Connectome

We describe the general structure of the mammalian connectome. Although the details of the neuronal network architecture are not fully known, several levels of cortical connectivity can be defined [111].

Microscopic connectivity

In the human brain, approximately 10^{11} neurons are linked together by 10^{14-15} connections, which corresponds to about 10^4 synapses per neuron on average. The network is rather sparsely connected, with mainly local connectivity. Usually, each neuron makes contact to its closest neighbor only by one synapse or not at all [21, 95]. The interneuron connectivity patterns are very plastic, where changes are partially predetermined by genetic constraints and later modified by factors like learning and nutrition. Since for a long time it has not been possible to extract the microscale connectivity [18, 78, 104], the neural connections are commonly modelled as a graph. The architecture often takes the

form of a small-world network [71, 72, 79]. Other topologies are also considered, ranging from random [23, 59, 70] or globally coupled networks [15, 48, 53] to more realistic topologies reflecting spatial growth of the cortex [62].

Mesoscopic connectivity

The next level in the brain anatomical network is made up of cortical minicolumns. A cortical minicolumn, a narrow chain of neurons organized in the vertical direction across cortical layers II–VI, is considered to be a basic functional unit for processing information in the brains of mammals [18, 94, 95]. Such local circuits consist of only 80–100 neurons with an architecture more complex than just random or distance dependent connections patterns. Further, the minicolumn is deemed to be a basic building block of the complete connectome [25, 111]. A set of these functionally specialized and precisely rewired small neuronal populations (usually 60–80 units) later gives rise to the cortical column (macrocolumn).

Macroscopic connectivity

In the cerebral cortex, neurons are also organized into numerous regions (areas) that differ in cytoarchitecture and function. These areas, originally defined and listed by Brodmann at the beginning of the 20th century, may be assumed to be basic elements at the macroscale [21]. The architecture and function of the areas, as well as the topology of the neuronal fiber connections linking different areas have been the subject of intensive investigation. The anatomical network of visual cortex of monkey was described for the first time in 1991 by Felleman and van Essen [41]. More recently, cortical maps of other species like rat [24] and cat [99, 100] have been published. Analysis of the obtained cat anatomical cortical network revealed that the network possesses the small-world properties [11, 108].

This detailed knowledge of the anatomical connectivity at the systems level of functional brain areas offers a good starting point to explore the undergoing dynamical processes.

2.3.2 Data extraction and databases

Anatomical information collected about the different levels of connectome has comes exclusively by invasive techniques (e.g., cutting axons and observing degeneration of cells, study of postmortem brains, microinjection of dyes followed by autoradiographic imaging), meaning that such information was mainly collected from animal studies. Several other factors like the high number of neurons, complex network topology or plasticity, make it impractical to extract the precise connectivity at the anatomical microlevel. Newly developed imaging methods like *Diffusive Tensor Imaging* may later help to obtain the details of human anatomical connectivity [37].

All the extracted information about the anatomical connectivity of a number of animal species has been summarized and presented in various databases on several web sites. At the

mesoscopic scale the databases 'Microcircuit' [3] or 'Wormatlas' [6] offer insights into local circuit connectivity. The database 'Cocomac' [2] contains connectivity maps of macroscopic cortical networks of macaque monkey, and 'BrainMaps' [1] maps the anatomical details of different animal species like domestic mouse, rat, cat, and several types of monkeys.

Our first task is to construct a topological model based on the known anatomical structure, which will provide the basis for modeling the dynamics of the system. We extract and investigate functional networks to understand how the anatomical connectivity corresponds to the dynamics. In the next section, we describe what functional connectivity and functional networks are and how we obtain them.

2.4 Functional connectivity

In the nervous system, processing and transmission of information are encoded in the form of electrical activity of individual neurons. The specific dynamical interactions between neural elements and their statistical dependencies give rise to functional connectivity (FC) [33, 46]. Being closely related to the underlying anatomical network [110], FC can be also estimated at different levels of brain hierarchy, as described in Section 2.3. At the microscopic level, single neuron activity can be recorded with an intracellular microelectrode. The change of membrane voltage is expressed in the form of an action potential (AP). The dendritic synaptic activity of all neurons within a certain volume, a local field potential (LFP), can be measured by a single extracellular electrode. Synchronized firing of neighboring neurons and summated postsynaptic potentials plus the AP of the active neuron give rise to the LFP. On this mesoscopic level, a large number of summed postsynaptic potentials from the surface of several square centimeters of cortex creates the EEG signal. This signal can be divided into several frequency bands, each related to a certain mental state. The EEG signal is complex, reflecting the strongly nonlinear neural dynamics and the intricate structure of the neuronal connections. The different types of neurophysiological data can be obtained under different conditions, either in the basic resting state or while the brain is being stimulated, directly by strychnine injections [118] and by transcranial magnetic stimulation or indirectly in the form of mental tasks. In addition to the records of the physiological signals, various neural models allow us to simulate neuronal activity at different levels: action potentials, local field potentials or mean field activities of whole areas (see review [11]).

To obtain functional networks from data (physiological records or neural simulations), we proceed in two steps:

1. Evaluation of functional connectivity
To evaluate the FC between a pair of nodes or in a specific frequency band, we can use either *linear* measures like cross-correlation, coherence and partial correlation [33, 98] or *nonlinear* measures like mutual information [110], generalized synchronization [13], synchronization likelihood [114, 116, 117], phase synchronization measures [90] or wavelet analysis [4].

It is difficult to decide which method allows us to extract functional connectivity most effectively [33]. Linear methods are more sensitive in the detection of the presence of neuronal coupling and allow a fast characterization of data, but they are not able to capture nonlinear features. Nonlinear techniques better handle nonlinearity in the data, but they are computationally demanding.

2. Extraction of functional networks
The pairwise FC between different regions forms a matrix from which the functional network can be extracted. A specific threshold is applied to this matrix and as a result an undirected graph is derived. If the value of the functional connectivity is larger than the threshold, a functional link between two corresponding elements is established. Connections with the FC smaller than the threshold are removed. The final structure of the functional network, represented by a binary matrix, depends on the number of regions included, the method chosen for the estimation of the functional connectivity and the thresholding rule [11].

Similar to anatomical networks, the topological properties of functional networks are the subject of intensive investigation. There is evidence of SW properties in functional networks, based mainly on the presence of network characteristics such as short average path length and high clustering coefficient [4, 11, 12, 98]. Degree distribution offers additional information about the network: It might vary from the power law distribution of SF networks [38] to the exponential truncated power law somewhere between the exponential law of SW and power law of SF networks. The resulting degree distribution guarantees the presence of a few hubs, but not as many as in SF networks. This property protects functional networks from attack and makes the network more resilient [4, 115]. Recently, functional networks were also described as fractal SW networks [12]. The small-world topology may play an important role in cognitive processes, e.g., the change in cognitive ability associated with Alzheimer's disease has been linked to the increased path length in the functional network [115].

2.5 Summary of the chapter

We have defined the three basic types of brain connectivity (anatomical, functional and effective) and introduced the basics of graph theory, allowing us to represent the connectivity as a network and estimate the network properties. Details and properties of anatomical and functional connectivity were mentioned together with how to obtain and analyze the anatomical and physiological data. At the end, we discussed the extraction of functional networks from the data.

Chapter 3

Network topology of a large-scale model

After introducing the idea of the connectome in the previous chapter, we use the anatomical information to build a hierarchical model of the brain. First, we describe the anatomical connectivity of the brain at the macroscale found in the cat cortical network. Each cortical area is modeled by a subnetwork resembling basic features of the microscale connectivity. The resulting system is then a *network of networks*.

3.1 Cat cortical network

One of the most detailed brain anatomical connectivities known is that of a cat cortical network, see Fig. 3.1 [100]. This system serves as the basis for our model. The first collation of cat corticocortical connections, including 65 areas and 1139 reported links, was presented by Scannell et al. [99]. The results of the study were later completed and reorganized, which led to the origin of a corticocortical network of 53 cortical areas and additional thalamo-cortical network of 42 thalamic areas [100].

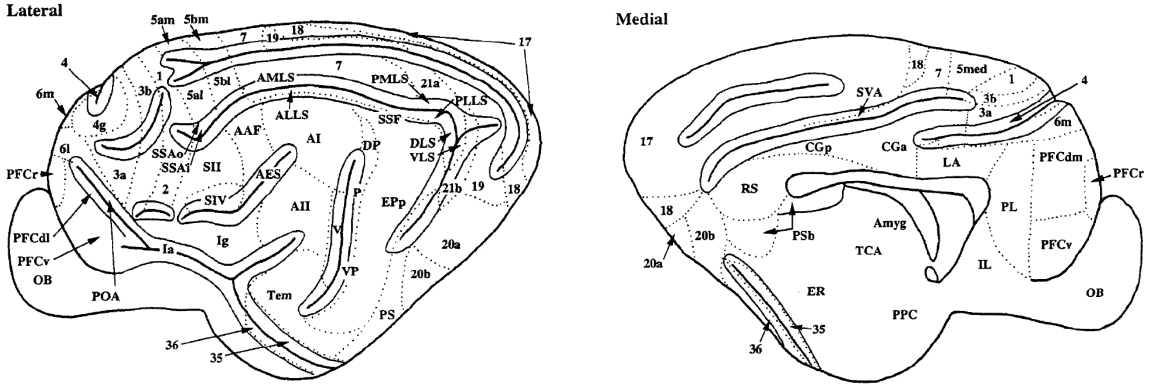

Figure 3.1: Topographical map of cat cerebral cortex (taken from [99]).

The corticocortical network of cat used in our model is composed of 53 highly reciprocally interconnected brain areas, see Fig. 3.2. The density of afferent and efferent axonal fibres is expressed in three levels — '3' for the densest bundles of fibres, '2' for intermediate or unknown density and '1' for the weakest connections. The value 0 characterizes absent or unknown connections. These values convey more the ranks of the links than the absolute density of the fibres, in the sense that a '2' is stronger than a '1' but weaker than a '3' [99, 100]. All together, there are around 830 connections in the corticocortical network with an average of 15 incoming links and with average incoming strength of 26 per area.

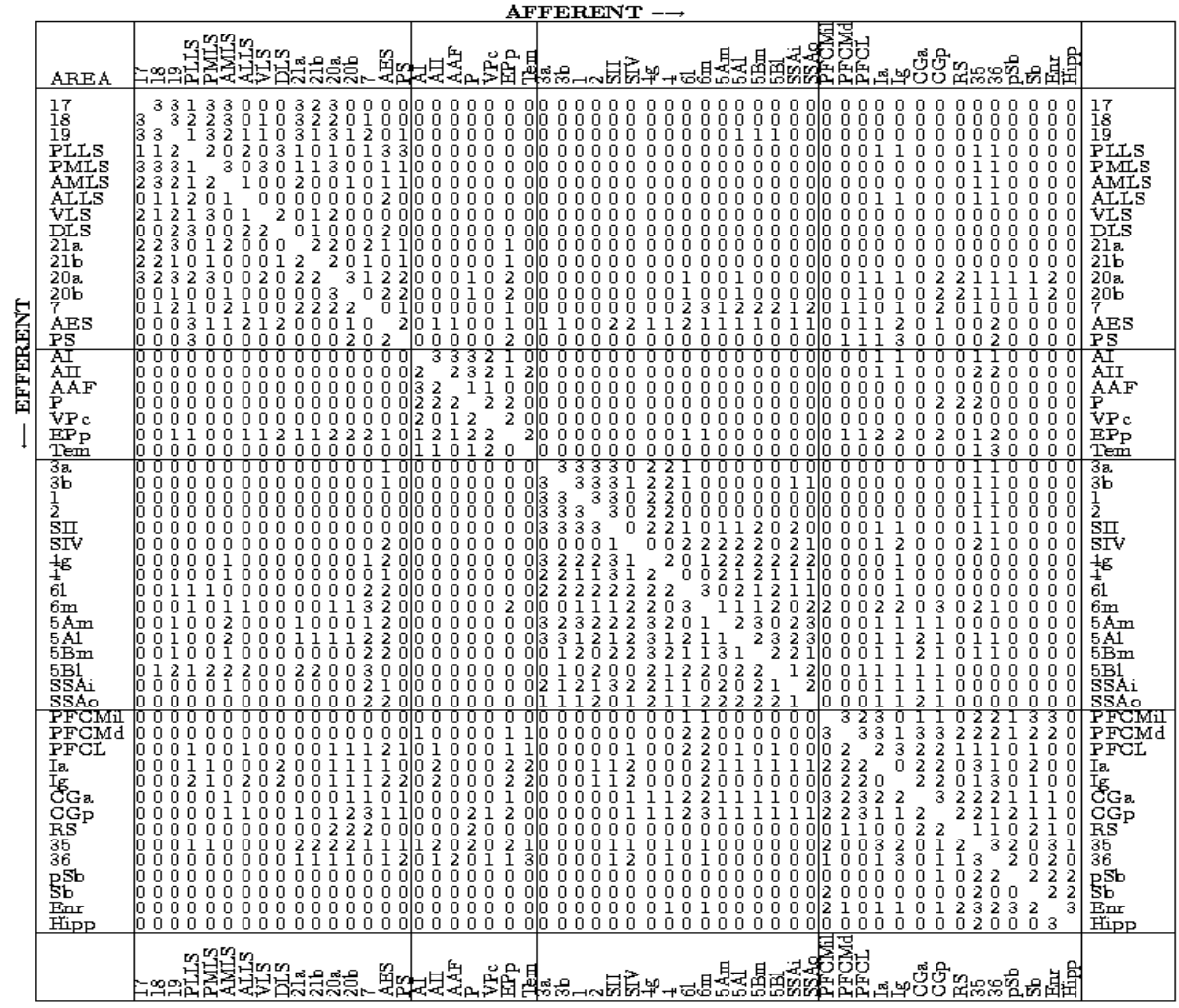

Figure 3.2: Connectivity matrix representing connections between 53 cortical areas of cat brain.

In the network of cat cortical connections, four distinct subsystems can be identified. Three of the subsystems — visual (V, 16 areas), auditory (A, 7 areas) and somato-motor (SM, 16 areas) — involve regions participating in the processing of sensory information and execution of motoric function. The fourth subsystem — fronto-limbic (FL, 14 areas) — consists of various cortical areas related to higher brain functions, like cognition and consciousness.

The optimal placement of the cortical areas in the connectivity matrix was found by using a nonmetric multidimensional scaling optimization method and already presented in the paper of Scannell et al. [99]. Such rearrangement of the areas led to the origin of these 4 subsystems described above. Later, several other methods based on network connectivity were applied to confirm this optimal arrangement [49, 50, 100]. As a very relevant method we only mention the evolutionary optimization algorithm [49], where the number of connections between units of the cluster is maximized while inter-cluster connections are minimized. The resulting four clusters agreed with the functional subsystems defined previously.

The corticocortical network has been subject to much detailed analysis based on graph theory (e.g., clustering coefficient, average path length, matching index and many other statistical properties) [108, 112] and theoretical neuroanatomy (e.g., segregation and integration) [107]. Most of the studies focused on revealing the small-world nature of the structure of the cortex. The presence of clusters is one of the cortical characteristics. Parcellation of the cortex into areas performing specialized functions corresponds to functional segregation. Cortical networks are also characterized by short path length between areas due to the few long-range connections; this short path length allows efficient inter-areal communication. This corresponds to the idea of functional integration of information. The robustness of such networks [61] and their hierarchical organization in the anatomical structure [31] have also been examined.

Because the properties of the structure of the cat cortex are well known, we chose the model of cat cortical connectivity as the basis for our model of macroscopic anatomical connectivity. We distinguish two types of model, differing in their representation of the areas: (i) In one case, we extend the network structure and build a two-level network, i.e., a network of networks. Cortical areas appear in the model as subnetworks. The global dynamics of each area arise from the interaction and superposition of the dynamics of individual neurons. (ii) In the second case, the dynamics of the area are modeled directly by a population model and the structure of the network corresponds to the basic cat cortical matrix. Now we concentrate only on the topology of the multilevel model.

3.2 Hierarchical model — network of networks

Due to the modular and hierarchical organization of the human connectome, simple models of individual cortical levels do not offer an appropriate insight into the complex dynamics occurring in such a complex topology. Thus, our model combines two cortical levels into one framework. The higher level copies the known connectivity of real neuroanatomical data, particularly the interconnectivity between 53 cat cortical areas [99, 100]. At the lower level, single cortical areas are modeled by large neuronal ensembles. Implementation of these two layers gives rise to a specific topology—a *network of networks*, see Fig. 3.3. Some of the previous studies have already dealt with such two level models (neuronal and areal) [109, 120]; however, none of them has introduced a detailed network topology in such an extension. As we will show in Chapter 5, this type of hierarchical network structure plays a crucial role in the uncovering of dynamical properties of the system, see also [132, 138, 139]. In the following section, we describe the details of the topology of the model and discuss possible modifications.

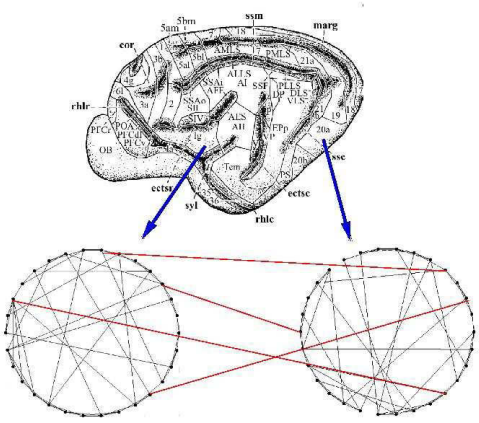

Figure 3.3: The modeled system—a network of networks. Note that the local subnetworks representing cortical areas have small-world structure.

3.2.1 Global cortical network

We chose the cat cortical map (see Fig. 3.1) as the representation of the large scale connectivity in our model. The cat cortex, together with the cerebral cortex of the macaque monkey, are the most completely described brain systems among the mammals. We will consider only cat corticocortical connections (cortical map) in our modeling, omitting corticothalamic connections. Our knowledge of the topological properties provides a good starting point for the investigation of the relationship between structure and dynamics. The model, however, is flexible enough to allow for the inclusion of any known cortical connectivity or artificially created network of long-range cortical connections. The cat cortical map is, in evolutionary terms, not so closely related to the structure of the human cortex. To minimize this difference, one can replace the cat matrix with the cortical map extracted from macaque monkey or possibly with a map of the human connectome in the future.

3.2.2 Local neuronal network

The individual cortical areas differ in cytoarchitecture and function. Due to these natural distinctions, we model each area as a local network, i.e., a population of neurons having its own topology.

It has already been reported in several studies [21] that local connections are more frequent than long-range ones, although the exact neuronal topology is unknown. Considering this fact, we have chosen a small-world architecture as a minimal model [79].

As soon as the local connections were established, we distinguished two types of neurons — excitatory and inhibitory. It is known that approximately 75–80% of the neurons are excitatory (pyramidal type with spines for specific excitatory synapses) and the remaining 20–25% are inhibitory neurons (interneurons, smooth cells with inhibitory synapses) [59, 64]. In our

simulations, we randomly selected the inhibitory neurons with a probability $p_{inh} = 0.25$. We considered all inter-areal links to be excitatory, since only pyramidal neurons are involved in the long-range inter-areal connections. Inhibitory connections are involved in long-range connectivity only at the local level (within cortical columns [26]); due to the absence of a myelin layer, they are not able to reach the speed necessary for signal transmission without significant delay and loss of data [21]. Additionally, we also have to take into account signals coming from other cortical areas (inter-areal links). If two areas are connected, only 5% of neurons within each area receive or send signals to the other area. On average, up to 30–40% of neurons of one area can be involved in communication with other areas [131].

We performed two studies which differed in the topology of long-range connections and the neuronal model together with the art of the neuronal coupling (discussed later in Chapter 4). We summarize the properties of the model topology for each case:

1. In the first part of our research, neurons communicate through the mean field signal, i.e., the selected 5% of neurons of one area get the mean field signal $\bar{x} = (1/n)\sum_i^n x_i$ of averaged activity of n neurons from another linked area I. The coupling strengths for intra-areal coupling g_{int}, i.e., the local excitatory and inhibitory synapses, have the same values. The inter-areal coupling strength g_{ext} differs from the local ones and both g_{int} and g_{ext} play a key role in identifying different dynamical regimes.

2. In the second study, we randomly selected $p_{ext} = 5\%$ of the neurons of a 'receiving' area to receive signals from $p_{ext} = 5\%$ of the neurons of a 'sending' area. Basically, we fix a total number of long-range connections between areas I and J as $(n * k_a * p_{ext})$. The selected receiving neurons of area I receive numerous inputs from selected sending excitatory neurons of area J. We avoid multiple links, i.e., two neurons from different areas can be connected only once. All established connections are directional. As we vary the coupling strength of the connections, here, for excitatory g_{exc} and inhibitory g_{inh} neurons, we obtain different dynamical regimes.

Table 3.1 offers an overview of all network parameters presented in the model of the network topology.

3.3 Summary of the chapter

Let us briefly summarize the structures of the model networks:

(i) In the first case, the system represents a *network of networks*, see Fig. 3.3. The upper level corresponds to the known anatomical connectivity map of 53 cat cortical areas. At the lower level, a single cortical area is modeled by a large neuronal population of excitatory and inhibitory neurons. The topology and the size of the local network can be adjusted by changing the network parameters. We randomly choose 5% of the neurons to receive an input from

Parameter	Description
N	Number of areas
n	Number of neurons per area
k_a	Number of connections per neuron within an area
p_{rew}	Probability of rewiring
p_{inh}	Ratio of inhibitory neurons
p_{ext}	Ratio of neurons of one area involved in long-range connections
g_{int}	Non-normalized intra-areal (internal) strength of synapses
g_{ext}	Non-normalized inter-areal (external) strength of synapses
g_{exc}	Non-normalized strength of excitatory synapses
g_{inh}	Non-normalized strength of inhibitory synapses

Table 3.1: Parameters of the network—structure and connections

another connected cortical area, thus forgetting the layered structure of the cortical area and corresponding topological details. Here, we consider two different topologies. In the first topology, the neurons receive an input in the form of average mean field signal of a sending area. We examine dynamical regimes obtained by variation of inter-areal and intra-areal coupling strengths. In the second topology, 5% of the neurons of area J receive an input from 5% of the neurons (only excitatory) in connected area I.

(ii) The second investigated model of connected neural populations mimics the neural dynamics on the macroscopic level. The number of neural populations and the connections between them reflect the topology of the cat cortical network.

The following chapter deals with the dynamics occurring in all types of model topology.

Chapter 4

Modeling the global dynamics of the neuronal population

Up to now we have presented the brain as a complex network of interacting elements and mainly discussed the details of brain anatomy and connectivity at different levels (Chapter 2). Based on this knowledge we have built a hierarchical model of brain, a network of networks (Chapter 3). In this chapter, we will concentrate on the neuronal dynamics and discuss the most relevant neuronal properties needed to model brain activity. The resulting dynamical patterns will be used to determine the functional networks. The linkage between the anatomical and functional networks will be examined later (see Chapter 5, 6).

In attempt to model the global dynamics of the neuronal populations, usually measured as EEG or LFP (Section 2.4), two main approaches are widely applied. The first approach simulates a network of neurons, where the combination of the nontrivial connectivity of neurons and the nonlinear behavior of the single neuron gives rise to complex dynamics. Following this idea, we have constructed a model with a network of neurons representing a cortical area. A set of neurons is connected according to a specific pattern of small-world network connectivity observed commonly in nature. The second approach models the mean activity of the entire ensemble of neurons. Such a population can represent a cortical column, or part of or the entire cortical area. The output signal is generated from sets of different types of neurons like pyramidal cells and excitatory and inhibitory neurons. Our model of neural mass mimics the activity of a brain area. In this chapter, we present the details of both approaches.

4.1 Single neuron model

Neurons possess a complex morphology to handle the specific tasks of information transmission and communication. The representation of neurons as a spatially extended unit with an intricate geometry would lead to a composite structural model of the neuron, computationally very expensive (see, e.g., [77]). Therefore, to simplify the neuronal model, neurons can be modeled as dynamical systems with an emphasis on the various ionic currents that determine

the neuronal excitability and response to stimuli. The neuronal response can be captured by a simple threshold or excitable model and the dynamics of the neurons can be described by two variables V and W:

$$\dot{V}_i = f(V_i, I^{bias}) + I_i^{syn}(t) + I_i^{ext}(t) \quad (4.1)$$
$$\dot{W}_i = h(W_i) \quad (4.2)$$

The dynamics of the fast variable V, imitating the membrane potential, are predetermined by a function f of two parameters: the membrane potential V and the basic current I^{bias}, which flows into the neuron and sets up the neuronal excitability. Moreover, the membrane potential V is modified by the total synaptic current I^{syn} coming from other connected neurons and the external current I^{ext}, representing perturbations from lower brain parts. The dynamics of slow recovery variable W, modeled by a function h, account for the activity of various ion channels.

Excitable neurons can be categorized into two classes based on their excitability and their response to an input [55, 57, 71]. Class 1 excitability contains those neurons able to encode the strength of the input into their firing activity, even with a weak input (Fig. 4.1(a)). Such neurons undergo a saddle-node bifurcation, with firing frequencies ranging from 2 to 200 Hz. Typical cells with such activity are pyramidal neurons, representing the majority of the cortical units. Class 2 excitability neurons do not respond to the input so flexibly and cannot fire at low frequencies (Fig. 4.1(b)). Their dynamics are characterized by a Hopf bifurcation, with an on/off behavior: Either the neuron does not fire, or it fires at a high frequency (like 40 Hz) [55, 71, 113].

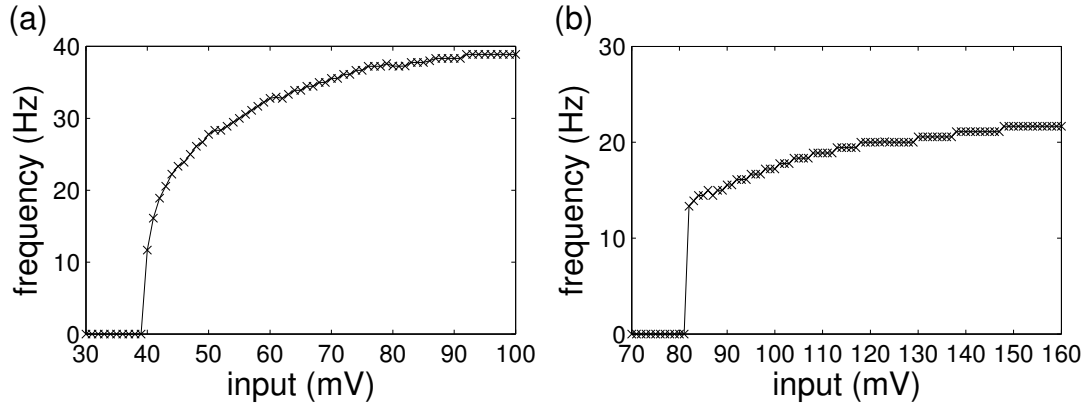

Figure 4.1: Dependence of the firing rate on the intensity of the applied current (Morris-Lecar model adopted from [123]): (a) Class 1 excitability, (b) Class 2 excitability.

From a variety of point spike models, e.g., Integrate-and-fire model, Hindmarsh–Rose model, Izhikevich model (see [55, 92]), we chose two different types of model. In addition to the details of the neuronal models, the properties of the neuronal coupling and stimulation are described and discussed in the following section.

4.1.1 Model of a single neuron

We introduce two neuronal models that capture the main features of neuronal dynamics like spiking, resting state, etc. The first model, the FitzHugh-Nagumo model, is an excellent example of an excitable system of class 2. This simple model of a relaxation oscillator is commonly used in neuroscience but has also various other applications, like in the kinetics of chemical reactions, or in solid state physics [89]. The second model is the Morris-Lecar model (ML), which is a canonical prototype for different classes of neuronal membranes. With a slight variation of the parameters, the ML model is able to exhibit both class 1 and class 2 neuronal dynamics.

4.1.1.1 FitzHugh-Nagumo model

FitzHugh proposed a model in 1961 [42], which was originally called the Bonhoeffer-van der Pol model. His main aim was to investigate basic dynamic interrelations between state variables of a cell membrane. At the same time, Nagumo constructed an electronic circuit exhibiting the same properties as the FitzHugh model [58] and now the model is known as the FitzHugh-Nagumo model (FHN). We adopted the version of the FHN introduced by Pikovsky et al. [89] and later used in numerous studies [52, 101, 135, 140]:

$$\varepsilon \dot{x}_i = x_i - \frac{x_i^3}{3} - y_i, \tag{4.3}$$

$$\dot{y}_i = x_i + a_i. \tag{4.4}$$

The fast excitable variable x represents the membrane potential; its cubic nonlinearity allows regenerative self-excitation via positive feedback (Eq. 4.3). The slow recovery variable y is responsible for accommodation and refractory behavior; its linear dynamics produce slower negative feedback (Eq. 4.4).

The small value of the time scale parameter ($\varepsilon = 0.01$) allows the separation of the motion of the two variables x and y. The parameter a is a bifurcation parameter responsible for excitatory properties of the system, where $|a| > 1$ corresponds to a stable fixed point and $|a| < 1$ to a limit cycle. We set $a_i \in (1.05, 1.15)$, and thus the neurons are in the excitable state, close to the bifurcation threshold. A small perturbation of such a state switches the activity to the oscillatory regime (see Fig. 4.2). We use the FHN model to describe the dynamics of individual neurons mainly because of its simplicity and biological plausibility [55]. This model is not a quantitative representation of a neuron, but it rather concentrates on the qualitative properties of neuron, modeling the dynamics of class 2 excitability. Even though it does not capture all features of the neuronal dynamics, the model still provides a signal similar to simple neuronal activity with properties like resting state and neuronal firing.

4.1.1.2 Morris-Lecar model

The second neuronal model we used in our simulations was the Morris-Lecar model, considered to be a canonical prototype for two classes of neuronal membranes. The Morris-Lecar model

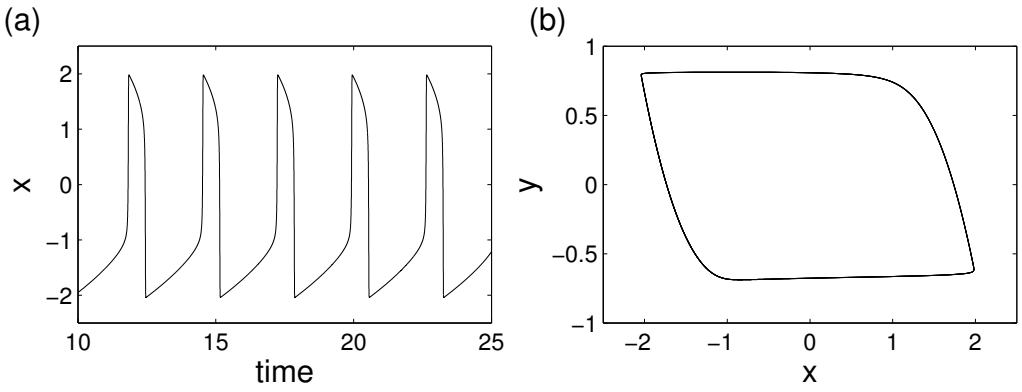

Figure 4.2: (a) FHN neuron in oscillatory state. (b) Phase portrait for FHN neuron.

was introduced by Morris and Lecar in 1981 during a series of studies of the excitability of the barnacle giant muscle fiber [93]. The dynamics of the cell membrane was determined by transmembranar currents — the voltage-gated Ca^{2+} current, the voltage-gated delayed-rectifier K^+ current and the leak current. The original third-order system of nonlinear equations denotes the voltage V and the activity of the depolarizing Ca^{2+} and hyperpolarizing K^+ channels. Due to the fact that calcium channels respond to V very rapidly, instantaneous activation is assumed and the model can be reduced to the two-dimensional form (Eqs. 4.5– 4.6) [93]:

$$C\dot{V} = I - g_L(V - V_L) - g_K W(V - V_K) - g_{Ca} M_{\inf}(V)(V - V_{Ca}), \tag{4.5}$$

$$\dot{W} = \lambda(V)(W_{\inf}(V) - W), \tag{4.6}$$

where

$$M_{\inf}(V) = 0.5\left[1 + \tanh\left(\frac{V - V_1}{V_2}\right)\right], \tag{4.7}$$

$$W_{\inf}(V) = 0.5\left[1 + \tanh\left(\frac{V - V_3}{V_4}\right)\right], \tag{4.8}$$

$$\lambda(V) = \phi \cosh\left(\frac{V - V_3}{2V_4}\right). \tag{4.9}$$

The activity of Ca^{2+} channels is included in the membrane voltage V, whereas the variable W represents the fraction of the open K^+ channels. C stands for the membrane capacitance per unit area and ϕ is a temperature-like scale factor, a decay rate of W, here considered to be a constant. g_a are the conductances and V_a resting potentials for calcium, potassium and leak channels $(a = Ca, K, L)$. Each neuron receives a constant input I, which determines the state of the neuron — either the resting (excitable) state, when the input is smaller than a critical bias current ($I < I_c$), or the oscillatory state, when the input is above the threshold ($I > I_c$). Fig. 4.3 shows the phase portrait of the oscillatory regime with corresponding voltage dynamics. We set $I_i \in (37.0, 38.0)$, when neurons are in the excitable state, close to the bifurcation threshold. Oscillations are achieved after perturbation of dynamics either through noise or signals from other neurons. All other parameter values were taken from Tsumoto [123] (Tab. 4.1) to model the dynamics of a single class 1 excitability neuron. The ML model is special since it can, with

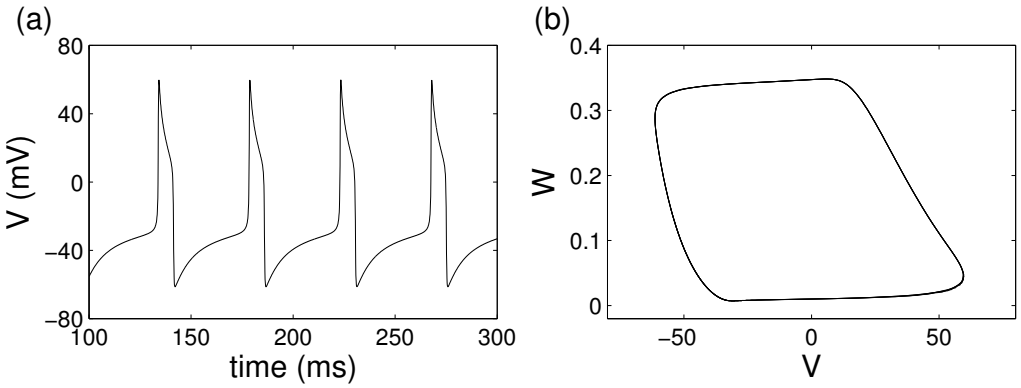

Figure 4.3: (a) Oscillatory dynamics of a ML neuron, class 1 excitability. (b) Phase portrait for ML neuron.

small change of parameters, also exhibit dynamical features of class 2 excitability (Fig 4.1(b)). Tsumoto has also shown that the parameters g_{Ca}, ϕ, V_3 and V_4 are crucial in the switching of the dynamics. When I_{ext} is relatively small, the simple change of the value of V_3 from 12 to 2 mV causes the dynamics to switch from class 1 to class 2 excitability, see [8, 123]. Thus, this model is suitable for modeling of heterogeneous groups of neurons. The same model with slightly different parameters was also used in our large-scale simulations of a neural network [10].

$g_L[\mu\text{S/cm}^2]$	2	V_L[mV]	-60	V_1[mV]	-1.2
$g_K[\mu\text{S/cm}^2]$	8	V_K[mV]	-80	V_2[mV]	18
$g_{Ca}[\mu\text{S/cm}^2]$	4	V_{Ca}[mV]	120	V_3[mV]	12
$\phi[s^{-1}]$	$\frac{1.0}{15.0}$	I[mA]	38.5	V_4[mV]	17.4

Table 4.1: Parameters of ML model of neuron (adopted from Tsumoto et al. [123]).

4.1.2 Factors influencing dynamics of a neuron

Previously described neuronal models can truly mimic the dynamics of a single neuron under certain conditions (in steady or oscillatory state, under stimulus). In the modeling of simple neuronal systems, two additional features are of great importance — (i) the presence of noise in the system, which determines the dynamical state of the neuron (oscillation) and (ii) the art of coupling of the basic elements, i.e., neurons or areas, expressing the influence of one system upon another one.

4.1.2.1 Role of noise in neural system

In the living brain, neurons in the normal state usually do not exhibit strong activity. According to some estimates, they are silent 99% of the time, just sitting below the critical threshold and

being ready to fire [44]. In our models, the neurons are also initially set to the excitable state (parameters a in the FHN model and I in the ML model are below the critical threshold).

We add Gaussian white noise $\langle \xi_i(t)\xi_j(t-\tau)\rangle = \delta_{ij}\delta(\tau)$ to mimic the intrinsic stochastic character of neuronal dynamics, caused by stochastic processes like synaptic transmission or spontaneous release of neurotransmitter into the synaptic cleft [28, 113]. The tunable parameter D (see later Eqs. 5.2, 5.13) scales the intensity of this random input. To obtain the natural firing rate of individual neurons (1–3 Hz), we can vary the intensity D until the expected firing rate is reached.

In some work, neurons are stimulated by multiple inputs of Poissonian noise to simulate external influences, e.g., from subcortical areas [23, 44, 56, 70]. In the study of a large-scale neuronal system [10, 133], we implemented both Gaussian and Poissonian noise.

4.1.2.2 Synaptic coupling between cortical neurons

10^{11} neurons in the human brain form a sparse network, where an average neuron forms about $10^3 - 10^4$ synaptic connections. There are two distinct types of synaptic coupling: electrical and chemical [64].

Electrical coupling (linear) appears only locally through the close contact of the cell membrane of the neurons (3.5 nm) without the presence of synaptic neurotransmitter. The information about the change of membrane potential of one neuron is transmitted directly as a current flowing through ion channels called gap junctions. The simplest linear coupling between two neurons i and j would take the form

$$x_i = f(x_i) + g(x_j - x_i),$$

where g is a strength of the connection [54]. Such diffusive coupling is not the most typical case in the mammalian cortex (occurs mainly in interneurons), but we use it in one part of our study to simplify that stage of our simulation (see later Section 5.1, Eq. 5.1).

Chemical connections (nonlinear) represent the majority of connections between neurons in the neocortex. The principle of signal transmission is based on the release of chemical messengers from the depolarized presynaptic neuron, which consequently bind to the receptors of the postsynaptic neuron. This causes the flow of ions in the postsynaptic neuron leading to the polarization of the membrane. Depending on the type of the receptor, we can distinguish excitatory or inhibitory neurons, which occur in the ratio of about 3:1 (implemented in the model as $p_{inh} = 0.25$). Excitatory neurons enhance the spreading of the action potential and excite the postsynaptic neuron. Inhibitory neurons inhibit neuronal activity and act to hyperpolarize the postsynaptic membrane.

Several models of chemical coupling are widely used, varying from a simple one expressed by a ‘threshold’ function [54] to more complex ones described by sets of equations [48, 64, 71,

Parameter		Excitatory	Inhibitory
E_s	(mV)	0	-80
α_s	(ms^{-1} mM^{-1})	2	0.5
β_s	(ms^{-1})	1	0.1

Table 4.2: Parameters of the synaptic coupling for excitatory and inhibitory neurons.

72]. In the second part of our study (Section 5.2), we adopted the model of chemical coupling described by Lago-Fernández [71], which will be now discussed in detail. The input from the synapses to the neuron I_i^{syn} (see Eq. (5.13)) is added to the fast voltage variable V. This synaptic term represents the total synaptic current to the ith cell, i.e., the sum of signals (spikes) from all pre-synaptic neurons, $k = 1,\ldots,n_{total}$. n_{total} is the number of afferent synaptic connections from all local and extra-areal neurons to neuron i:

$$I_i^{syn}(t) = \sum_{k}^{n_{total}} g_{ij} r_j [V_i(t) - E_s]. \tag{4.10}$$

The response from an individual synapse is modeled by the difference between the membrane potential of the postsynaptic neuron V_i and the reversal potential E_s (see a similar approach in [70, 71, 72]). E_s stands for E_{exc} or E_{inh} depending on whether the presynaptic neuron is excitatory or inhibitory. The parameter g_{ij} is the maximum conductance per unit area, which determines the connectivity and coupling strength between the postsynaptic i and presynaptic j neurons. In the case of disconnected neurons, we have $g_{ij} = 0$; $g_{ij} > 0$ indicates the presence of excitatory links and $g_{ij} < 0$ the presence of inhibitory ones.

The amount of released neurotransmitter into the synaptic cleft determines the fraction of the open channels r in the postsynaptic neuron:

$$\dot{r}_j = \alpha_s x_j (1 - r_j) - \beta_s r_j, \tag{4.11}$$

where α_s and β_s are time-dependent rise and decay constants, with s symbolizing whether the neurons are excitatory or inhibitory. The corresponding values of the parameters for synaptic coupling are summarized in Table 4.2. Neurotransmitter concentration x_j is typically modelled as a square pulse, see Destexhe et al. [36]. To make the change in the concentration smoother, the limits in the transmitter concentration at a constant presynaptic potential V_{pre} are expressed by the function $f(V_{pre})$:

$$\dot{x}_j = \alpha(f(V_{pre}) - x_j), \tag{4.12}$$

$$f(V_{pre}) = \frac{\sigma}{1 + \exp(-(V_{pre} - \theta)/T)}, \tag{4.13}$$

where $\alpha = 5$ ms^{-1}, $\sigma = 2.84$ mM, $\theta = 2$ mV, $T = 5$ mV [72].

With this model of the chemical synapses, the coupling gains nonlinear terms and the dynamics of the network become even more complex.

4.1.2.3 Other neuronal properties

There are several other neuronal properties modulating neuronal reaction and activity propagation within the network that we did not consider in our research. One of them is the spreading of the signal in the network, influenced by transduction delays t_{del}. Delays typically vary between 0.1–20 ms [68] and depend on the neuronal morphology [40]. Further, the strength of the synaptic connection is plastic; the mechanism of spike-timing-dependent plasticity (STDP) [17, 106] modifies the weight of connection between the neurons in dependence on the exact time difference between postsynaptic t_i and presynaptic t_j spike arrival, see [56, 106].

These properties also play a significant role in the dynamics of the brain, but because of the added model complexity, high computational costs would incurred when adding such properties. Example of their implementation in a large-scale model of brain can be found in [10, 14, 133].

As one can see, the modeling of a network of coupled neurons with many biological details of neuronal dynamics and coupling can be quite complex. A neural mass model offers an alternative way to model the dynamics of the neuronal population; we discuss its properties in the next section.

4.2 Neural mass model

EEG measurements record the mean activity of a population of neurons in the brain, often exhibiting rhythmic oscillations within well-defined frequency bands. A neural mass model describes the activity of such populations of cortical neurons and can reproduce the main features of EEG dynamics.

The first models of neuronal dynamics on the macroscopic scale appeared in the early 1970s [32, 43]. Lopes da Silva constructed a simple lumped parameter model of two populations of neurons (excitatory and inhibitory) coupled with negative feedback, generating an alpha rhythm [32]. Later, Jansen et al. [16] extended this model by modeling three subgroups: excitatory pyramidal cells and excitatory and inhibitory interneurons, adding also nonlinear terms to the equations. Wendling et al. [128, 129] concentrated in their works on modeling different patterns of EEG signals observed in epileptic patients. An improved version of the previous two models [16, 32] was able to generate EEG signals from multiple coupled neuronal populations in various frequency bands. The next variant of the model contained four neuronal subsets; the inhibitory neurons were further distinguished with fast or slow kinetics [128]. Recently, David mimicked EEG/MEG dynamics using hierarchically coupled models of neuronal populations [34, 35] and Ursino et al. [124] presented a model with parallel implementation of three different populations reproducing different rhythms of brain activity.

In our work, we use the neural mass model and parameters presented in [129], see Fig. 4.4 for a graphical representation of the model.

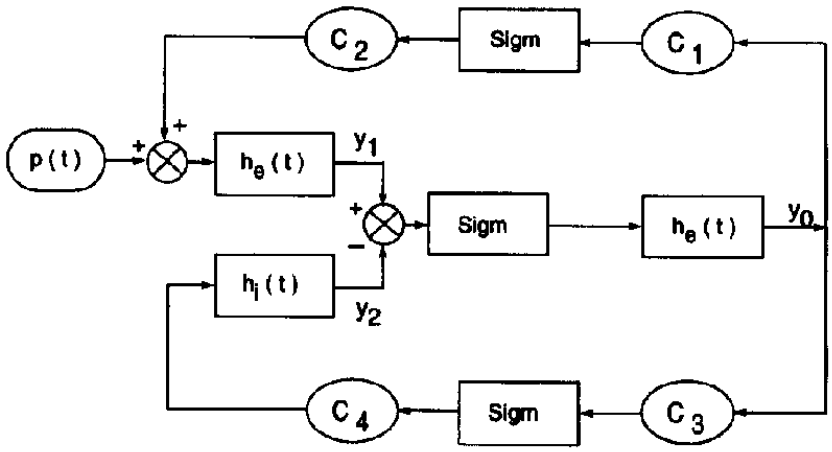

Figure 4.4: Neural mass model, adopted from [16]. Here, y_0 stands for v^p, y_1 for v^e and y_2 for v^i, p(t) is the noise input, as shown later in Chapter 6.

Here, a population of neurons contains two subpopulations: subset 1 consists of pyramidal cells receiving excitatory or inhibitory feedback from subset 2. Subset 2 is composed of local interneurons receiving excitatory inputs. This model describes the evolution of the macroscopic variables, i.e., average postsynaptic membrane potentials v^p for pyramidal cells, and v^e, v^i for the excitatory and inhibitory interneurons, respectively. A static nonlinear sigmoid function $f(v) = 2e_0/(1+e^{r(v_0-v)})$ converts the average membrane potential into an average pulse density of action potentials. v_0 is the postsynaptic potential corresponding to a firing rate of e_0, and r is the steepness of the activation. The dynamical equations for a single population are:

$$\ddot{v}_I^p = Aaf(v_I^e - v_I^i) - 2a\dot{v}_I^p - a^2 v_I^p, \tag{4.14}$$

$$\ddot{v}_I^i = BbC_4 f(C_3 v_I^p) - 2b\dot{v}_I^i - b^2 v_I^i, \tag{4.15}$$

$$\ddot{v}_I^e = AaC_2 f(C_1 v_I^p) - 2a\dot{v}_I^e - a^2 v_I^e, \tag{4.16}$$

where v_I^p, v_I^i and v_I^e are the postsynaptic membrane potentials of the area I. A detailed interpretation and the standard parameter values of this model are presented in Table 4.3. The details of the dynamics of multiple coupled populations and their relationship to the underlying anatomy will be discussed in the next chapter (Chapter 6).

4.3 Summary of the chapter

We have presented two different approaches to model the dynamics of neural ensemble. (i) The first approach considers the single neuron to be the basic element of the population. Connecting numerous neurons gives rise to the population dynamics representing a cortical area in our

Parameter	Value	Interpretation
A	3.25 mV	average E synaptic gain
B	22 mV	average I synaptic gain
$1/a$	100 s^{-1}	dendritic average time constant in the feedback E loop
$1/b$	50 s^{-1}	aver. time constant in the feedback I loop
C_1	C=135	aver. number of synaptic contacts in the E feedback loop,
C_2	0.8 C	
C_3	0.25 C	aver. number of synaptic contacts in the I feedback loop
C_4	0.25 C	
v_0, e_0, r	(mV)	parameters of the nonlinear asymmetric sigmoid function

Table 4.3: Model parameters, their values and interpretation (E = excitatory, I = inhibitory), adopted from [128, 129].

study. We have shown two point models with different excitability classes — the FitzHugh-Nagumo (FHN) and Morris-Lecar (ML) models. The FHN model captures the basic features of the neuronal dynamics and has class 1 excitability. It is a rather simple model, computationally inexpensive and thus suitable for the modeling of large networks. We coupled the set of FHN neurons by simple electrical coupling. However, in reality, around 70% of neurons are pyramidal cells with class 2 excitability and the neuronal coupling is mediated by chemical transmitter with complex dynamics. The ML model is suitable for simulations of such properties and moreover by the change of only a few variables, it can switch its behavior to class 1 excitability. The neuronal model composed of ML neurons is coupled by chemical synapses. These features increase the biological relevance of the model but also the computational difficulties. (ii) The second approach uses a neural mass model to imitate the dynamics of neuronal ensembles. This model substitutes the modeling of the dynamics of the network of neurons representing one cortical area.

The general dynamics generated by these diverse models will be presented and discussed in the next chapters (Chapter 5 and 6).

Chapter 5

Hierarchical model of cat cortex

We investigated the behavior of the multilevel model with two different types of neuronal dynamics. In the first case, the neurons represented by FitzHugh-Nagumo model are electrically coupled and the areas communicate through the mean field signal. The second case employs the neuronal model of Morris-Lecar coupled through chemical synapses with neuron-to-neuron communication between areas. This synaptic coupling has a nonlinear character, which makes the neuronal dynamics more complex. Here, we will describe the main features of the dynamics induced by both models, reveal the hierarchy of functional networks, that is similar to the structure of the underlying anatomical network, and show the presence of functional clusters. We will also discuss the reasons for such behavior and its biological relevance.

5.1 Network of electrically coupled FHN neurons

5.1.1 General dynamics of the model

As we have already introduced in Chapter 3, in our model of the cat cortex the neurons stand for the basic elements of the two-level hierarchical network. The general set of equations of the whole system in the case of FHN neurons takes the form:

$$\begin{aligned} \varepsilon \dot{x}_{I,i} &= f_{FHN}(x_{I,i}, y_{I,i}) + \frac{g_{int}}{k_a} \sum_{j}^{n} M_I^L(i,j)(x_{I,j} - x_{I,i}) \\ &+ \frac{g_{ext}}{\langle w \rangle} \sum_{J}^{N} M^C(I,J) L_{I,J}(i)(\bar{x}_J - x_{I,i}), \qquad (5.1) \\ \dot{y}_{I,i} &= h_{FHN}(x_{I,i}, y_{I,i}) + D\xi_{I,i}(t), \qquad (5.2) \end{aligned}$$

where x is the membrane potential modelled by a particular function f, see Eq. 4.3. It is also modulated by the input from neighboring neurons from the local network (coupling represented

by local connectivity matrix M^L) and input from remote neurons from other areas (coupling represented by cat cortex connectivity matrix M^C). Here, we set up that the connected areas communicate through their mean field activity $\bar{x} = (1/n)\sum_j^n x_j$. The label $L_{I,J}(i)$ is 1 if neuron i is among the 5% within area I receiving the mean field signal from area J, otherwise, $L_{I,J}(i)$ is 0 [131]. In spite of the fact that diffusive electrical coupling occurs only in a minority of the neuronal synapses, we use it in our model in order to simplify the connections between the neurons. Once the dynamical principles of the simpler model are understood, we will use more realistic chemical coupling (see Section 5.2). To each neuron, we add the weak Gaussian white noise ξ with intensity $D = 0.03$ to the slower variable to simulate the natural perturbation of the dynamics (Eqs. 4.4, 5.2). We tune the parameter D until we do not obtain signal for one area, similar to the background irregular neuronal activity of a silent neuron. Such signal corresponds to the average neuronal activity of the set of coupled neurons in the resting state with occasional bursts of activity, similar to EEG signal at resting state [87]. The coupling properties and the role of the noise in the system have been described in details in Section 4.1.2. We would like to emphasize that the Euler method, used for numerical integration, is appropriate due to the stochastic term ξ in the system. The model is coded in the Fortran 90 programming language.

Parameter study

We simulate the above system of Eqs. 5.1–5.2, the network of networks of FHN neurons, up to time $t = 2000$. A time step $\Delta t = 0.001$ is applied which is sufficiently small for the stochastic dynamics. To keep the simulation time reasonable, we fix the small-world subnetworks to have $n = 200$ neurons, $k_a = 12$ neighboring links, and a probability of rewiring of $p_{rew} = 0.3$. Despite the relatively large value of the rewiring probability we still obtain the small-world properties of the network. We select $n = 200$ as large enough to exclude the system size effects by checking the amplitudes (standard deviation) of the mean field $\bar{x}$ of the individual SWNs without external coupling ($g_{ext} = 0$). We also ran the whole system with other values of p_{rew} and n, and two different settings of the parameters g_{int} and g_{ext} that select the two main dynamical regimes (see later in this section); the obtained results confirm the robustness of the dynamics to changes in the local network topology.

Except for the noise intensity parameter D, here fixed to a constant level, the dynamics of the system are controlled only by the internal g_{int} and external g_{ext} coupling strengths. We explore the parameter space for g_{int} and g_{ext} and investigate how the dynamics of the individual areas are synchronized. To evaluate the degree of synchronization among these stochastic signals, a simple but effective linear measure, the Pearson correlation coefficient r, is used. We compute this correlation coefficient between the the mean field activities $\bar{x}_I$ of the areas using long time series after the transient, namely,

$$r(I,J) = \frac{\langle \bar{x}_I \bar{x}_J \rangle - \langle \bar{x}_I \rangle \langle \bar{x}_J \rangle}{\sigma(\bar{x}_I)\sigma(\bar{x}_J)}, \tag{5.3}$$

where $\langle \cdot \rangle$ denotes averaging over time. Further, the average correlation coefficient over all the $N(N-1)$ pairs of areas,

$$R = [1/N(N-1)] \sum_{I \neq J}^{N} r(I,J), \tag{5.4}$$

quantifies the overall level of synchronization in the whole network system.

In the local SWNs, the spiking dynamics and the synchronization of the neurons are mainly controlled by the internal coupling g_{int} [135] that determines the mutual excitation between any pair of neurons. For small g_{int}, a neuron is primarily activated by the noise, and not usually by the spiking activity of its neighbors. Thus, we observe irregular spiking patterns for individual neurons. The mean field $\bar{x}$ is characterized by some clear deviations from the baseline, demonstrating the weak synchronization within and also between the subnetworks (Fig. 5.1(a)). Such mean field activity of individual areas can be regarded as an analogue of the EEG signal [87]. The weak synchronization between such signals of the different areas is also shown by a small average correlation coefficient R (Fig. 5.4(a)). Increase of the coupling strength g_{int} leads to the increase of the synchronization between the neurons within the local subnetworks, manifested by the presence of some apparent peaks in $\bar{x}$ (Fig. 5.1(b)). With large enough g_{int}, the neurons are mutually excited, achieving both strongly synchronized and regular spiking behavior (Fig. 5.1(c)), indicating an almost global synchronization of the network.

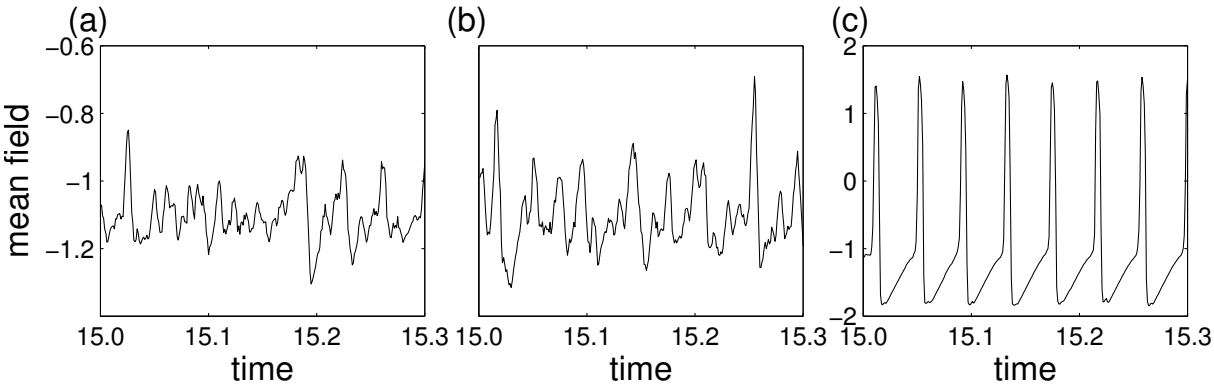

Figure 5.1: Typical time series of the mean field dynamics $\bar{x}$ of one area with different coupling strengths ($g_{int} = g_{ext}$): (a) $g_{int} = 0.06$, (b) $g_{int} = 0.082$ and (c) $g_{int} = 0.12$. Notice the different scales on the vertical axes.

Additionally to the main driving parameter of the network, g_{int}, the external coupling g_{ext} has also an effect on the synchronization of the neurons in the local network (amplitudes of $\bar{x}$), as well as on the control of the synchronization between the areas. For small g_{int}, the infrequent and irregular spiking activity of one area does not very much affect the behavior of the other connected areas. The correlations between the areas are not strong even for significantly large g_{ext} ($r \leq 0.1$). This is mainly due to the fact that only 5% of the neurons receive signals from another connected area [131]. For intermediate g_{int} (e.g., 0.080 ± 0.003), the effect of g_{ext} on the total synchronization of the network is clearly visible (Fig. 5.3(a)). With large values of g_{int}, the frequent and regular spiking activity of one area has significant effects on the spike timing of the other connected areas. The whole network exhibits strong synchronization even for relatively small g_{ext}. Fig. 5.2 illustrates the typical behavior in three regimes. We can observe some weakly synchronized activities among certain areas in Fig. 5.2(a), the slight increase in the amplitude of the spikes in the transient regime in Fig. 5.2(b) and the high spiking amplitude with some temporal interruption of the strong synchronization in some areas in Fig. 5.2(c).

The behavior of the system in the weak synchronization regime, i.e., the infrequent spiking of neurons and the irregular activity of the weakly synchronized brain areas, is biological plausible and comparable to normal brain activity. On the other hand, the regular spiking characteristically found in the strong synchronization regime, both in the dynamics of single neurons and brain areas, could correspond to pathological states such as epileptic seizure [70, 74].

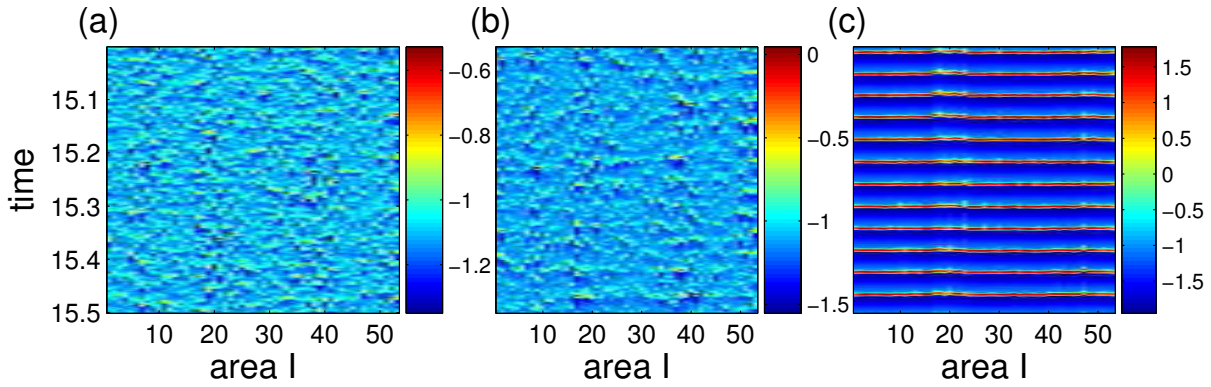

Figure 5.2: Spatio-temporal patterns of the mean activity $\bar{x}_I$ at different coupling strengths ($g_{int} = g_{ext}$): (a) $g_{int} = 0.06$ (b) $g_{int} = 0.082$ and (c) $g_{int} = 0.12$. Note the different scales in the colorbars.

Further, we focus on the correlation of the areas, R, at various coupling strengths. A plot of R as a function of the coupling strengths g_{int} and g_{ext} is shown in Fig. 5.3(a). We have averaged the results over 10 realizations of the initial conditions and the topology of the SW subnetworks for each set of the parameters. As already discussed, an increase of the coupling strengths g_{int} leads to stronger interaction of the neurons and to a rapid growth of their synchronous activity within and across areas for non-vanishing g_{ext} (Fig. 5.3(b)).

The correlation matrices $r(I,J)$ for the three regimes are shown in Fig. 5.4. Although the average levels of synchronization R are very different, the correlation patterns display some dynamical clusters, where a *dynamical (functional) cluster* is defined as a group of brain areas communicating much more strongly within this set than with the areas in the rest of the brain [122] (see also the definition of functional connectivity in Section 2.1). In the weak synchronization regime with the correlation $r \in [0, 0.1]$, four dynamical clusters are visible that resemble the underlying anatomical structure (Fig. 5.4(a)). The transient regime, correlations in the range $[0, 0.4]$, captures the reorganization of areas into three dynamical clusters. Figure 5.4(b) does not clearly show these three clusters, but such separation is later revealed by clustering analysis. Finally, in the strong synchronization regime with $r \in [0.6, 1.0]$, we can observe two dominant clusters (Fig. 5.4(c)). These clusters are also evidently present in the spatio-temporal patterns in Fig. 5.2(c).

The characterization of these dynamical clusters and their precise relation to the underlying anatomical communities was our main concern and will be presented in the next section.

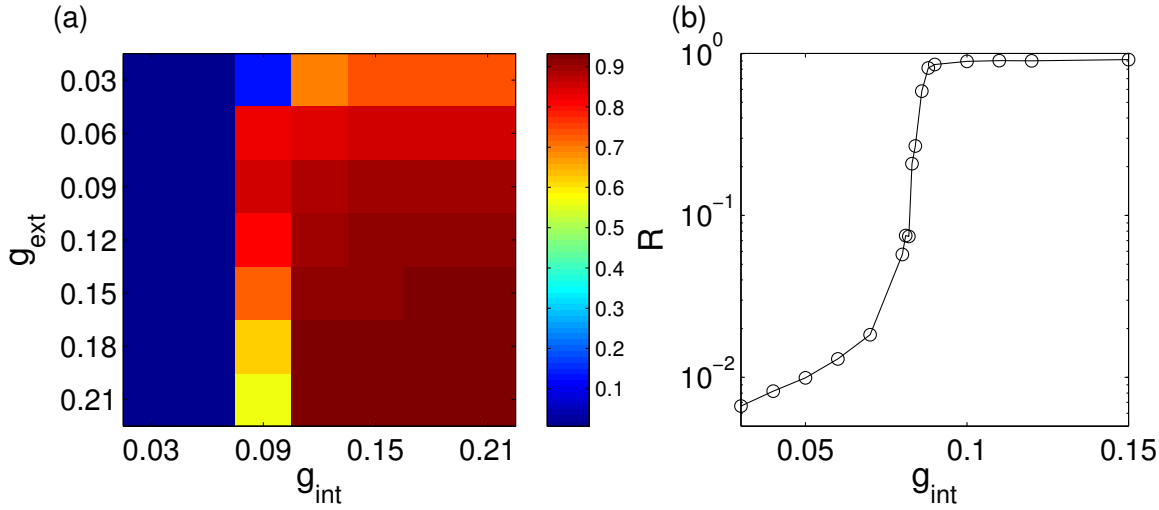

Figure 5.3: (a) Dependence of the average correlation coefficient R on the internal and external coupling strength g_{int} and g_{ext}. (b) The effect of the internal coupling strength g_{int} on the global correlation R (with fixed $g_{ext} = 0.06$).

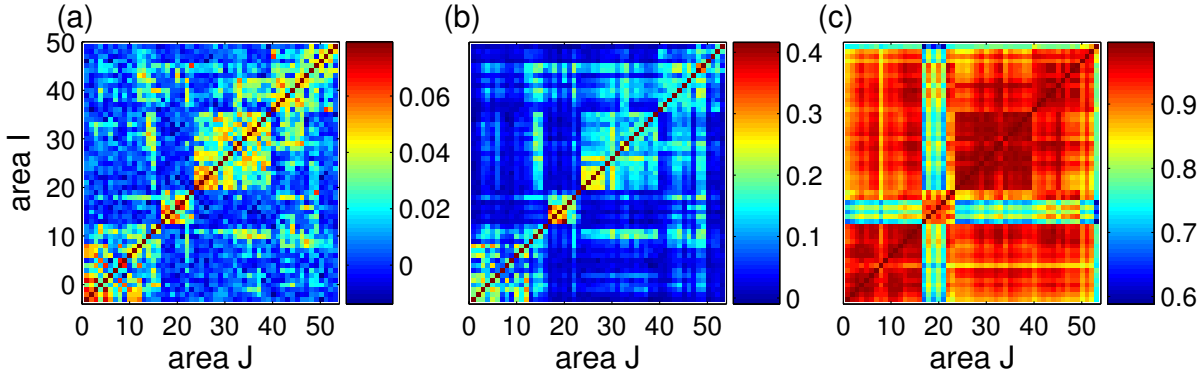

Figure 5.4: Correlation matrices $r(I,J)$ corresponding to the spatio-temporal patterns in Fig. 5.2. (a) $g_{int} = 0.06$, (b) $g_{int} = 0.082$ and (c) $g_{int} = 0.12$. In all cases $r(I,I) = 1.0$. Note also the different scales in the colorbars.

5.1.2 Revealing the network hierarchy

Visual inspection of the correlation matrix $r(I,J)$ shows a good match between the dynamical clusters in the weak synchronization regime and the underlying anatomical communities. Fig. 5.4(a) suggests that the dynamics of the present multilevel model has a nontrivial organization and an intriguing relationship with the network topology. To better characterize this relationship, let us now concentrate on the distribution of the correlation under four conditions. First, we are interested in the distribution of $r(I,J)$ among all pairs of areas: this exhibits a Gaussian peak around zero, but with a long tail toward large positive values. The significance of these large values is confirmed by comparison to correlation $r(I,J)$ of surrogate data obtained by random shuffling of the original time series $\bar{x}_I$. Further, based on the argument of the signal propagation, we distinguish three types of connections between any pair of areas in the network:

- reciprocal connections (P2)
- uni-directional connections (P1)
- non-connections (P0)

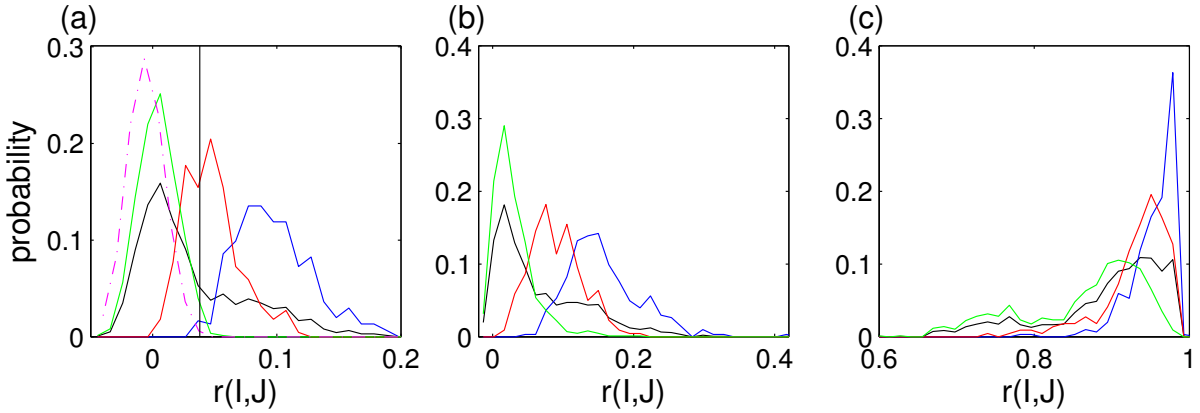

Figure 5.5: Distribution of the correlation $r(I,J)$ (a) $g = 0.07$, (b) $g = 0.082$ and (c) $g = 0.12$ for all nodes (black line), P2 (blue line), P1 (red line) and P0 (green line). The dashed-dotted line denotes the results for the surrogate data.

The distributions of $r(I,J)$ for these three cases display well-separated peaks in the weak coupling regime (Fig. 5.5(a)). The dynamics of the cortical areas connected by reciprocal anatomical links, P2, tends to be more strongly correlated than the dynamics of areas connected by one link, P1. Compared to the surrogate data, almost all the P2 pairs have significant correlations. With strong coupling (e.g., $g \geq 0.09$), the excitation propagates through the whole network and the separation of distributions of correlations is no longer so clearly pronounced (Fig. 5.5(c)). Generally, with increase of the reciprocity and the strength of the connection, we observe a shift of the peak of the distribution towards larger correlation values.

The weak coupling regime is biologically more realistic with a low frequency and irregular spiking behavior. Here, the propagation of the signal between connected areas is mediated by synchronized activities (peaks in $\bar{x}$). A temporal correlation is most likely established when the receivers produce similar synchronized activities by this input, or when two areas are excited by correlated signals from common neighbors. Due to the weak coupling and the existence of subnetworks, such a synchronized response does not always occur, thus a local signal (excitation) does not propagate through the whole network. As a result, the correlation patterns are closely related to the network topology, although the values are relatively small due to infrequent signal propagation. With strong coupling, the signal can propagate through the whole network strongly influencing also distant areas and leading to high correlation among areas, as corresponds to pathological situations, such as epileptic seizures [70].

5.1.2.1 Functional connectivity

To characterize the obtained dynamical networks, their topology and relation to the underlying anatomy, we use several graph theoretical measures described previously in Section 2.2. First, link reciprocity and its impact on the correlation of the activity between areas is considered. Figure 5.5 displays larger values of correlation between areas that are anatomically connected by reciprocal links. Furthermore, correlation is also expected to depend on the connection weights. We define the *reciprocal weight*, w_{IJ}, as the normalized sum of the link strengths between I and J. In Fig. 5.6(a), the pairwise w_{IJ} is shown for the anatomical connectivity matrix M^A.

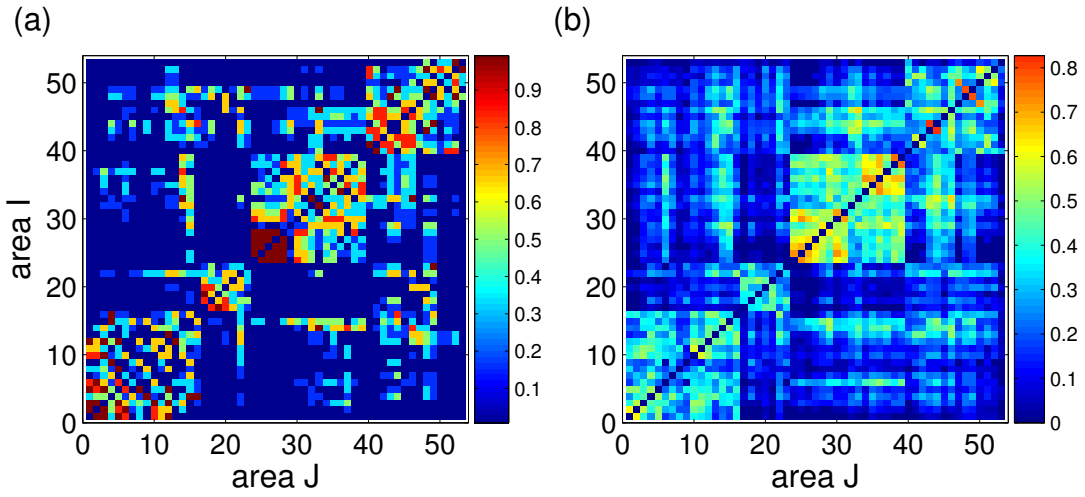

Figure 5.6: Properties of the anatomical network M^A: (a) reciprocal weight w_{IJ} of the anatomical links and (b) matching index MI of input neighbors.

However, pairwise connection weight alone does not completely explain the strength of correlation between two areas; the common environment of areas might also play an important role. The *matching index MI* quantifies the number of common neighbors between the nodes. For illustration, the MI matrix from the anatomical connectivity of cat cortex is presented in Fig. 5.6(b). As can be seen, the MI values of the areas within the anatomical communities V,

A, SM and FL are high (internal *MI*). On the contrary, the *MI* of areas in different communities (external *MI*) is heterogeneous, i.e., only some areas share many common neighbors with areas in other communities.

Our goal is to study how much the correlation between cortical areas depends on these measures. We extract *functional networks* M^F to analyze more closely the relationship between the anatomical topology and functional connectivity. The approach, commonly used in experimental studies working with a set of recorded brain data, consists of applying a threshold R_{th} to the correlation matrix $r(I,J)$ (see detailed description in Section 2.4 and [4, 38, 98, 117]). A pair of areas is considered to be functionally connected if the correlation between them is larger than the threshold :

$$M^F(I,J) = \begin{cases} 1 & \text{if } r(I,J) \geq R_{th}; \\ 0 & \text{otherwise.} \end{cases}$$

We compare these functional networks M^F at different R_{th} to the topological features of the anatomical network M^A and examine how the various levels of synchronization reveal different scales in the topology. We focus on the biologically meaningful weak coupling regime and take $g = 0.07$ as the typical case. (See Fig. 5.7 for several selected functional networks.)

In each M^F we consider *only* expressed areas and links. An area is expressed when it has at least one functional link to another area, i.e., their correlation is higher than the threshold R_{th}. We calculate the average $\langle w_{IJ} \rangle$ (Fig. 5.8(a)) and average *MI* of functional connections, distinguishing whether areas belong to the same community (Fig. 5.8(b), black line) or to different communities (red line).

Additionally, due to the sparseness of functional links at high R_{th} thresholds, functional networks are separated into several *connected components*, i.e., areas form groups that are internally connected, but disconnected between them. In Fig. 5.9, the number of connected components within each M^F is presented.

Now we proceed to discuss the organization properties of functional networks at different levels of synchronization.

1. When R_{th} is very close to the maximal value of the correlation matrix $r(I,J)$, only a few areas with P2 links within the auditory system A are functionally expressed, because of their strong anatomical links and sharing of many common neighbors. In Fig. 5.8(a), $\langle w_{IJ} \rangle = 1$ for the highest thresholds, meaning that these nodes are anatomically connected by strong bidirectional links. With lower values, e.g., $R_{th} = 0.07$ (Fig. 5.7(a)), about two-thirds of the areas are active but only 10% of the P2 links and none of the P1 links are present. This is manifested in high values of $\langle w_{IJ} \rangle$. Interestingly, all functional links correspond to anatomical connections within the communities V, A, SM, and FL, forming "core" functional subnetworks. However, M^F is distributed into several components (Fig. 5.9).

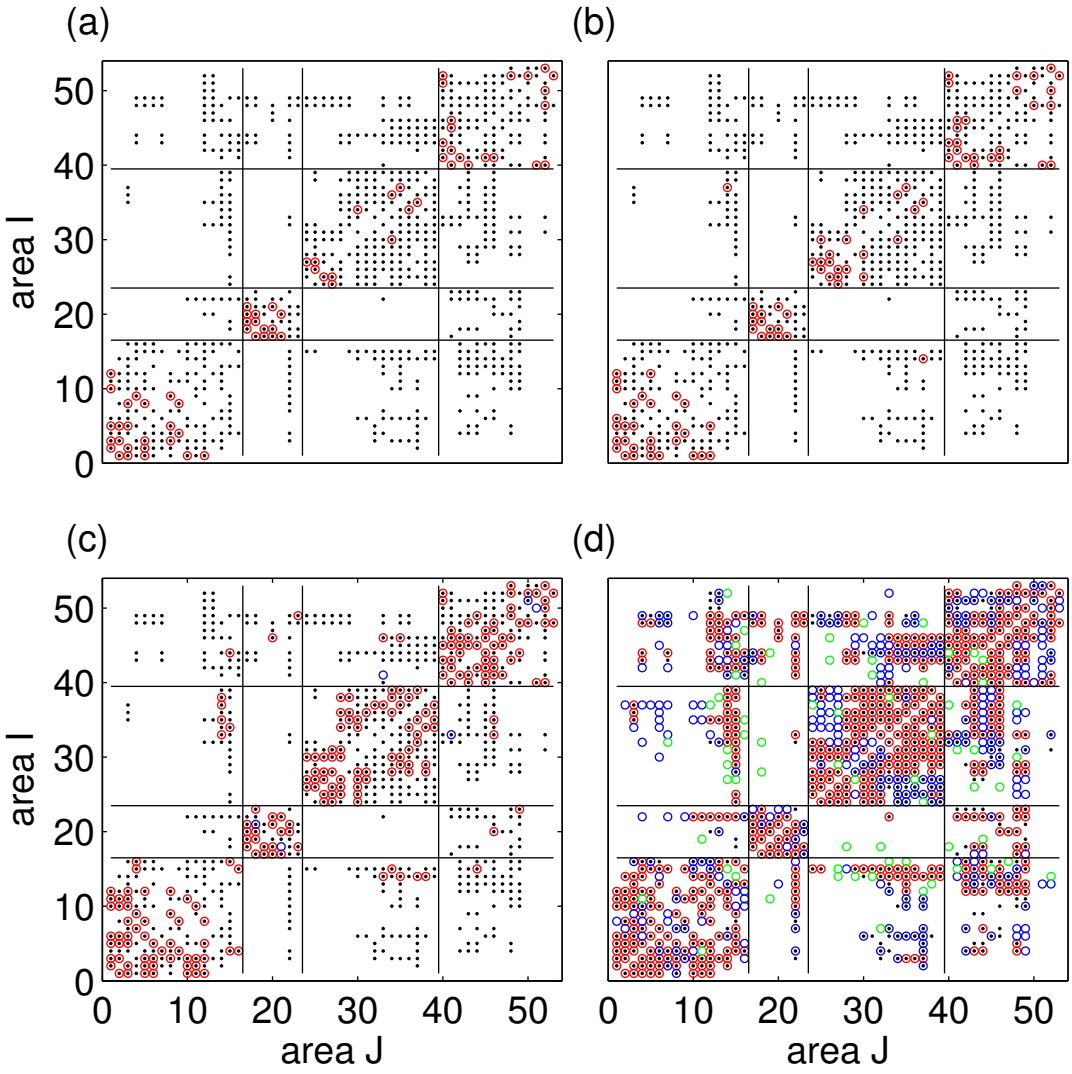

Figure 5.7: The functional networks at various thresholds for $g = 0.07$: (a) $R_{th} = 0.070$, (b) $R_{th} = 0.065$, (c) $R_{th} = 0.055$ and (d) $R_{th} = 0.019$. The red $\circ$ stand for P2 connections, blue ones for P1 and green ones for P0 links. The small black dots indicate the anatomical connections.

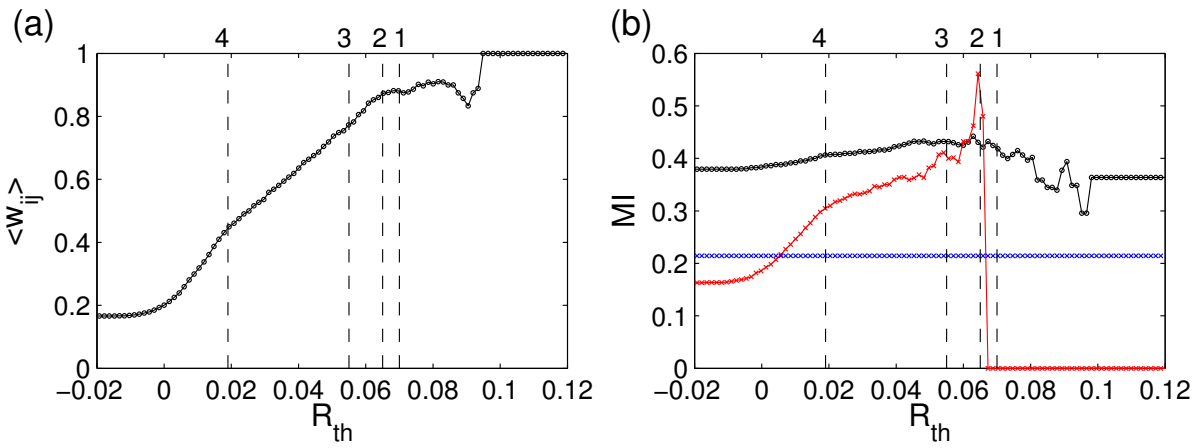

Figure 5.8: Properties of functional networks with various correlation thresholds. (a) Average reciprocal weight of links expressed in M^F. (b) Anatomical matching index of M^F. Black line: average MI of intracommunity links; red line: average MI of intercommunity links; and horizontal blue line: global average of MI matrix (in Fig. 5.6(b)). Vertical lines correspond to the four snapshots in Fig. 5.7: (1) $R_{th} = 0.070$, (2) $R_{th} = 0.065$, (3) $R_{th} = 0.055$ and (4) $R_{th} = 0.019$.

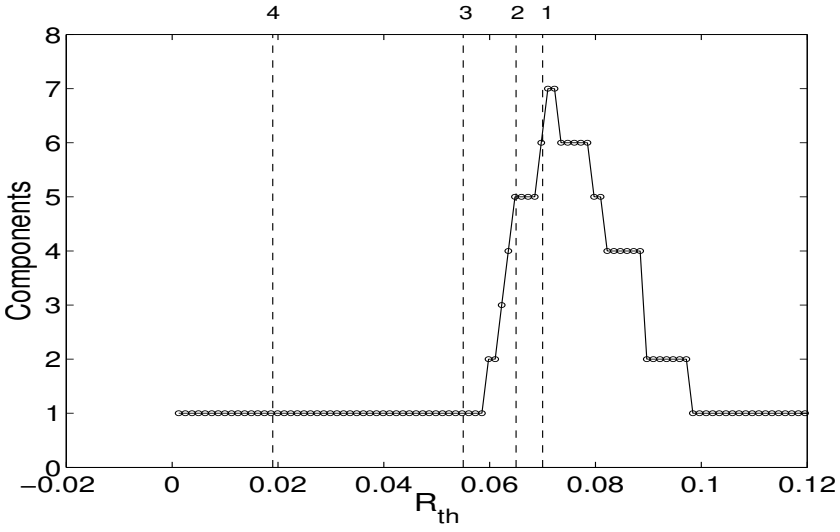

Figure 5.9: Number of connected components of M^F at various thresholds: (1) $R_{th} = 0.070$, (2) $R_{th} = 0.065$, (3) $R_{th} = 0.055$ and (4) $R_{th} = 0.019$.

2. At lower values, e.g., $R_{th} = 0.065$ (Fig. 5.7(b)), as more areas from the respective communities are expressed, the small components grow and merge. There are only five components closely following the anatomical communities. The small decrease of $\langle w_{IJ} \rangle$ shows that the new functional links still correspond to strong and bidirectional anatomical connections. The internal $\langle MI \rangle$ remains high (Fig. 5.8(b), black line), denoting that anatomical communities are densely connected. Here, the first intercommunity functional links are also expressed. Precisely, these links functionally connect the cortical areas that have many common neighbors belonging to different communities, as manifested by the peak in the external $\langle MI \rangle$ (Fig. 5.8(b), red line). In the core subnetwork the areas communicate more frequently within respective community. Such activity suggests a specialized function of this community.

3. Moving to a slightly lower threshold, e.g., $R_{th} = 0.055$ (Fig. 5.7(c)), a transition occurs in the organization of M^F. Even though, the majority of links occur within the anatomical communities V, A, SM and FL, a few intercommunity connections lead to the merging of all components into a single connected functional network (Fig. 5.9). In this way, communication between all the cortical areas is possible and determines the clustered structure of the functional network. At this stage, still only about one third of the anatomical P2 links and very few P1 links are expressed. With such a low connection density, M^F already reflects the main properties of M^A: high clustering and community structure, although the anatomical connectivity is much denser. This suggests high robustness and the existence of many parallel paths of information processing.

4. With additional reduction of the threshold, e.g., at $R_{th} = 0.019$ (Fig. 5.7(d)), all P2 links are just fully expressed and about 70% of P1 links too. Meanwhile, about 4% of nonconnected pairs (P0) establish significant functional connections (significance level ≈ 0.004), since they have many common neighbors. The functional network reflects rather faithfully the anatomical network (Fig. 5.7(d)). A further reduction of R_{th} is not very meaningful because too many insignificant correlations could be mistaken as functional connections.

Several cortical areas with the highest correlations have been observed to form the cores of the subsystems. When identifying these nodes, we realize that these areas are those known to perform the primary and highly specialized functional tasks. For example, areas 17 ($I = 1$) and 18 ($I = 2$) are the primary visual areas, processing visual stimuli to the higher visual centers (Fig. 5.7(a)). Later expressed areas, which are involved in the dynamics of two subsystems, e.g., area AES ($I = 15$) visible in Fig. 5.7(c), correspond to the areas where information from different sensory modalities converges [100]. We call them *bridging nodes* and they will be discussed in detail in Section 5.1.3.4.

Moreover, to compare the matrices M^F and M^A in a more quantitative manner, we take the binary matrix of M^A, symmetrize all P1 links and compute the *Hamming distance* H. The Hamming distance is a measure used to compare two networks, and equals to the number of different values in two adjacency matrices [30]; we use it to tell us the percentage of elements between M^F and the binary M^A that are different (see Eq. 5.5).

$$H(M^F, M^A) = \frac{1}{2N^2}\{N^2 - \sum_{i=1}^{N}\sum_{i=j}^{N}\delta(M^F(i,j), M^A(i,j))\}, \tag{5.5}$$

where δ is the Kronecker delta.

The distance between M^F and M^A is minimal when $R_{th} \approx 0.019$, with a very small Hamming distance $H = 0.074$ (Fig. 5.10). Interestingly, this threshold is exactly where the full distribution of R starts to deviate from the Gaussian and the distribution of P2 links separates from that of the surrogate data, at a significance level $\approx 0.4\%$ (Fig. 5.5(a), vertical solid line). We find that such a natural choice of R_{th} always reproduces the network topology well, and maintains a minimal H (≈ 0.06) for all coupling strengths $0.04 \leq g \leq 0.08$.

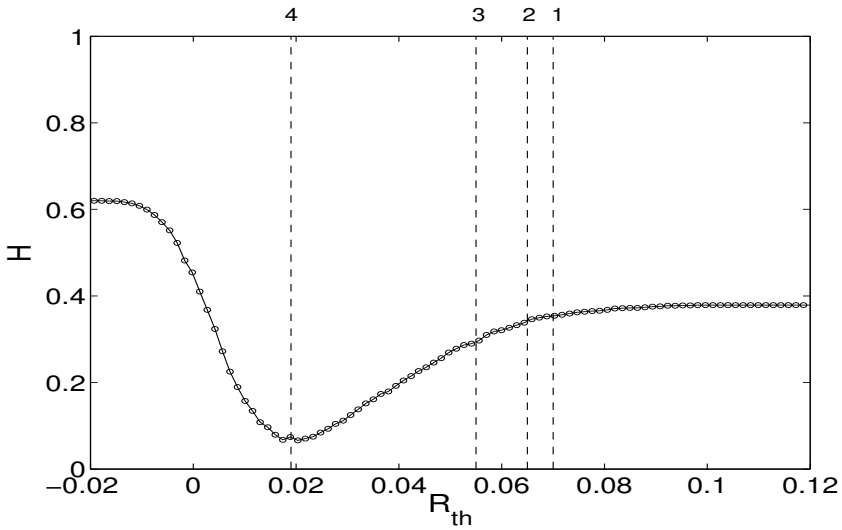

Figure 5.10: Hamming distance H between M^A and M^F vs. R_{th}. Vertical lines correspond to the four snapshots in Figure 5.7

In summary, we have observed that nodes connected by strong bidirectional links and having many common neighbors are highly correlated, and thus, they are the first to be expressed as functionally interacting. The strongest correlation occurs between nodes within the same anatomical community. Besides, the internal $\langle MI \rangle$ (Fig. 5.8(b), black line) remains stable over all R_{th}, and much higher than the global $\langle MI \rangle$ between all areas (Fig. 5.8(b), horizontal blue line). This confirms a high functional similarity between areas within the same community even when they are not anatomically connected. It also illustrates the capability of different communities (V, A, SM and FL) to perform specialized information processing. Generally, cortical areas belonging to different communities have a few common neighbors, as seen in Fig. 5.6(b). The fast decrease of external $\langle MI \rangle$ confirms this fact, as the number of functional links increases with decreasing R_{th} (Fig. 5.8(b), red line). However, the peak at $R_{th} \sim 0.06 - 0.07$ points out a transition in the dynamics. The change in the systems activity is triggered by a few intercommunity functional links between certain cortical areas in different communities,

but which have high functional similarity. All areas of the network merge into a single connected component. This potentially permits the integration of specialized information.

5.1.2.2 Detecting the network communities

As we have shown the complex network has a tendency to form clusters and we have revealed a hierarchy in its dynamical organization similar to the structural one. At different thresholds, various number of components, consisting of the areas having the dynamics in certain range, can be detected. Our next point is to find out the optimal number of communities into which areas should be separated, based on the similarity of their dynamics.

First, let us introduce the modularity measure which quantifies the diverse formations of communities and allows to choose optimal partitions. This measure was defined by Newman and Girvan [7, 85, 86] for the evaluation of community structure in complex networks. The modularity measure Q is defined as follows:

$$Q = \sum_k e_{kk} - a_k^2, \tag{5.6}$$

where e_{kk} is the fraction of all links in the network that connect the nodes within community k, and $a_k = \sum_l e_{kl}$ is the fraction of links from the whole network that connect to nodes in the community k. The value of $Q > 0$ indicates the presence of community structure, with the limiting case $Q = 1$ occurring when the division of elements into the communities is perfect.

To characterize the formation of functional clusters according to the anatomical communities, we consider the four communities ($k =$ V, A, SM, FL). The functional modularity Q^F based on the functional connectivity of M^F at various R_{th} is measured (Fig. 5.11, black line). Further, the modularity Q^4 based on the anatomical connectivity M^A (here we use the binary matrix) is also calculated as $Q^4 = 0.284$ (horizontal red line in Fig. 5.11). In a broad range of R_{th}, Q^F is much larger than Q^4, and they coincide at the natural threshold $R_{th} = 0.019$ (Fig. 5.11). This provides meaningful insights into how the densely connected cortical subsystems (e.g., communities V, A, SM, FL) can perform highly specialized functions (the strongest synchronization) by a subset of areas and connections.

The above analysis based on functional networks reveals that the most prominent clusters of the hierarchically organized network are consistent with the four known anatomical communities.

Next, we use the agglomerative method of hierarchical clustering [76] (the algorithm comes from the Statistics Toolbox in Matlab, version 7.0.1) and construct a typical hierarchical tree of the dynamical network (for the weak coupling regime, see Fig. 5.12(a)). The method is based on the grouping of objects into subsets (clusters) in a series of steps. In this case, the fusion of

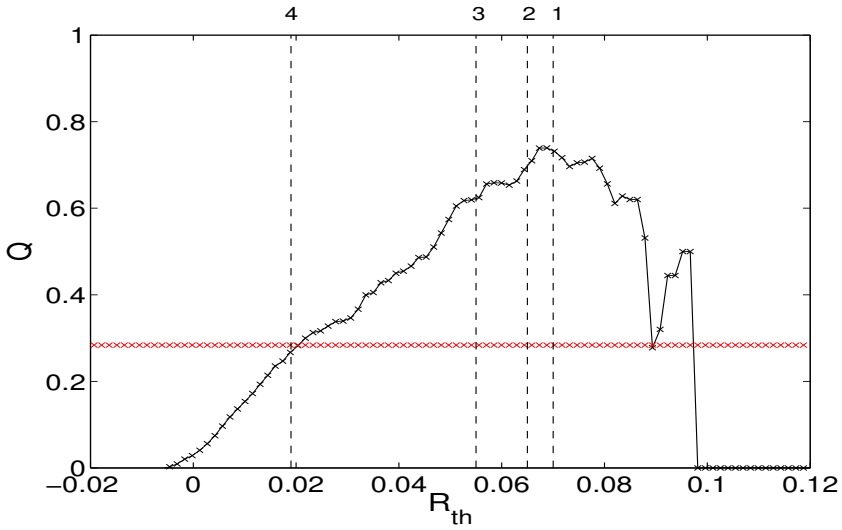

Figure 5.11: Modularity of anatomical network Q^4 (red line) and modularity Q^F (black line) of M^F considering the four subdivisions (V, A, SM, FL) vs. R_{th}. Vertical lines correspond to the four snapshots in Fig. 5.7

objects into clusters is determined by the similarity or distance between them. The procedure 'linkage' specifies how the distance should be evaluated.

Here, we calculate the dissimilarity matrix $d = [d(I,J) = 1 - r(I,J)]$ and apply 'average linkage', which defines the distance between the clusters as an average of distances between all pairs of objects coming from two groups. The segmentation of areas into the clusters was optimal, confirmed also by the control algorithm.

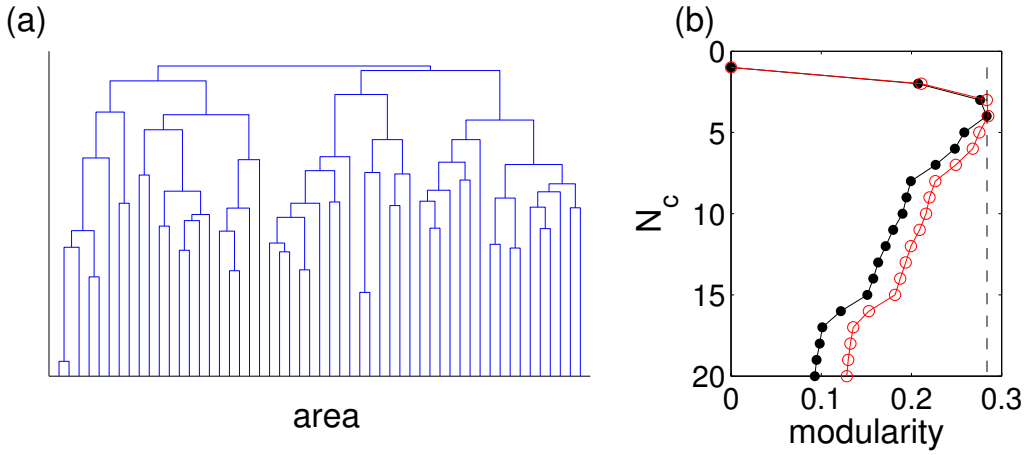

Figure 5.12: (a) The hierarchical tree of the dynamical clusters at $g = 0.07$. (b) Modularities Q^C (red ○) and Q^A (black ●) vs. the number of clusters N_c. The dashed line denotes Q^4.

At each level of the hierarchical tree, a set of N_c functional clusters is detected. The next intriguing question coming out is what are the underlying topological links within and across

Table 5.1: Overview of different types of modularity

.

modularity	using network	number of communities
Q^A	M^A	various
Q^C	$r(I,J)$	various
Q^F	M^F	4 anatomical
Q^4	binary M^A	4 anatomical

these dynamical clusters? We calculate both the anatomical modularity Q^A (using the anatomical matrix M^A) and the functional modularity Q^C (using the correlation matrix $r(I,J)$). In order to avoid thresholding the correlation matrix and to use all its values, we define Q^C as an extension of Q in Eq. 5.6:

$$e_{kl} = \sum_{I \neq J} r(I,J), \text{ where } I \in k, J \in l. \quad k,l = 1,\cdots,N_c. \tag{5.7}$$

Here e_{kl} is the fraction of the total strength of correlation between communities k and l. Strikingly, at different levels of the hierarchy (varying N_c), Q^C and Q^A follow each other closely (Fig. 5.12(b)). This proves that the dynamical organization reveals hierarchical scales in the network topology. At $N_c = 4$, both Q^C and Q^A are maximal, approaching Q^4 of the four communities in the anatomical network.

Table 5.1 summarizes the difference of Q^C and Q^A from Q^F and Q^4. Q^F and Q^4 are obtained for the *4 cortical subsystems V, A, SM, FL* using the particular extracted functional network M^F and the binarized anatomical matrix M^A, respectively. Q^C and Q^A are calculated for *various numbers of communities* in the dynamics of correlation matrix $r(I,J)$ and the original anatomical matrix M^A.

The behavior described above is common for coupling strength $g \leq 0.08$, although the average and maximal values of the correlation R increase with g. However, for $g \geq 0.084$ the system achieves strong local synchronization, and each area becomes significantly correlated with the rest of the network.

5.1.3 Clustered structure of functional networks

As we have already confirmed in the previous Section 5.1.2, the optimal number of clusters, coming out from the most natural division of the areas in the weak coupling regime, is four. In the original matrix of the cat cortical network, the anatomical connections create also four specific communities consistent with the functional subsystems V, A, SM and FL, see Section 3.1. Here, we will explore the distribution of areas into the dynamical clusters using cluster analysis and discuss how the resulting clusters correspond to the underlying anatomical communities.

To analyze the dynamical clusters we apply a hierarchical clustering algorithm, described in Section 5.1.2, to create a cluster tree. A typical hierarchy of the clusters (dendrogram) is shown in Fig. 5.13(a), (b) and (c) for three different types of synchronization regimes.

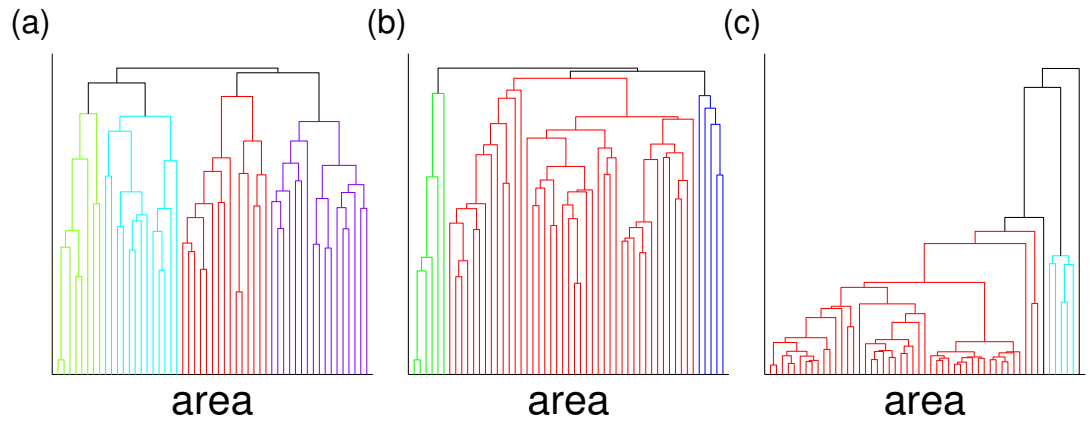

Figure 5.13: A typical hierarchical tree of the dynamical clusters in the weak coupling regime (a) $g = 0.07$, transient regime (b) $g = 0.082$ and strong coupling regime (c) $g = 0.12$.

In dendrograms, the distance between two objects (areas or clusters) is represented by the height of each line connecting two objects together. The higher the lines, the more distant the objects are, and so they are less likely to belong to the same group. With weak coupling, the nodes preserve their own dynamics without being influenced very much by other nodes, and the correlation is low and thus the distance between individual areas is relatively high (Fig. 5.13(a)). The highest levels of the hierarchical tree point out how the brain areas agglomerate to form the four main dynamical clusters. The different colors correspond to different clusters. By increasing the coupling strength, the activity of the areas is interrelated and becomes more correlated. Such behavior leads to the formation of one dominant and three small additional clusters (Fig. 5.13(b)). When the coupling is large, the mean activities of the majority of areas are strongly synchronized; this is also expressed by the short distance between the individual objects on the lower levels of the dendrogram. The areas merge into two clusters, but there are still several nodes preserving their own dynamics (Fig. 5.13(c)). The distance between the two main clusters is large because of different dynamics.

The hierarchical clustering algorithm does not directly indicate the optimal number of clusters into which the areas should be divided. To compare the anatomical and the correlation clusters, we concentrate on the level in the hierarchy of the cluster where the correlation matrix decomposes into the four clusters. Such a number of clusters corresponds to the natural division coming out from the modularity measure and the number of anatomical communities. At this level, the cluster formation in the weak, transient and the strong synchronization regimes is demonstrated and described. The details of the distribution of areas into the clusters in all these three cases of coupling strength are presented in Figs. 5.14, 5.16 and 5.18.

5.1.3.1 Weak synchronization regime

In the weak synchronization regime, neurons fire with low frequencies characterized by irregular spiking sequences and irregular mean activity as we have seen in Fig. 5.1(a). The integration of areas into the dynamical clusters due to the synchronization of areas closely resembles the pattern of communities obtained using the graph theoretical tools based on the anatomical structures, see Fig. 2.1 and [49, 50]. Typical dynamical clusters for the weak synchronization regimes are shown in Fig. 5.14. The four dynamical clusters C coincide with the functional subdivision

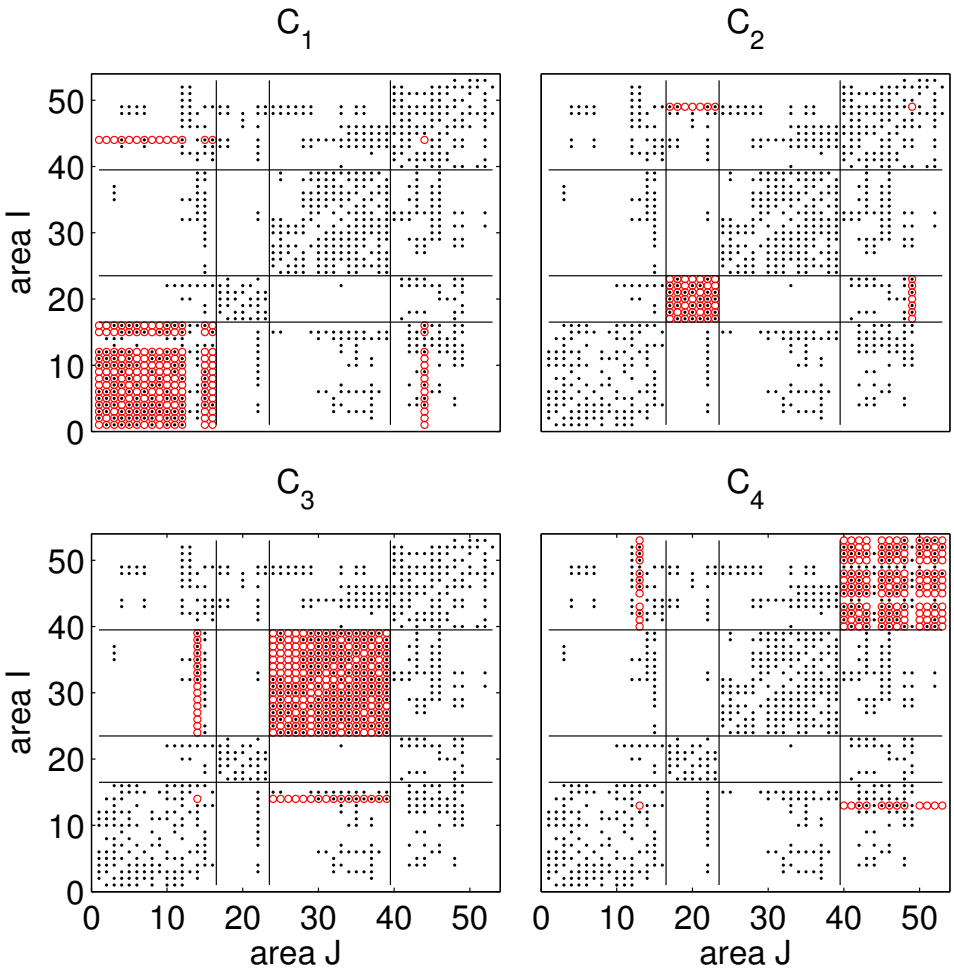

Figure 5.14: Dynamical clusters (red ○) with weak coupling strength $g = 0.07$, compared to the underlying anatomical connections (black ·).

(anatomical communities) of the cortex — C_1 (V), C_2 (A), C_3 (SM), C_4 (FL). However, it is also important to note that there are a few bridging nodes which belong to one anatomical community but join another dynamical cluster. For example, the area $I = 49$ (anatomically named as '36' in the cat cortex) coming from the fronto-limbic system appears in the dynamical cluster C_2, which is mainly composed of areas from the auditory system (Fig. 5.14 (C_2)). A closer inspection shows that these nodes bridging different anatomical communities and dynamical

clusters are exactly the areas sitting in one anatomical community but in close connectional association with the areas in other communities [100]. Detailed analysis of these bridging areas will follow later.

To measure in a more quantitative way the coincidence of the dynamical clusters and the anatomical communities, we examine each dynamical cluster and check which anatomical communities the areas come from. Additionally, we also investigate how the areas of a topological community are involved into different dynamical clusters. The distribution of the dynamical clusters into the anatomical communities and vice versa is summarized in Fig. 5.15. A dominant bar with a ratio ≈ 1 in the respective histograms points out the agreement between the dynamical clusters and topological communities. The presence of the small bars indicates the intercluster connections, the bridging nodes.

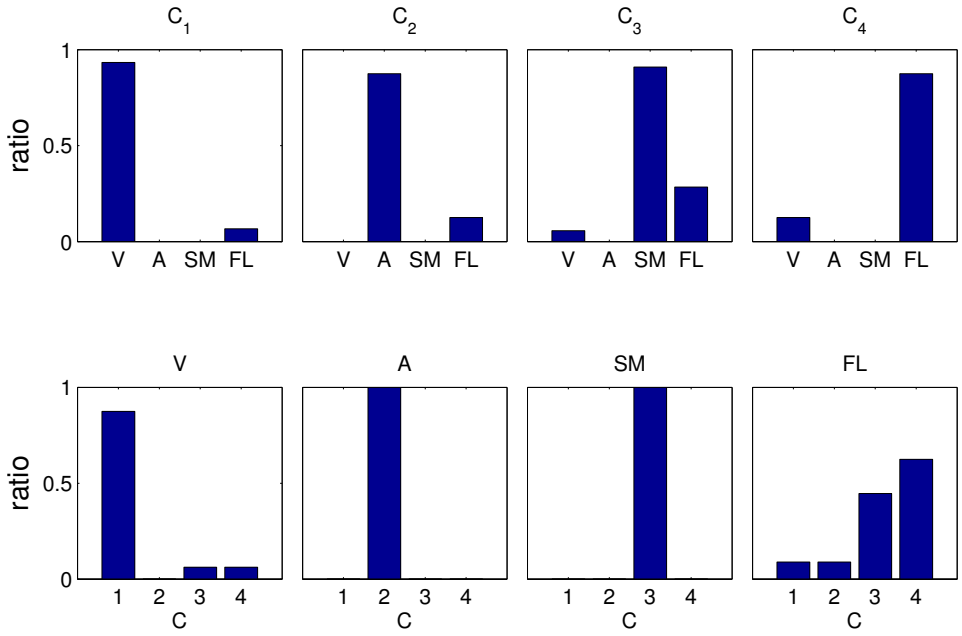

Figure 5.15: Upper panel: composition of dynamical clusters from different anatomical communities. Lower panel: participation of the areas of a community in different dynamical clusters. The results correspond to the clusters in Fig. 5.14 at $g = 0.07$.

.

5.1.3.2 Intermediate synchronization regime

The transient regime between the weak and strong couplings typical for $g \in (0.080 \pm 0.003)$ is characterized by the formation of one major cluster and three small clusters (Fig. 5.16). The major cluster C_3 consists of the somato-motor system and absorbs almost half of the areas from FL system and several areas from the V and A systems (Fig. 5.16 (C_3)). Remarkably, areas from V ($I = 13, 14$) are the same as the bridging nodes which connect at weak coupling the visual part to the other systems. The number of areas in the cluster C_4 is markedly reduced in

comparison to the size of the FL. Only the cluster C_2 corresponding to the auditory system A remains relatively independent, linked only through area $I = 22$ (Epp) to the central cluster C_3 (Fig. 5.16 (C_2)).

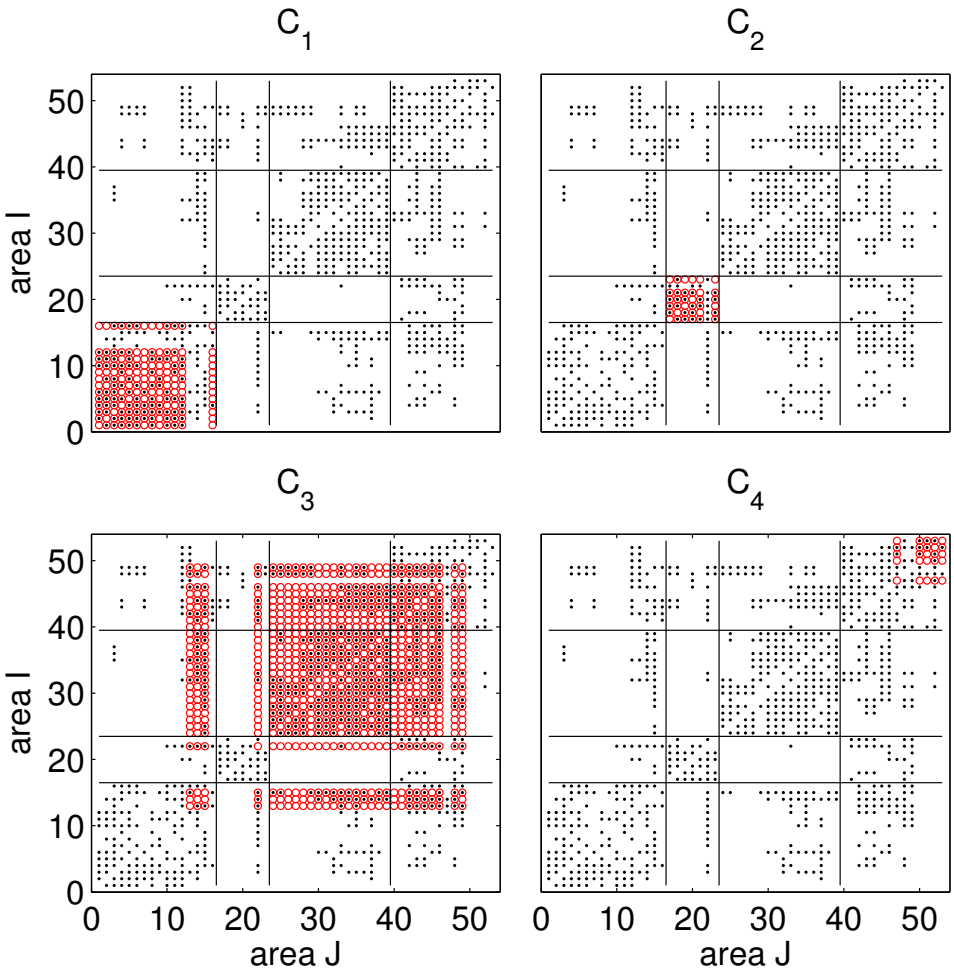

Figure 5.16: Dynamical clusters (red ∘) with intermediated coupling strength $g = 0.82$, compared to the underlying anatomical connections (black ·).

We evaluate again the correspondence of the dynamical clusters and the anatomical communities. These distributions (of the dynamical clusters in the anatomical communities and vice versa) are presented in Fig. 5.17.

The agreement between the dynamical clusters and topological communities is clearly seen by a dominant bar with a ratio ≈ 1 in the respective histograms. Clusters C_1, C_2 and C_4 are created each only by areas from one specific community. Only cluster C_3 contains areas from all communities and links them all together. Investigating the structure of C_3, community SM can be found exclusively here and thus somato-motor areas are dynamically joining the other three communities.

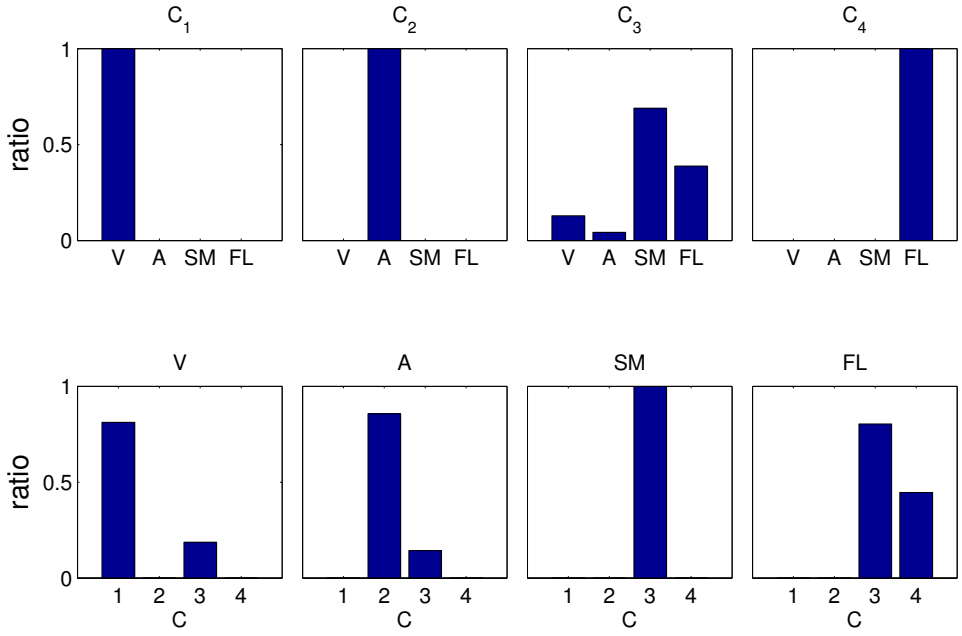

Figure 5.17: Upper panel: composition of dynamical clusters from different anatomical communities. Lower panel: participation of the areas of a community in different dynamical clusters. The results correspond to the clusters in Fig. 5.16 at $g = 0.082$.

5.1.3.3 Strong synchronization regime

In the third synchronization regime, typical for stronger internal coupling ($g \gtrsim 0.09$), the mean field signals of the areas exhibit regular spikes with high amplitude and frequency, which have a higher correlation between the areas. This type of clustering dynamics is mainly characterized by two dominant clusters that contain the majority of nodes and with a few single areas as separate clusters (Fig. 5.18). When the coupling strength g_{int} is increased (e.g., from 0.08 to 0.09), the three dynamical clusters corresponding to the major parts of the V, SM and FL communities as in Fig. 5.16 (C_1, C_3, C_4) merge to a single large cluster containing most of the nodes of the network (Fig. 5.18 (C_3)). The community SM plays a crucial role in the formation of this large dynamical cluster: by increasing the coupling strength, the C_3 cluster expands and absorbs large parts from the V and FL communities due to the strong intercommunity connections of the SM community with them (see also Fig. 5.19).

The auditory system A remains independent (Fig. 5.18 (C_2) and Fig. 5.19). The cluster formation behavior in the strong coupling regime is also in good agreement with the intercommunity connectivity summarized in Table 5.2. There are also two single areas showing themselves as independent clusters — area $I = 8$ from V system representing C_1 and area $I = 53$ from FL as the C_4 cluster. It turns out that these are the nodes with the minimal intensities in the network ($S_{53} = 8$ and $S_8 = 11$). For other parameter combinations, different areas may remain independent, e.g., $I = 1$ (17), 8 (VLS), 21 (VPc), 23 (Tem), 47 (RS) and 53 (Hipp). The dynamical independency of these several areas may arise from their specific biological origin. For example, the exclusion of the hippocampus, $I = 53$ (Hipp), from the dominant network dynamics can

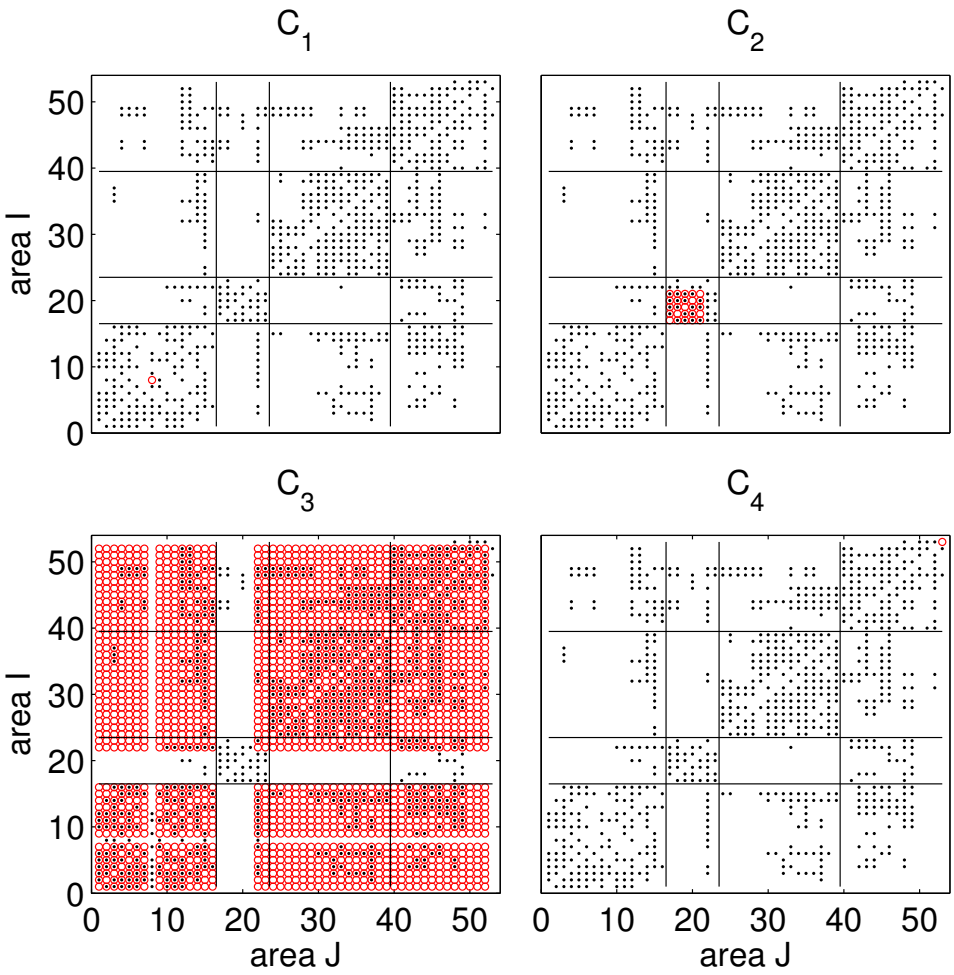

Figure 5.18: Dynamical clusters (red ∘) with strong coupling strength $g = 0.12$, compared to the underlying anatomical connections (black ·). C_1 and C_4 contain only a single node, $I = 8$ from V and $I = 53$ from FL.

be caused by its distance from the sensory periphery [100].

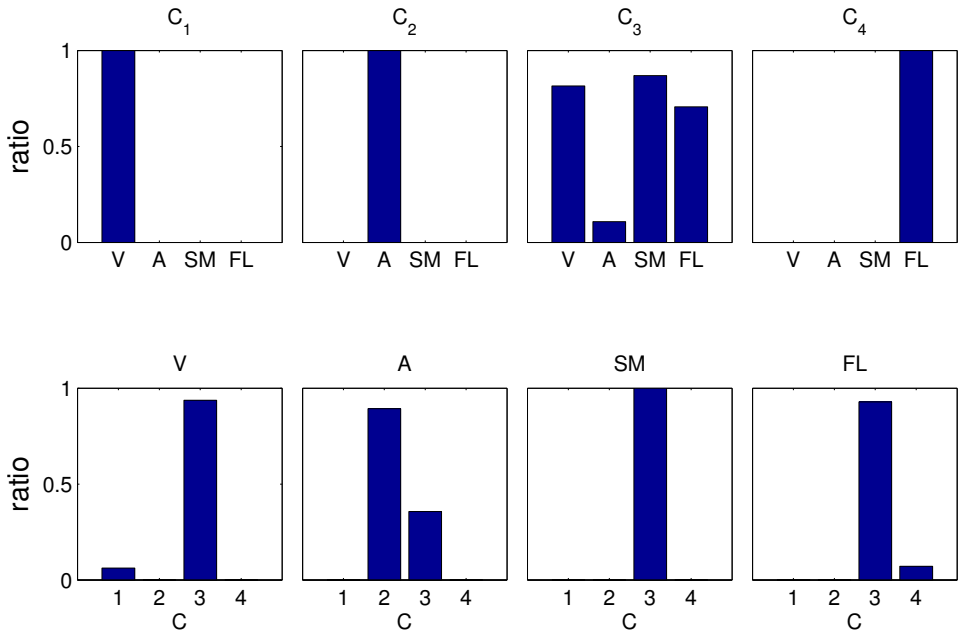

Figure 5.19: Upper panel: composition of dynamical clusters from different anatomical communities. Lower panel: participation of the areas in a community into different dynamical clusters. The results correspond to the clusters in Fig. 5.18 ($g = 0.12$).

We have found that variation of the internal and the external coupling strengths g_{int} and g_{ext} does not much affect the formation of the cluster C_2. The formation of this independent cluster, mainly composed of areas from the auditory system in the weak (Fig. 5.14), intermediate (Fig. 5.16), and the strong (Fig. 5.18) synchronization regimes, is due to strong (weight=2–3) and almost global internal connections within A and few intercommunity connections to other communities. Such connectivity provides a reason for the strong stability of this dynamical cluster in all synchronization regimes, irrespective of the coupling strength.

Later we will show that the clustering patterns from the strong synchronization regime remain almost the same in randomized networks. These randomized networks preserve the same size of the network and the incoming and outgoing intensities S_I of individual areas as in the cat cortical network. In these networks, the auditory system A no longer forms a distinct cluster when the pronounced intracommunity connections are destroyed in the randomized networks.

5.1.3.4 Presence of bridging nodes

As we have already mentioned (see Section 5.1.3.1), the dynamical clusters in the weak and transient synchronization regimes are characteristized by the presence of the bridging nodes. These nodes vary between different realizations and for different coupling strengths. For example, in the weak regime we can observe slightly different combinations of such bridging areas

Table 5.2: Input degree (intensity) of the areas in and among the four anatomical communities. E.g., the community V receives 51 connections from SM.

CM	V	A	SM	FL
V	140 (264)	11 (15)	51 (76)	53 (71)
A	11 (14)	34 (63)	1 (2)	27 (42)
SM	28 (38)	2 (2)	178 (340)	53 (67)
FL	45 (57)	20 (31)	54 (65)	118 (225)

like: $I = 12$ (20a), 13 (20b), 14 (7), 15 (AES), 16 (PS), 22 (EPp), 23 (Tem), 33 (6m), 43 (Ia), 44 (Ig), 46 (CGp) and 49 (36). Here we try to describe the nodes' structural properties by using graph theoretical measures, and point out their biological tasks and functions.

One of the basic characteristics of the nodes in the network is their degree k_i (number of connections) and intensity S_i (total strength of connections), previously introduced in Section 2.2. Not all connections in the cat matrix are reciprocal, so we can distinguish incoming and outgoing degree and the intensity of the node. Fig. 5.20 displays the information about the degree and intensity of the areas in the network of the cat cortex.

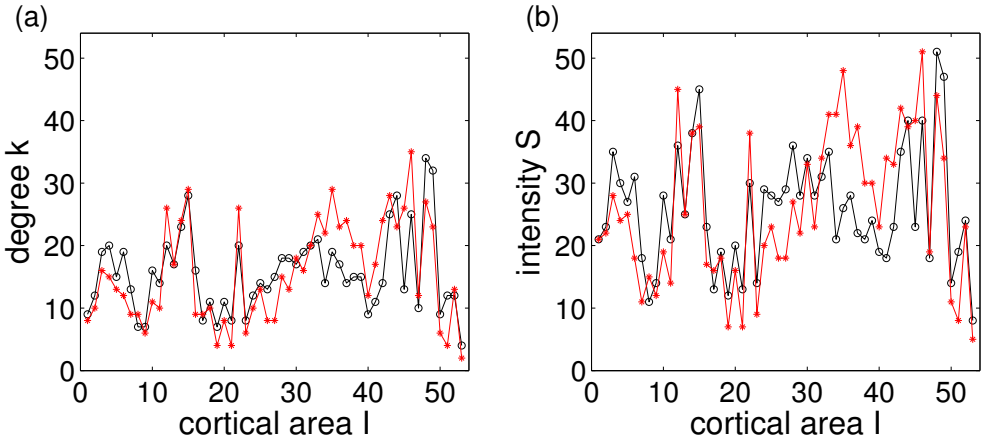

Figure 5.20: (a) degree and (b) intensity of areas of the cat cortex (incoming - black line, outgoing - red line)

Table 5.2 summarizes the overall connection degrees and intensities among the four anatomical communities. As is also clear from the table, the number of intracommunity connections (placed on the diagonal) confirms the dense communication within the community compared to weaker connections to the other communities (low nondiagonal values for intercommunity connections).

Coming back to the areas we have identified as bridging nodes, we concentrate on the incoming degree and the intensity of these areas from other areas within the respective communities

Table 5.3: Input degree (intensity) from the four communities (V, A, SM, FL) to the bridging nodes (identified across various parameters), which are in one topological community (CM) but in another dynamical cluster (CL).

area	(name)	CM(CL)	V	A	SM	FL
12	20a	V(C_4)	10(23)	1(2)	2(2)	7(9)
13	20b	V(C_4)	6(10)	1(2)	2(2)	8(11)
14	7	V($C_{3,4}$)	6(8)	1(2)	9(18)	7(10)
15	AES	V($C_{2,3}$)	9(16)	1(1)	12(20)	6(8)
16	PS	V(C_4)	10(15)	0(0)	0(0)	6(8)
22	EPp	A($C_{1,4}$)	7(10)	4(6)	1(2)	8(12)
23	Tem	A($C_{1,4}$)	0(0)	2(4)	0(0)	6(10)
43	Ia	FL(C_3)	5(5)	3(4)	9(10)	8(16)
44	Ig	FL(C_1)	6(9)	3(4)	12(14)	7(13)
46	CGp	FL($C_{2,3}$)	4(7)	2(4)	7(9)	11(19)
49	36	FL($C_{1,2}$)	8(10)	4(8)	9(9)	11(20)

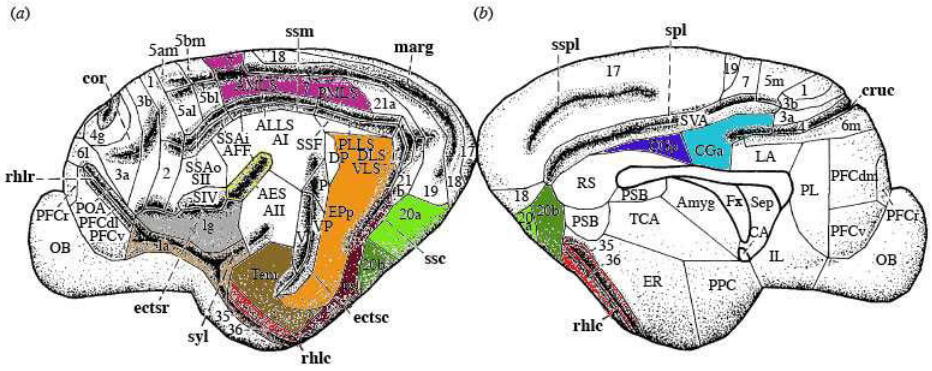

Figure 5.21: Cat cortex with colour marked bridging areas, corresponding to Table 5.4.

and from other communities (Table 5.3). Comparing to the global connection degrees (intensities) of the communities presented in Table 5.2, we can see that these few bridging nodes identified in our dynamical clustering analysis can form a significant part of the intercommunity connections. In particular, the the area $I = 14$ from the V community accounts for almost one fifth of the afferent connections from SM to V, and dynamically it joins the cluster C_3 in Fig 5.14.

Table 5.4 summarizes once again the most commonly appearing bridging areas, their location in the cortex, and the function with which they are associated. This list is in strikingly good agreement with all those special areas pointed out previously [100] that may play special multifunctional roles in information processing in the brain. Additionally, for a better overview of the crucial areas we have marked their position in the map of the cat cortex, see Fig. 5.21.

Our results suggest that, due to the role of the intercommunity association played by these nodes, they are acting as the bridge of communication among the functional communities. We

Table 5.4: List of the bridging nodes together with their location and functions with which they are involved.

name	area	location	function/involved in task
20a	12	temporal cx.	high level visual processing, recognition memory
20b	13	temporal cx.	static object vision, similar to 20a
7	14	parietal cx.	cells responsive to sensory stimuli visuomotor coordination
AES	15	ectosylvian g.	a region of multimodal cortex, sensitive to motion and visuospatial and other sensory stimuli
PS	16	suprasylvian area	visual system, related to limbic structures
EPp	22	ectosylvian g.	visual and auditory association area
Tem	23	tempor. aud. f.	higher auditory area
Ia	43	insular cx.	related to limbic cortex and to homeostatic function
Ig	44	insular cx.	response to visual stimuli and multimodal stimulation
CGa	45	cingulate cx.	central station for top-down and bottom-up processes
CGp	46	cingulate cx.	input from thalamus, hippocampus
35	47	perirhinal cx.	sensory information from all sensory regions
36	49	perirhinal cx.	important for memory, links to hippoc. and vis. areas

assume that the dynamics of these nodes integrates the dynamics of different anatomical communities.

5.1.3.5 Role of intensity in the network dynamics

We have seen that the connectivity of nodes within and between clusters plays an important role in the dynamics of the network. To better understand the different mechanisms of cluster formation in different synchronization regimes, we compare the cat cortical network with equivalent random networks. We generate random networks (M^R) using a rewiring algorithm proposed by Milo et al. [80]. The main idea is that the degrees and weights of the incoming connections of the cat cortical network M^C are preserved, but any other topological organization is destroyed. Specifically, two pairs of connected nodes are randomly selected, (x_1, y_1) and (x_2, y_2), and the connections are changed to (x_2, y_1) and (x_1, y_2) if such connections do not exist. This procedure is repeated until the network becomes random. We perform simulations of the dynamics using the randomized matrix M^R and analyze the clusters for the weak ($g_{int} = 0.06, g_{ext} = 0.12$) and strong ($g_{int} = 0.12, g_{ext} = 0.12$) synchronization regimes. The behavior of the mean activities of the subnetworks and the overall degree of synchronization are very similar to the original cat cortical network (compare Fig. 5.22 with Figs. 5.1 and 5.3), but the dynamical organization changes substantially, see Figs. 5.23 and 5.24.

As seen in Figs. 5.23 and 5.24, which show one typical realization of the random networks for both the weak and the strong synchronization regimes, we have one major cluster and several other clusters each containing only a few (1–3) nodes. In the strong synchronization regime

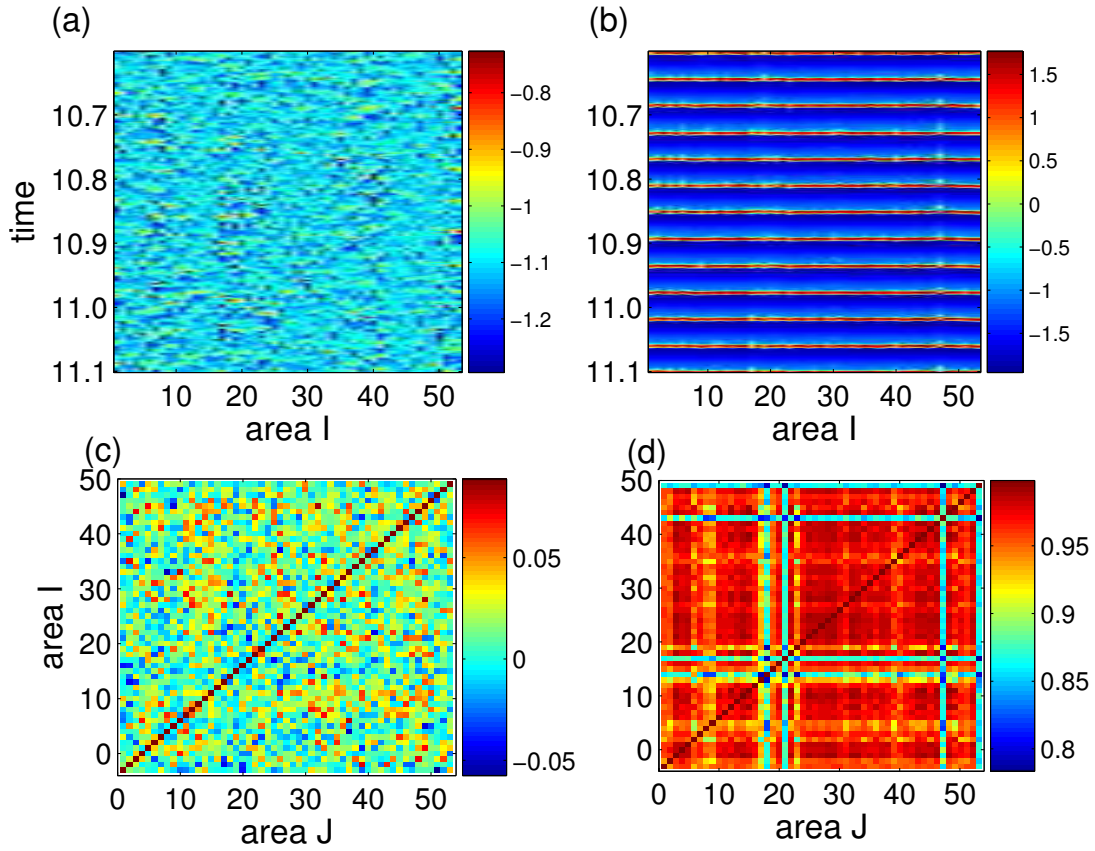

Figure 5.22: Spatio-temporal patterns of the mean activity $\bar{x}_I$ in random networks at different coupling strengths g_{int} keeping g_{ext} fixed at $g_{ext} = 0.12$: (a) $g_{int} = 0.06$ and (b) $g_{int} = 0.12$. The corresponding correlation patterns for the same parameters are shown in (c) and (d). Note the different scales in the colorbars.

the auditory cluster is destroyed (compare C_2 in Fig. 5.16 and Fig. 5.24); most of its areas join the major cluster, since these areas are no longer strongly connected among themselves. Nevertheless, the major cluster C_3 and the independent single nodes C_1 and C_4 in Fig. 5.16 remain largely unchanged in the random network (see Fig. 5.24). This suggests that the dynamical organization in the strong synchronization regime is mainly determined by the input degrees and intensities of the nodes, which are the same in the original and in the randomized networks.

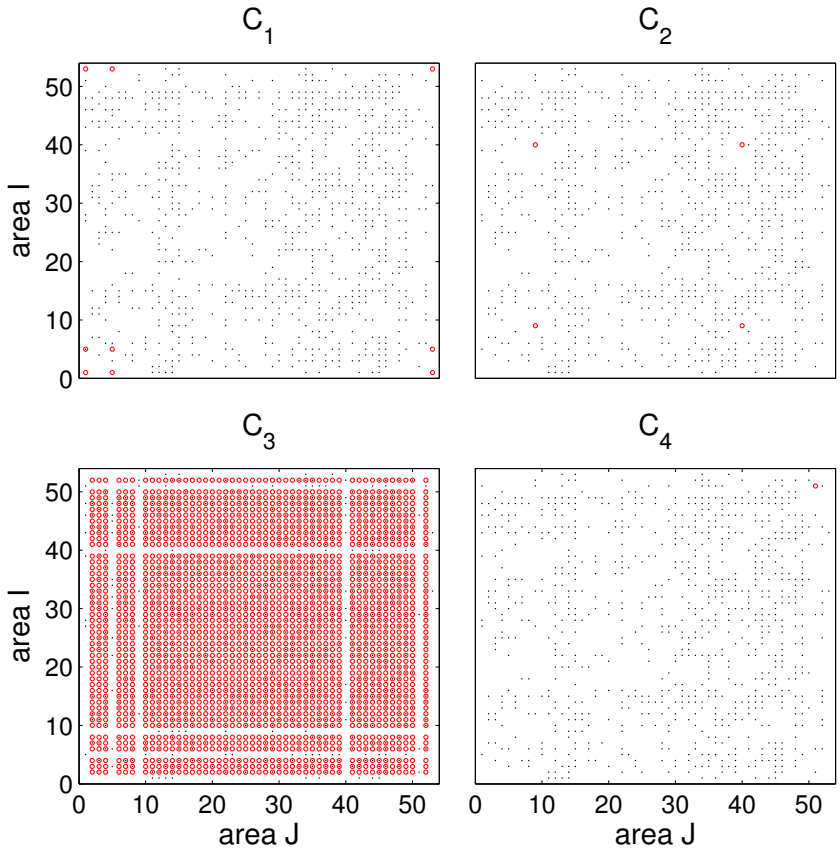

Figure 5.23: Dynamical clusters (red ∘) with weak internal coupling strength $g_{int} = 0.06$ ($g_{ext} = 0.12$), compared to the underlying random connections (black ·).

The next analysis concentrates on the strong synchronization regime, where the dependence of synchronization on the intensities is confirmed. First, we can assume the following dynamics for the mean activity of the subnetworks:

$$\dot{\bar{x}}_I = F(\bar{x}_I) + g_{\text{eff}} \sum_J^N M^R(I,J)(\bar{x}_J - \bar{x}_I), \tag{5.8}$$

where $F(\bar{x}_I)$ represents the complicated collective dynamics of the subnetworks and g_{eff} denotes the effective coupling between the mean activities, both depending on g_{int} and g_{ext}. According to some recent analysis on general weighted networks of oscillators [134, 136], when the network is sufficiently random, the input to a node I from its k_I neighbors is already close to the global mean field $X = (1/N)\sum_J^N \bar{x}_J$ if the degree k_I is large enough, namely, we can take

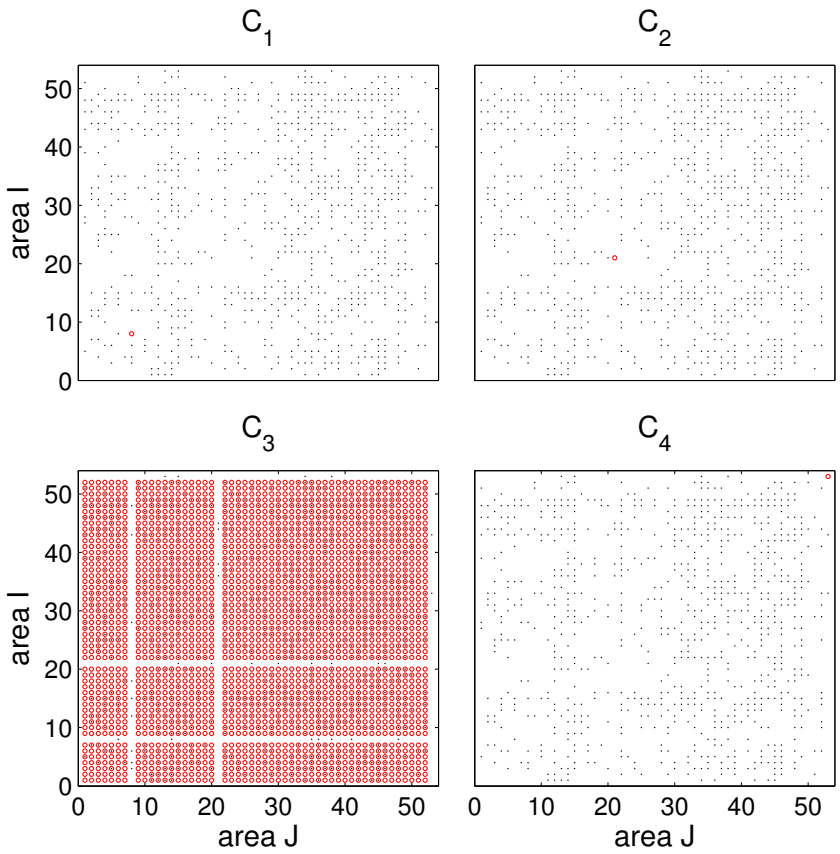

Figure 5.24: Dynamical clusters in the random network with strong internal coupling strength $g_{int} = 0.12$ ($g_{ext} = 0.12$).

$$\sum_J^N M^R(I,J)\bar{x}_J \approx \big[\sum_J^N M^R(I,J)\big]X \tag{5.9}$$

with intensity S_I as the sum of the total input weights to the node I

$$S_I = \sum_J^N M^R(I,J) \tag{5.10}$$

and get the following approximation

$$\dot{\bar{x}}_I = F(\bar{x}_I) + g_{\text{eff}} S_I (X - \bar{x}_I), \quad k_I \gg 1. \tag{5.11}$$

This first-order approximation in Eq. 5.11 means that nodes with large intensities S are more strongly coupled to the global mean field X and synchronize closer to it. The nodes usually synchronizing with X form an effective cluster, while the nodes with small intensities S are not significantly influenced by the activity of other nodes and preserve their own rather independent dynamics. A comparison of the intensities of the nodes in Fig. 5.20(b) with the clusters in Fig. 5.23 already provides some evidence for the above argument.

To prove the results of the theoretical analysis that with increasing intensity the activity of areas corresponds closer to mean field activity, we compute the correlation between the local mean field $\bar{x}_I$ and the global mean field X, denoted by $r_X(I)$, for each area I. A plot of r_X as a function of the intensity S is shown in Fig. 5.25. Hence several nodes have identical intensity,

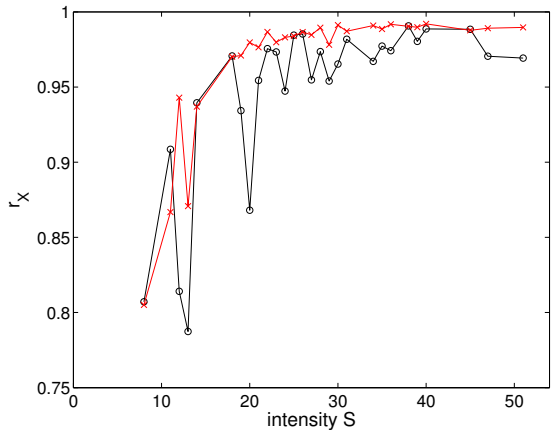

Figure 5.25: The correlation r_X between the local and global mean field, as a function of the intensity S of the nodes, for the randomized network (red line) and for the original cat network (black line).

we take the average value among nodes with the same intensity S. We can see that for the random network, r_X is an almost monotonously increasing function as we would expect from Eq. 5.11. An exception is node 19 (degree $k = 7$) with intensity $S = 11$ which connects to several neighbors with large intensities in this realization of the random network so that it has a larger r_X. From this, we conclude that the major cluster is composed of nodes with intensities S larger than some threshold S_{th}, because these nodes are dynamically close enough to the global

mean field X. Thus, we create a set of effective clusters C^S based on the incoming intensities S in the following way:

$$C^S(I,J) = \begin{cases} 1 & \text{if } S_I \geq S_{th} \text{ and } S_J \geq S_{th}; \\ 0 & \text{otherwise.} \end{cases} \tag{5.12}$$

A suitable value of the threshold S_{th} can be obtained by examining the correlation r_C between the matrix of the dynamical cluster C_3 in Fig. 5.24 and the matrix of the effective cluster C^S defined in Eq. 5.12. The relationship of this correlation coefficient r_C to the threshold value S_{th} is shown in Fig. 5.26(c). The matrix C^S corresponding to the maximal correlation r_C at $S_{th} = 12$ is shown in Fig. 5.26(b). We can see that it differs from the dynamical cluster (plotted again in Fig. 5.26(a)) only by a single area $I = 21$ in this realization of the random network. The area 21 has an intensity $S = 13$ just beyond the threshold S_{th} and the dynamics are marginal to the major cluster. The other two areas $I = 8$ and $I = 53$ having intensities smaller than the threshold S_{th} are considered to be independent clusters, which is also consistent with the observation directly from the dynamical pattern.

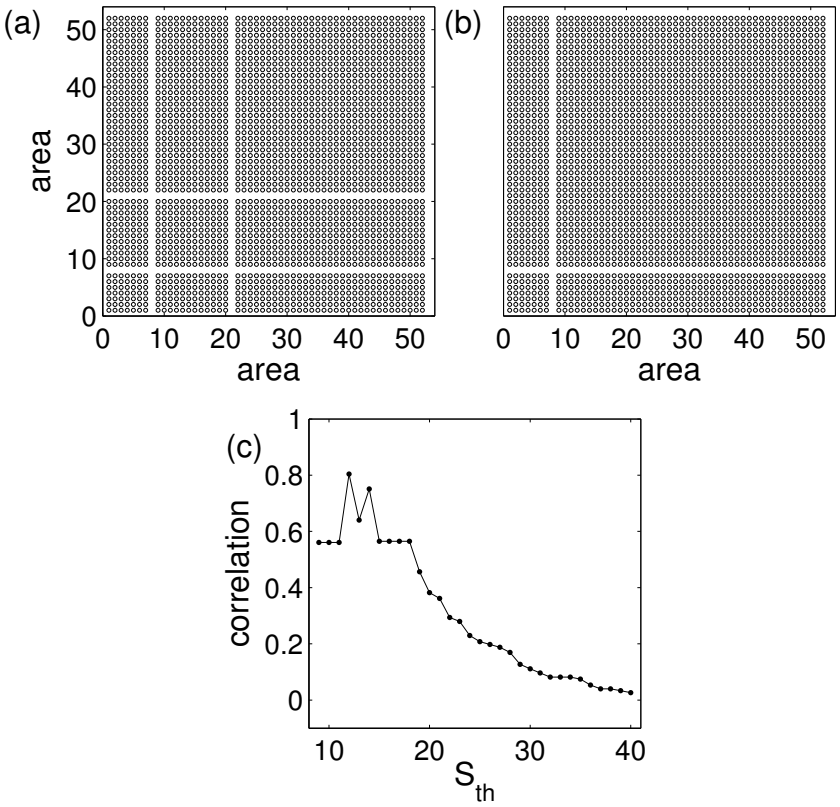

Figure 5.26: The relationship between dynamical clustering and node intensity in random networks. (a) Major dynamical cluster as in Fig. 5.24 (C_3). (b) Effective cluster C^S defined by Eq. (5.12) with the threshold $S_{th} = 12$. (c) The correlation r_C between the dynamical cluster in (a) and the effective cluster C^S, as a function of the threshold S_{th}.

Now we perform the same analysis for the original cat cortical network. The correlation r_X between the local mean field $\bar{x}_I$ and global mean field X displays a similar trend as the random networks (Fig. 5.25). The lowest correlation corresponds to the area $I = 53$ (Hippocampus) from the FL system with the minimal intensity $S = 8$. However, there are several areas with intermediate intensities $S \sim 12-13$ and $S \sim 20$, but with significantly lower correlation. These are the areas $I = 19, 17, 21, 20$ (AAF, AI, VPc, P) belonging to the auditory system which form another dynamical cluster (Fig. 5.16 (C_2)). The effective cluster C^S obtained by thresholding the intensities with the optimal value $S_{th} = 14$ is shown in Fig. 5.27(b). Apart from a few nodes ($I = 18, 20$) from the auditory system, the argument based on intensities also explains the major dynamical organization in the system.

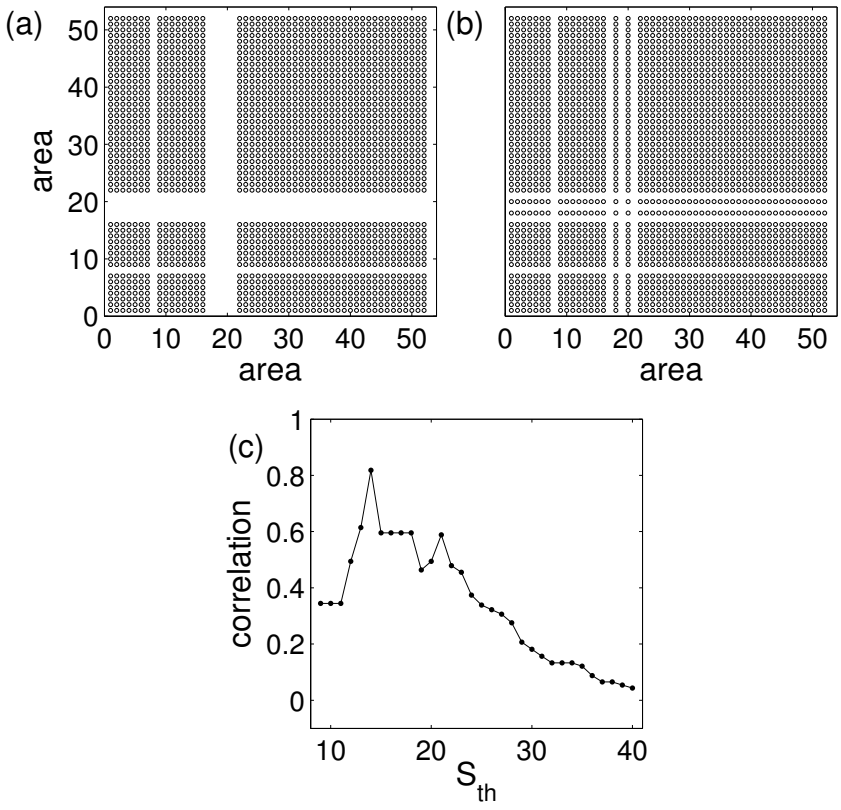

Figure 5.27: The relationship between dynamical clustering and node intensity in the original cat cortical network. (a) Major dynamical cluster as in Fig. 5.18 (C_3). (b) Effective cluster C^S defined by Eq. 5.12 with the threshold $S_{th} = 14$. (c) The correlation r_C between the dynamical cluster in (a) and the effective cluster C^S, as a function of the threshold S_{th}.

The above comparison shows that when the coupling is large and synchronization is strong, the organization of the systems into topological communities may not reveal dynamical specialization. The communities having significant intercommunity interactions (V, SF and ML) merge to form a single cluster, see also Table 5.2. The nodes having low connectivity to the rest of the network stay relatively independent, and the dynamical organization is mainly controlled by the intensities, regardless of the network topology.

5.2 Network of ML neurons with chemical coupling

5.2.1 General dynamics of network of coupled ML neurons

The previous model of the network of coupled FHN neurons has unveiled a hierarchical topology of the functional networks. For various dynamical regimes, different mechanisms of dynamical clustering were detected and described. However, the FHN neuronal model has class 1 excitability and such models do not show high sensitivity to external inputs. A sensitive coding of the synaptical input to the neuronal firing activity is one of the main tasks of neurons. Thus, in the second study, we have selected a model neuron of class 2 excitability: the Morris-Lecar model. Similar to the case of the FHN model in the global network 4.1.1.1, the membrane potential V is predeterminantly modeled by a particular function f_{ML}, see Eq. 4.5. This basic potential of a single neuron is modulated by the input from the local network — the neighboring neurons (coupling represented by M^L) and the input from remote neurons from the other cortical areas (coupling represented by M^C). Here, areas do not communicate through their mean field activity but through the individual activity of neurons involved in inter-areal communication (marked in the matrix L). The entire network contains only chemical synapses. The noise ξ stimulating the spontaneous activity of the neuron is added to the voltage variable V. A function h_{ML}, see Eq. 4.6, depicts the dynamics of the slow variable W. The dynamics of the model is described by:

$$\begin{aligned} C\dot{V}_{I,i} &= f_{ML}(V_{I,i},W_{I,i}) + D\xi_{I,i}(t) - \frac{g_{I,i,I,j}}{k_a}\sum_{j}^{n} M_I^L(i,j) r_{I,j}(V_{I,i}-E_s) \\ &\quad - \frac{g_{I,i,J,j}}{k_a\langle S_{in}\rangle p_{ext}}\sum_{J}^{N} M^C(I,J) L_{I,J}(i,j) r_{J,j}(V_{I,i}-E_s), \qquad (5.13) \\ \dot{W}_{I,i} &= h_{ML}(V_{I,i},W_{I,i}). \qquad (5.14) \end{aligned}$$

We fix the small-world subnetworks to have the following properties: the number of neurons $n = 200$, the number of neighboring links $k_a = n * 0.1$ and the probability of rewiring $p_{rew} = 0.3$. Such network properties allow us to keep the simulation time reasonable and also to compare the network of ML neurons with the previously simulated system of FHN neurons. Each neuron is in the excitable state, with $I_i < I_c$ and $I_i \in (37.0, 38.0)$. Additionally, neurons receive Gaussian noise ξ. The coupling between local neurons, connected according M^L matrix, is scaled by the average number of intra-areal connections k_a. In the case of long-range connections (L matrix), the synaptic coupling is averaged over the total number of neurons from the distant area sending signals to the specific neuron, i.e., $k_a\langle S_{in}\rangle p_{ext}$. $\langle S_{in}\rangle = 26$ is the average input intensity to all cortical areas and p_{ext} expresses the proportion of neurons from a single area involved in long-range communication, here $p_{ext} = 0.05$ [131]. The parameter E_S stands for the resting potential of the neuron and its value determines the type of synapses (0 mV for excitatory and -80 mV for inhibitory synapse, see Table 4.2).

We have simulated this system of Eqs. 5.13 and 5.14, the network of networks of ML neurons, up to time $t = 30$ s, and the first three seconds were ignored to remove the effects of

transients. The first order Euler algorithm was used during numerical integration, with a time step $\Delta t = 0.1$ ms. The model is coded in the Fortran 90 programming language. A simulation of 1 second of the neural activity of the whole model takes approximately 30 minutes on average on a Pentium 4 desktop PC.

Parameter study

We are interested in the specification of the strength of the different types of synapses whose variations allows us to investigate dynamics in various regimes. Generally, due to the smaller number of inhibitory neurons (and thus inhibitory synapses), these connections are usually stronger than the excitatory ones. Thus, we assume different coupling strengths for the excitatory ($g_{1,exc}$) and inhibitory ($g_{1,inh}$) synapses within a cortical area. The modification of $g_{1,exc}$ and $g_{1,inh}$ balances the excitatory and inhibitory inputs to the neurons within a single cortical area and achieves the 'natural' firing frequency of neurons in the range of 1–3 Hz (see Section 4.1.2 and [44, 56, 70]). To exclude the dependence of the neuron firing rate on the network size, we additionally normalize the coupling strength by the number of connections per area (k_a). In the work of Barbosa et al. [10], a description of an efficient search for the optimal coupling parameters was presented. We have followed this procedure, implementing it in three steps; the basic settings are done for a single SW network of 200 neurons and averaged over 10 different realizations of the network topology and initial conditions.

- Noise level

  As we have mentioned previously (Section 4.1.2), neurons in their natural state without the presence of an external input do not fire very frequently. Taking into account their 'resting' frequency, we stimulate them with Gaussian noise of different intensities D added to the fast variable V (Eq. 4.5) of each neuron. This is done for all 200 uncoupled neurons and we calculate their average frequency at specific a D (Fig. 5.28 (a)). Finally, the intensity $D = 4.9$ was selected, where the average frequency of firing is $f_{aver} = 2.5$ Hz; see also the individual frequencies of the neurons in Fig. 5.28(b).

- Strength of the excitatory connections

  After the neuronal background activity has been set to 2.5 Hz, we change the strength of the excitatory connections between neurons, $g_{1,exc}$. The inhibitory connections are neglected since $g_{1,inh} = 0$. As one would expect, the stronger the excitation $g_{1,exc}$, the higher the frequency of firing is. Neurons are mutually excited through their connections and due to the presence of the shortcuts in the SW structure the signal quickly spreads through the whole network. Fig. 5.29(a) shows the increase of the average frequency of neuronal firing with an increase of the coupling strength. For further simulations we select $g_{1,exc} = 0.9$, where slow saturation of the frequency starts, i.e., the speed of the signal transmission is almost maximal.

- Strength of the inhibitory connections

  As the last step, we activate inhibitory connections in the network. The 'natural firing frequency' of a neuron is the result of the balanced excitatory and inhibitory strengths affecting it. The inhibitory synapses compensate the excitation of the network and decrease the average frequency of neurons (Fig. 5.29(b)). We fix the inhibitory strength to be $g_{1,inh} = 1.8$, where the frequency of firing reaches approximately 3 Hz.

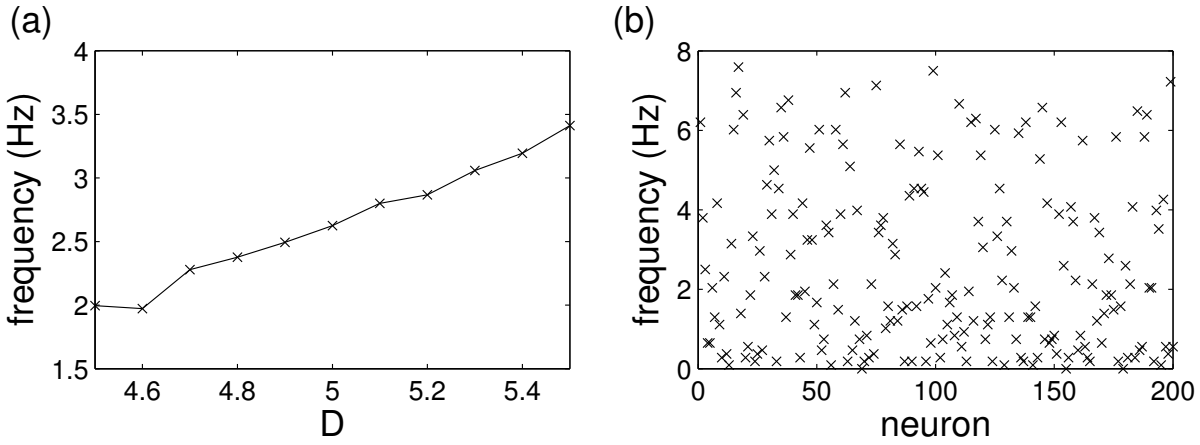

Figure 5.28: Dependence of the frequency of firing of neurons on the background noise (for a set of 200 neurons, averaged for 10 realizations with different initial conditions). (a) D is varied, $g_{1,exc} = g_{1,inh} = 0$, (b) frequency of the individual neurons at $D = 4.9$ for one realization; the difference is due to heterogeneity in the excitability.

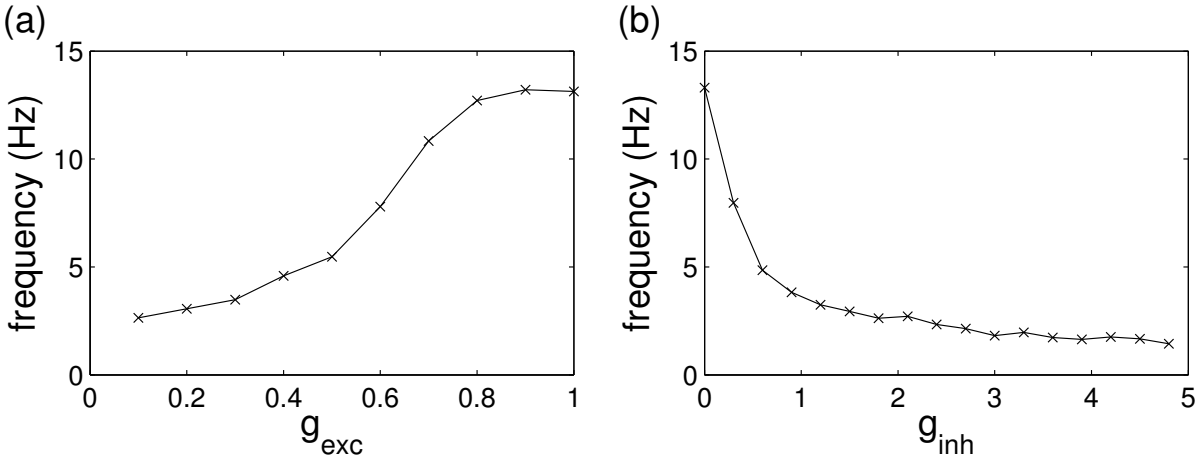

Figure 5.29: Dependence of the frequency of firing of neurons on the external input (for a set of 200 neurons). (a) $D = 4.9$, $g_{1,exc}$ is varied, $g_{1,inh} = 0$, (b) $D = 4.9$, $g_{1,exc} = 0.9$, $g_{1,inh}$ is varied.

Finally, we obtain parameters so that the local network of 200 neurons exhibits a natural frequency of firing. These parameters are: $D = 4.9$, $g_{1,exc} = 0.9$, $g_{1,inh} = 1.8$. Then, we simulate the whole network of 53 connected areas. The inter-areal connections are excitatory in character. We keep their value the same as for the local excitation within an area, i.e., $g_{1,exc} = g_{2,exc}$. The only difference is in the normalization of the coupling strength $g_{2,exc}$ of the inter-areal connections, as described previously. In the next parts we will distinguish only excitatory and inhibitory strengths and refer to them as g_{exc} and g_{inh}.

In comparison to the large-scale network of FHN neurons, here the situation is different. The internal dynamics of the areas are driven by both parameters g_{exc} and g_{inh}, whereas the interconnections are only excitatory. Thus, inhibitory coupling affects the dynamics of the system only at the local level. Starting with the coupling strengths $g_{exc} = 0.9$ and $g_{inh} = 1.8$ typical for the frequency of approximately 3 Hz for a single area, we coupled also areas with the $g_{exc} = 0.9$. The presence of inputs from other areas increases the average firing frequency of the areas and of the whole system to approximately 9 Hz. In the following section, the regimes of various frequencies, both higher and lower, obtained for couplings $g_{exc} \in (0.4 - 0.9)$ and $g_{inh} \in (1.8 - 4.8)$, are explored.

Here, we present three different regimes of the system dynamics. In the first regime of weak synchronization at $g_{exc} = 0.5$, the presence of the noise and the relatively strong value of inhibitory coupling ($g_{inh} = 3.8$) determine the neuronal dynamics. The excitatory couplings, internal and external, are not sufficient to stimulate a frequent firing activity of neurons; the neurons fire irregularly with some occasional spikes. The mean field signal of a single area $\bar{V}$ is relatively flat with small deviations from the baseline (Fig. 5.30(a)). Again, the mean field signal can be considered as an analogy of the EEG signal during resting state [87]. With $g_{exc} = 0.6$ and $g_{inh} = 1.8$, the mutual excitation of the neurons is stronger than the local inhibition. In this transient regime the global dynamics are not much suppressed and the mean field signal differs moderately from the signal occuring with weak excitatory coupling (Fig. 5.30(b)). Approaching a high value of $g_{exc} = 0.9$, with $g_{inh} = 3.8$, the incoming excitation from other areas enhances the activity of the whole neuronal ensemble. Several neurons, excited already by strong internal coupling, receive external signal and the SW topology allows a fast spreading of the positive activity across the subnetwork. All neurons fire more frequently with regular spiking behavior and the average mean field signal of a single area exhibits numerous prominent spikes (Fig. 5.30(c)).

The various dynamical regimes are also clearly present in the spatio-temporal patterns in Fig. 5.31. In the weak synchronization regime, the dynamics of the individual areas do not exhibit prominent peaks, the signals oscillate around $V = -34$ mV and most of the areas display similar behavior. In the transient regime (Fig. 5.31(b)), a few areas are more active, with a slightly higher average mean field signal. Strong excitation at $g_{exc} = 0.9$ leads to clearly visible oscillations of the mean field dynamics of all areas. The presence of the dynamical clusters is here not so visible (Fig. 5.31(c)).

We conclude that the global dynamics are under significant influence of excitation and inhibition. It seems that the dynamics of the subnetworks are more sensitive to the fragile balance between excitation and inhibition than to the strength of the global and local synaptic inputs. Changes to excitation can be compensated by changes in inhibition, but small deviations from

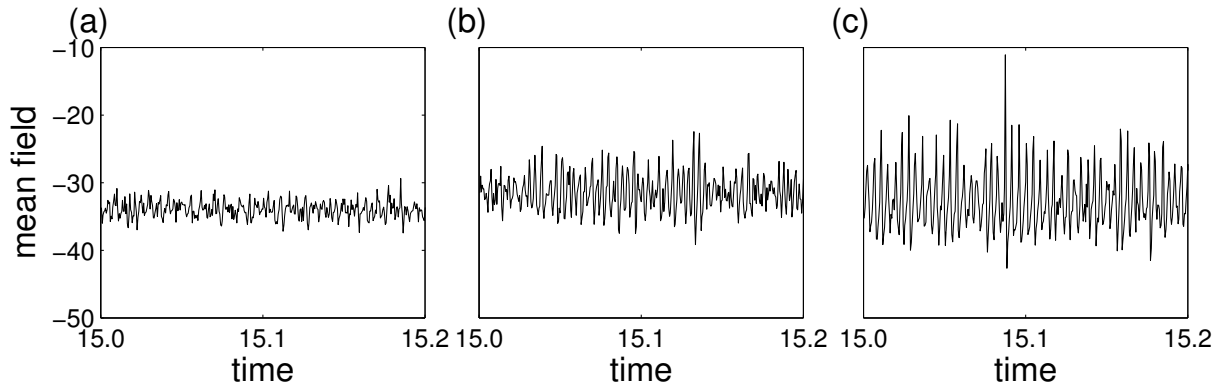

Figure 5.30: Typical time series of the mean field dynamics $\bar{x}$ of one area with different coupling strengths: (a) $g_{exc} = 0.5$ and $g_{inh} = 3.8$, (b) $g_{exc} = 0.6$ and $g_{inh} = 1.8$ (c) $g_{exc} = 0.9$ and $g_{inh} = 3.8$.

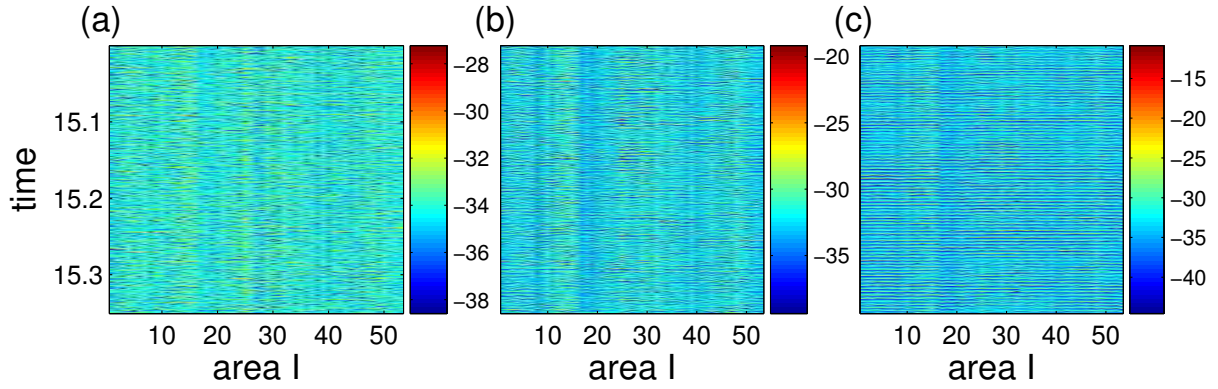

Figure 5.31: Spatio-temporal patterns of the mean activity $\bar{x}_I$ at different coupling strengths: (a) $g_{exc} = 0.5$ and $g_{inh} = 3.8$, (b) $g_{exc} = 0.6$ and $g_{inh} = 1.8$ (c) $g_{exc} = 0.9$ and $g_{inh} = 3.8$. Note the different scales in the colorbars.

the balanced state can lead to abnormal activity similar to the strongly synchronized neuronal activity during epileptic seizure [70, 74].

We apply the Pearson correlation coefficient r (Eq. 5.3) to quantify how the individual areas interact. The correlations between the mean field signals are computed and averaged over 10 realizations of different local network structures (SW network) and neurons involved in the long-range connections. Figure 5.32(a) shows the average correlation coefficient of all pairs of areas (Eq. 5.4) at specific g_{exc} and g_{inh} values. The plot reveals how the neural activity depends on the excitatory and inhibitory coupling strength. The size of increment for excitatory coupling is only 0.1, whereas the inhibition is incremented with a stepsize of 1.0. The system is more sensitive to change of the excitatory coupling: even with a small increase, the correlation can be substantially stronger. The effect of changing the inhibitory coupling is more pronounced in the more synchronized networks: with strong excitation (e.g., $g_{exc} = 1.0$), the decrease of synchronization caused by an increase of inhibition is clearly visible, see also [70].

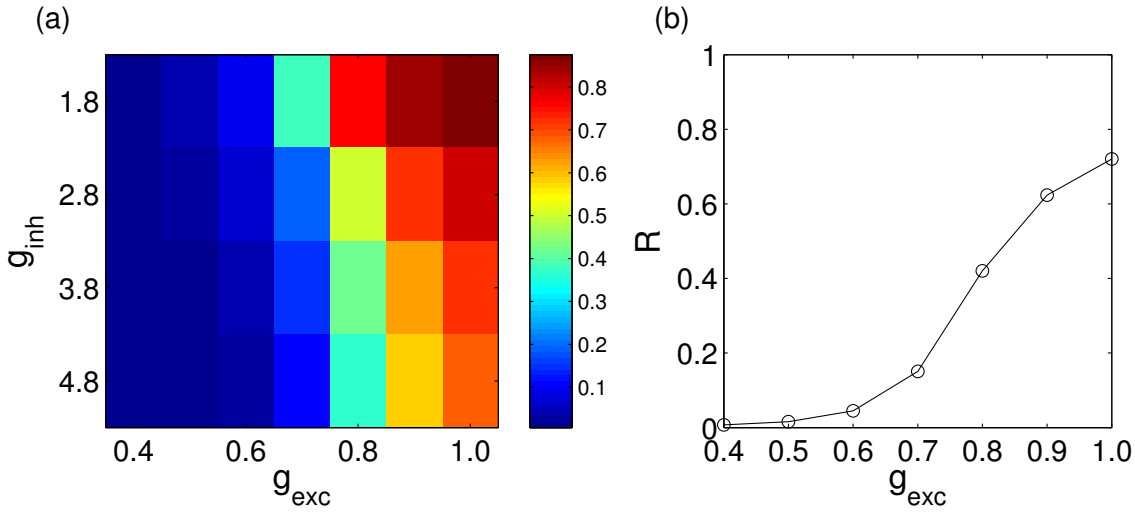

Figure 5.32: (a) Dependence of the average correlation coefficient R on the excitatory and inhibitory coupling strength g_{exc} and g_{inh}. (b) The effect of the internal coupling strength g_{exc} on the correlation (at fixed $g_{inh} = 3.8$).

The correlation matrices averaged over 10 realizations for three combinations of parameters g_{exc} and g_{inh} are shown in Fig. 5.33. The different realizations can result in slightly different correlation patterns and the averaged version of correlation matrix can have different correlation structure.

A weak synchronization regime (see Fig. 5.33(a)) is observed for values $g_{exc} \leq 0.5$ when $g_{inh} = 3.8$. Most of the cortical areas are weakly correlated since inhibitory couplings show a larger influence over the neuronal dynamics than excitatory ones. The maximal correlation between the area activity reaches 0.11 but the average correlation is very small ($R = 0.02$). In the correlation pattern four clusters are visible. A transient regime can be observed at, e.g., $g_{exc} = 0.6$ and $g_{inh} = 1.8$. Synchronization between the areas is larger, with the maximum at

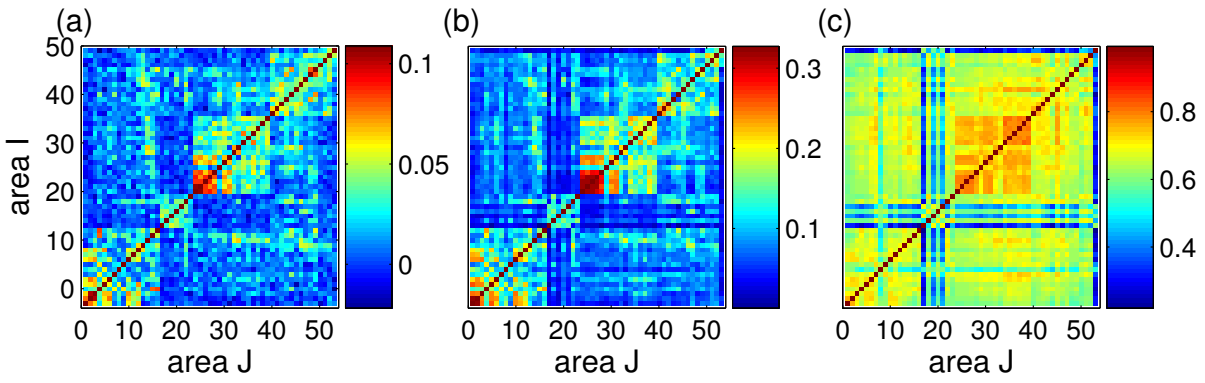

Figure 5.33: Correlation matrices $r(I,J)$ corresponding to the spatio-temporal patterns in Fig. 5.31. (a) $g_{exc} = 0.5$ and $g_{inh} = 3.8$, (b) $g_{exc} = 0.6$ and $g_{inh} = 1.8$ (c) $g_{exc} = 0.9$ and $g_{inh} = 3.8$. Note the different scales in the colorbars.

$r = 0.3$ leading to small changes in the dynamical patterns, see Fig. 5.33(b). The region of auditory areas becomes more independent, while new intercommunity connections appear between the SM and FL systems. The strong synchronization regime $g_{exc} \geq 0.9$ is characterized by strong interactions of the dynamics of cortical areas and the presence of two functional clusters (Fig. 5.33(c)). The correlations within those clusters are high (up to maximal $r = 0.82$ for $g_{exc} = 0.9$ and $g_{inh} = 3.8$). Intercluster correlation values are substantially smaller with a minimum of 0.21.

Similar to Section 5.1.2, we have calculated the distribution of correlation coefficients of all pairs of areas with respect to the underlying links, in order to evaluate the relation between topology and dynamics. Three different variants of node connectivity are considered — reciprocal links (P2), uni-directional links (P1) and an absence of connections (P0). Fig. 5.34 shows the distributions for three different coupling regimes.

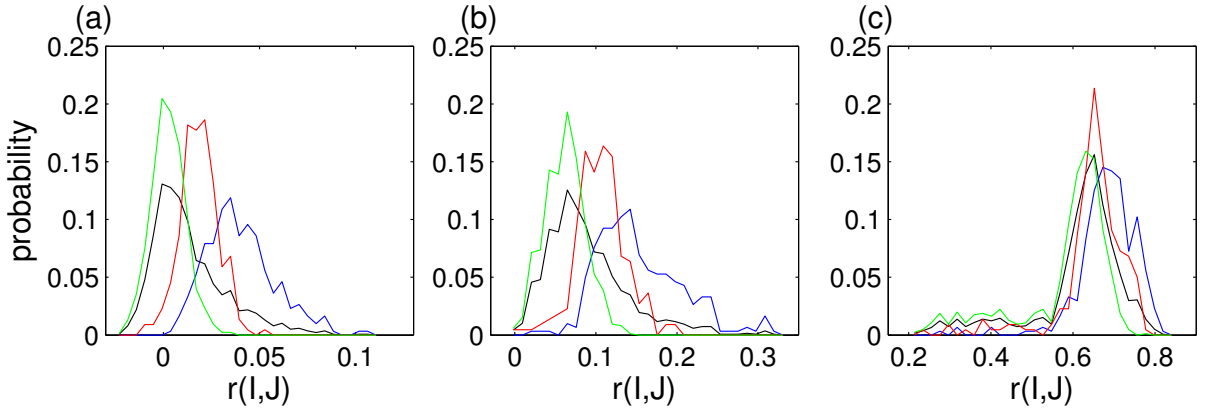

Figure 5.34: Distribution of the correlation $r(I,J)$ for (a) $g_{exc} = 0.5$ and $g_{inh} = 3.8$, (b) $g_{exc} = 0.6$ and $g_{inh} = 1.8$ (c) $g_{exc} = 0.9$ and $g_{inh} = 3.8$ for all nodes P_{all} (black line), P2 (blue line), P1 (red line) and P0 (green line).

The first dynamical regime is characterized by weak coupling, e.g., $g_{exc} = 0.5$ and $g_{inh} = 3.8$ with low correlation values between the areas, $r \in [-0.05, 0.1]$. The three distributions for P_{all} (general distribution of correlation), P2 and P1 are grouped around zero with a prominent Gaussian peak and long tail towards positive values (Fig. 5.34(a)). Most of the correlations with positive nonzero values are between reciprocally connected nodes (P2 distribution). The distributions of correlations in the transient regime are already shifted towards higher correlation again with the presence of long tails towards higher correlation values (Fig. 5.34(b)). Such forms of the distributions indicate the presence of several nodes with stronger activity and higher correlation between their mean field activities. For $g_{inh} = 0.6$ and $g_{inh} = 1.8$ the correlation values lie around $r \in [0, 0.3]$, comparable to the transient regime of FHN model dynamics $r \in [0, 0.35]$. At strong coupling values, e.g., $g_{exc} = 0.9$ and $g_{inh} = 3.8$, the distributions significantly overlap, with their peaks at around 0.65.

Stronger excitation leads to stronger synchronization of areas. The synaptic inputs from distant areas modifies the activity of the neuronal ensemble. The external coupling of areas enhances their common synchronization, here expressed as a higher correlation between their mean activities, see Fig. 5.32. Modulation of the inhibitory coupling strength has more impact on local activity than on global activity.

5.2.1.1 Firing frequency of areas vs. coupling strength and intensity of areas

We also recorded the spiking time of all neurons during simulations. Spikes were registered whenever V reached 10 mV. The firing frequency was calculated by averaging the number of spikes over the time of simulation and the number of neurons. Additionally, the firing frequency of individual areas was estimated. Figure 5.35 presents the average firing frequency of the whole system for various values of g_{exc} and g_{inh}.

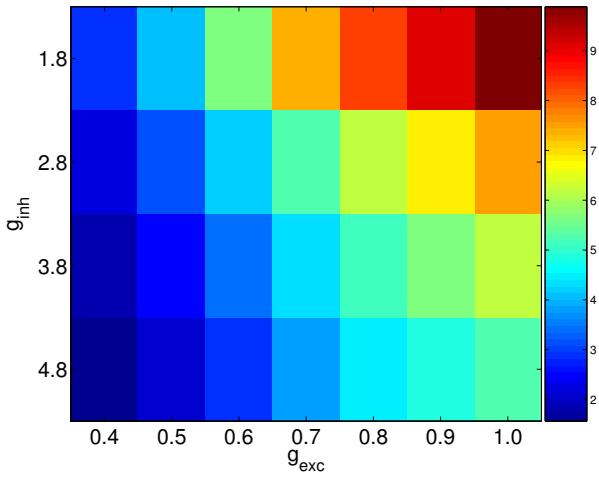

Figure 5.35: Dependence of the average frequency of neuronal firing on the internal and external coupling strength g_{exc} and g_{inh}.

We can clearly see the trend of increasing frequency with increased excitation at fixed values of g_{inh}, e.g., from $f_{aver} = 2.89$ Hz when $g_{exc} = 0.4$ to $f_{aver} = 9.95$ Hz when $g_{exc} = 1.0$ (here, $g_{inh} = 1.8$). Also, a decrease in the inhibitory coupling g_{inh} leads to a higher frequency of firing, e.g., from $f_{aver} = 4.9$ Hz when $g_{inh} = 4.8$ to $f_{aver} = 9.13$ Hz when $g_{inh} = 1.8$ (here, $g_{exc} = 0.9$). Again, the change of inhibition has a stronger effect in the strongly synchronized networks with large g_{exc}.

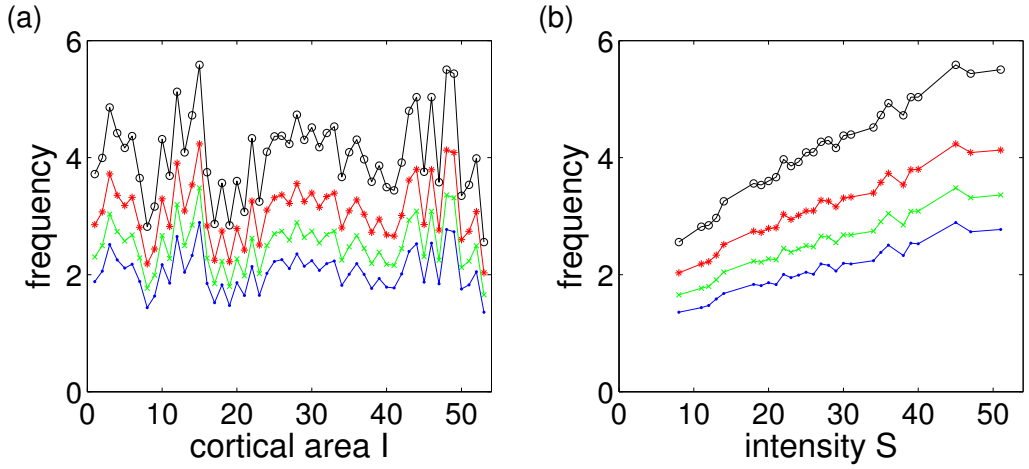

Figure 5.36: ML model with $g_{exc} = 0.5$ and various values of g_{inh}: 1.8 (black line), 2.8 (red), 3.8 (green) and 4.8 (blue line). (a) Firing frequency of cortical areas. (b) Dependence of the average firing frequency on the intensity of the area.

Changing the coupling strength between areas influences the neuronal response in the way of increase or decrease of firing frequency. However, such change is also due to strong influence of intensity, and varying of the coupling strengths causes mainly the shift of frequency in vertical direction (see Fig. 5.36). The higher the intensity of an area, the higher the firing frequency. The neural mass model exhibits a similar behavior in response to the external input to the neural mass (see later Chapter 6).

The network of FHN neurons has different frequency characteristics. In this case, for a weak synchronization regime, the higher the intensity of area, the lower the firing frequency (Fig. 5.37). The reason for this reversed dependence can be the presence of the electrical coupling in the system which occurs only occasionally in the nervous system. Here, we present the dynamics of the weak synchronization regime, where the intensity of the areas does not play a significant role. Neuron are mainly driven by local connections in the subnetworks and the long-range connections are very weak. Most of the neurons are silent and due to the diffusive homogeneous coupling, they influence the global dynamics of the whole network and decrease the activity of the firing neurons. The effect of coupling is continuous in contrast to the pulse character of chemical synapses.

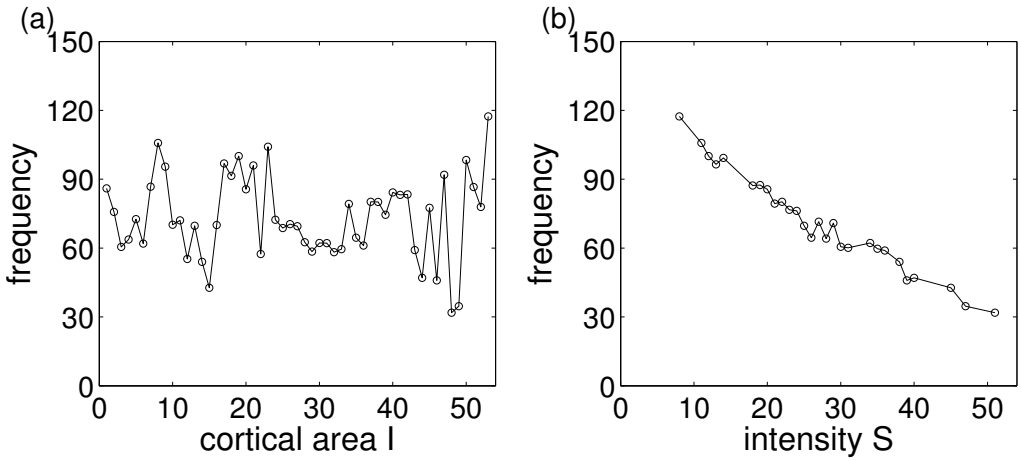

Figure 5.37: FHN model with coupling values $g_{int} = 0.7$ and $g_{ext} = 0.7$. (a) Firing frequency of cortical areas. (b) Dependence of the average firing frequency on the intensity of the area.

5.2.2 Functional clusters and networks

The correlation patterns visible in Fig. 5.33 point out the existence of several groups of areas with correlated dynamics. To further analyze the structure of such dynamical patterns at various coupling strengths, we apply the method of hierarchical clustering described previously (Section 5.1.2). The hierarchical trees for three different regimes are presented in Fig. 5.38. The dendrograms show the separation of areas into diverse groups and subgroups, where the length of the bar characterizes the similarity of the areal dynamics. Specific colors denote the clusters typical for those regimes. For the weak synchronization regime (Fig. 5.38(a)), the dynamics of the areas do not differ too much, and the intracluster distances at the lowest level of separation are significantly larger than the distances between the four major clusters. The transient regime (Fig. 5.38(b)) is characterized by the more closely related dynamics of areas. The intracluster structure is more complex, with distances of various lengths, displaying also stronger interactions between areas. Finally, in the strong synchronization regime (Fig. 5.38(c)), the mean field signals of areas from the major cluster are strongly correlated and thus, the intracluster distances are short. On the other hand, the distance between this cluster and the remaining areas is large and these few separate nodes preserve their rather independent dynamics.

In our analysis, we concentrate on the level of four clusters in various regimes, which we expect to agree with the four anatomical clusters.

5.2.2.1 Weak synchronization regime

As a typical representative of a weak synchronization regime we take $g_{exc} = 0.5$ and $g_{inh} = 3.8$. The neurons are only weakly mutually excited. The average frequency of firing of neurons is low, as is also the case for the correlation between areas. The activity does not spread through the entire network and is preserved mainly in the local structures. The areas group functionally

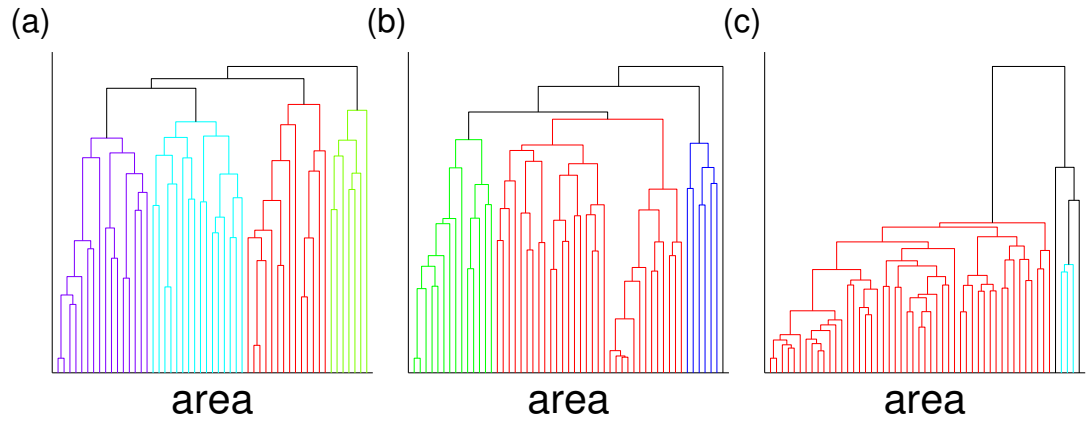

Figure 5.38: Typical hierarchical tree of the dynamical clusters in the weak coupling regime (a) $g_{exc} = 0.5$ and $g_{inh} = 3.8$, transient regime (b) $g_{exc} = 0.6$ and $g_{inh} = 1.8$ and strong coupling regime (c) $g_{exc} = 0.9$ and $g_{inh} = 3.8$..

into four clusters $C1$—$C4$, which are in good agreement with the anatomical communities ($C1$ corresponds to V, $C2$ to A, $C3$ to SM and $C4$ to FL systems). The functional clusters communicate through the several bridging nodes, here areas 13 (20b), 14 (7) and 39 (SSAo). These areas are known to be involved in multifunctional tasks. Typical dynamical clusters for this regime are shown in Fig. 5.39.

5.2.2.2 Intermediate synchronization regime

The system with parameters $g_{exc} = 0.6$ and $g_{inh} = 1.8$ represents an intermediate synchronization regime (see Fig. 5.40). From three visible functional clusters, two of them reflect the communities V and A. The rest of the areas from V and A and from both communities SM and FL are joined and form one dominant cluster. The exchange of the information between those three clusters is mediated by areas 13 and 14 from the visual system and area 22 situated in the auditory community. The fourth cluster, $C4$, has only a single area — area 53. The small intensity of this area, causing weaker external input, preserves its dynamical independence.

5.2.2.3 Strong synchronization regime

Figure 5.41 shows clusters in a strong synchronization regime with $g_{exc} = 0.9$ and $g_{inh} = 3.8$. The main cluster $C3$ is a set of areas belonging anatomically to the V, SM and FL systems. Cluster $C2$ contains only several auditory areas, where the remaining auditory areas are responsible for the communication between the clusters $C2$ and $C3$. The cluster $C2$ is stable across all dynamical regimes. Even at strong coupling, the core of the auditory system remains independent. Such behavior can be explained by strong interactions of the areas within the anatomical auditory system. Here, the intracommunity links are denser and stronger than intercommunity ones, see Table 5.2. The last two clusters consist of the single areas 8 and 53. As we can see,

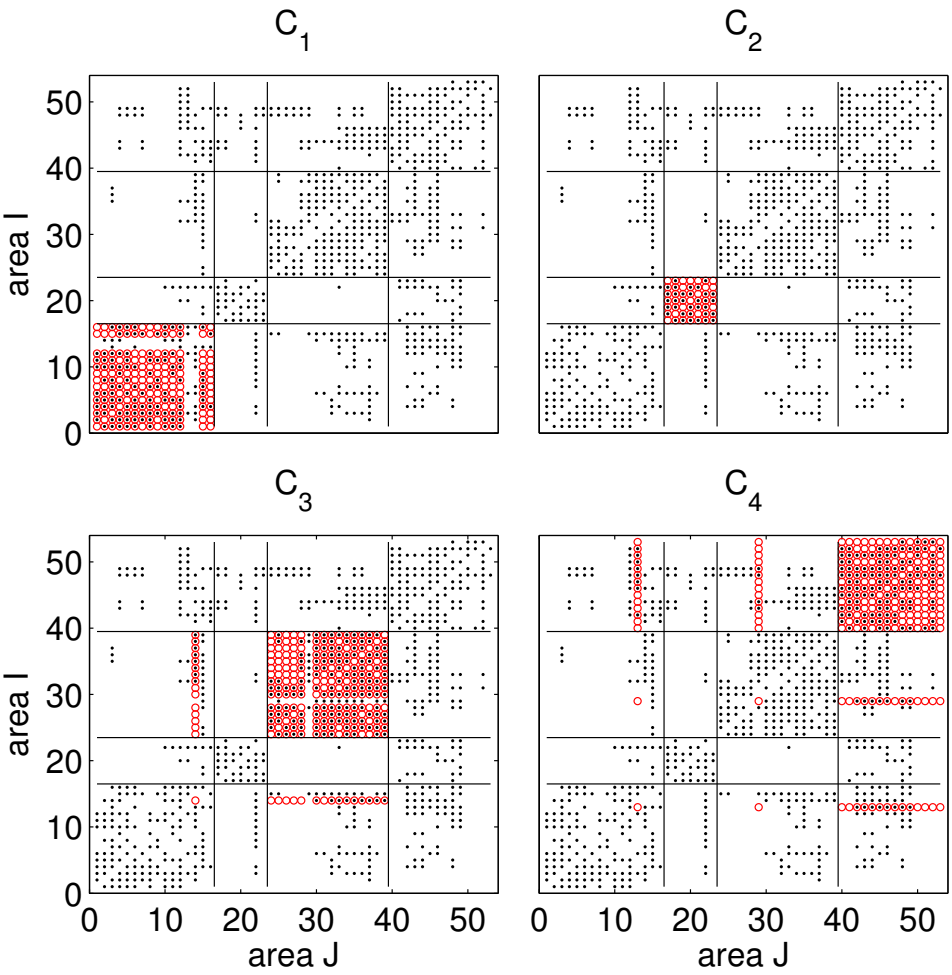

Figure 5.39: Dynamical clusters (red ∘) with weak coupling strength $g_{exc} = 0.5$ ($g_{inh} = 3.8$), compared to the underlying anatomical connections (black ·).

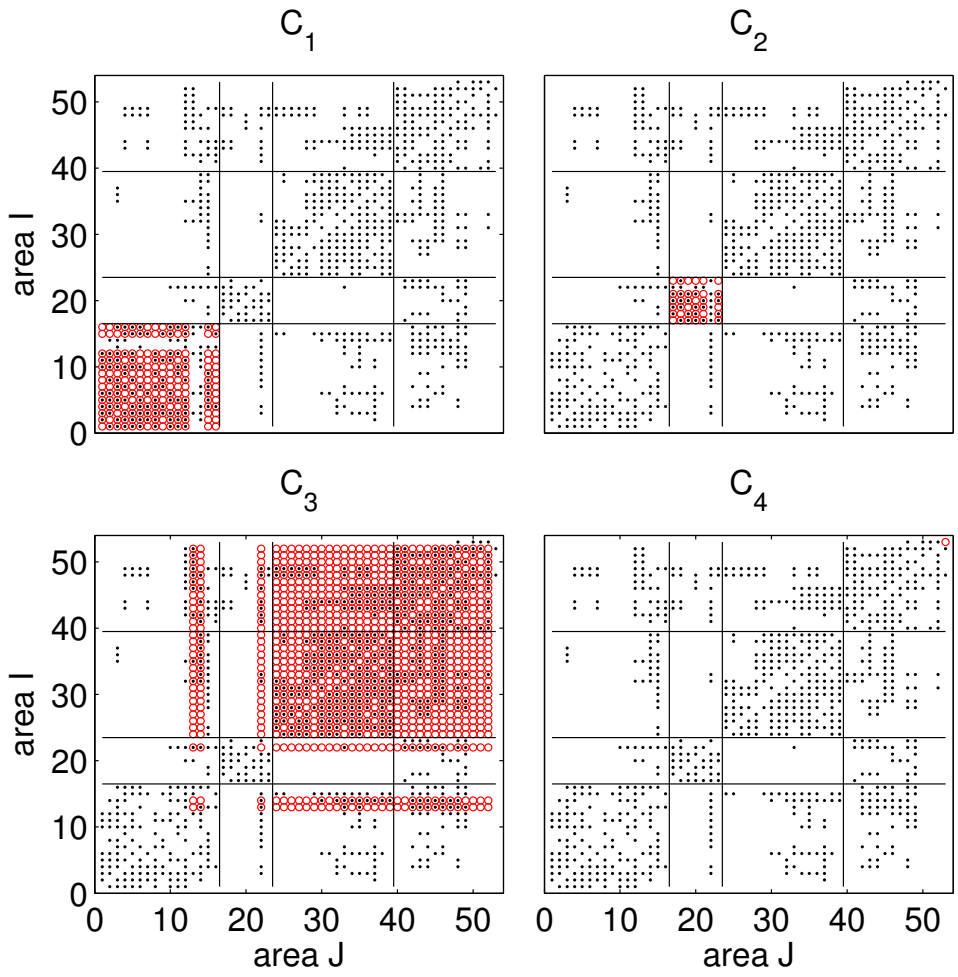

Figure 5.40: Dynamical clusters (red ∘) with intermediated coupling strength $g_{exc} = 0.6$ ($g_{inh} = 1.8$), compared to the underlying anatomical connections (black ·).

at this stage, the dynamics of areas are strongly predetermined by the area intensities. The areas with the lowest intensities stay independent, while strongly connected areas become highly correlated.

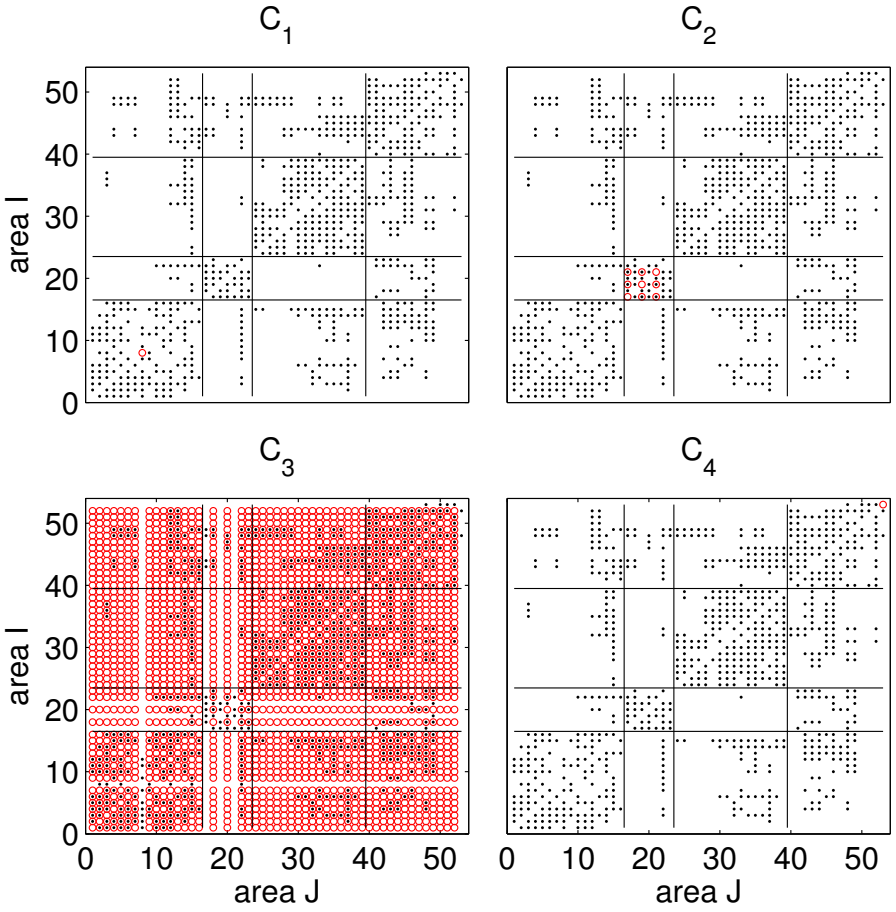

Figure 5.41: Dynamical clusters (red ○) with strong coupling strength $g_{exc} = 0.9$ ($g_{inh} = 3.8$), compared to the underlying anatomical connections (black ·). Note that clusters C_1 and C_4 comprise only the single areas 8 and 53, respectively.

5.2.2.4 Presence of bridging nodes

As is visible in Figs. 5.39–5.41, the dynamical clusters in weak and transient synchronization regimes communicate through the bridging nodes (areas sitting in one anatomical community but functionally located in other clusters, see Section 5.1.3.4). The occurrence of bridging nodes changes with the different realization and synchronization regimes. Here, we have selected three dynamical patterns with a characteristic number and location of the functional clusters. With weak coupling, four clusters with numerous bridging nodes are present — 4 (PLLS), 7 (ALLS), 9 (DLS), plus those found in the model network with electrical coupling, which are areas 12 (20a), 13 (20b), 14 (7), 15 (AES), 16 (PS). Latter five areas are involved in the multifunctional tasks, connecting the visual system, the place of their anatomical location, with

other basic systems like the somato-motor and fronto-limbic communities. Two other areas from the auditory system, 22 (EPp) and 23 (Tem), also participate in the communication with SM and FL systems. Table 5.4 shows the function and location of these bridging nodes in the cortex, which probably integrate the dynamics of different anatomical communities.

Other areas from Table 5.4 only occur occasionally. Area 53 (Hipp) is the most common bridging node and at the same time in strong synchronization regime it represents an independent node with preserving its own dynamics. This feature is caused by the small intensity of the area, which determines the amount of communication and information transmission with the rest of the network.

We would like to stress again, that each realization has a different cluster structure and the presented averaged correlation matrices already display average dynamical patterns. Here, the most important thing is that the ML model with chemical coupling reproduces the dynamical organization of the FHN model with electrical coupling. The results obtained for the biologically more plausible ML model with chemical coupling confirmed the presence of the complex hierarchical topology of the functional networks. Thus, it implies that the functional networks are independent of details of neurons representing dynamics, and are strongly related to the underlying anatomy, especially its hierarchical nature. Simple models like neural mass model do not show such behavior; the regime with hierarchical functional organization is not present.

5.3 Summary of the chapter

The results from the study of dynamics of large-scale hierarchical model can be summarized as follows:

- The only parameters that we varied in the models were the coupling strengths. The dynamics of the first model of FHN neurons with heterogeneous internal and external electrical coupling are mainly driven by local coupling strength and not so much by global coupling strength. The second model of ML neurons with distinguished excitatory and inhibitory chemical coupling shows a nontrivial dependence on the coupling strengths.
- We have identified three main dynamical regimes obtained for certain coupling strengths (weak, intermediate and strong synchronization regimes) in both models.
- The relationship between structure and function varies in these dynamical regimes. However, the dynamics of specific regimes exhibits similar correlation patterns for both types of multilevel models.
- In the biologically plausible regime of weak synchronization, the dynamical clusters closely correspond to the topological communities. In the light that structure determines dynamics and dynamics controls function, these results provide an explanation from the viewpoint of network dynamics for the coincidence between the topological communities and the functional subdivisions of the brain cortex [49, 50]. The dynamics are mainly controlled by the global structures in the network.

- The areas important for intercommunity communication and information integration act as bridges between different anatomical communities and dynamical clusters. These areas are the same as those previously found to be crucial for the global functioning of the system [100]. They have higher number of connections to the other areas, which predetermines that they will be 'integrators' in the cortical network.

- Different structures of the functional networks obtained by variation of the threshold of correlation unveil the hierarchical structure of dynamics. The lowest level comprises nodes that are strongly coupled and synchronized within their anatomical community, but with a low number of intercommunity links. The next areas to be expressed are the 'bridging' areas, which have numerous corticocortical links.

- The regime with intermediate coupling strengths shows a transition of the dynamics; the dynamics of cortical areas is more strongly correlated and creates three dynamical clusters.

- The abnormal synchronous activity of large neuronal ensembles, e.g., during epileptic seizures [70, 74], is a typical behavior for the regime of large couplings and strong synchronization. Here, the organization of the network into communities does not always separate the dynamics into the corresponding functional clusters. Only two functional clusters are observed. The failure to form different dynamical (functional) clusters indicates the failure to perform distinct functional tasks in different functional subsystems of the cortex during pathological events.

- The synchronization patterns in the strong synchronization regimes are mainly controlled by the local structural statistics of the nodes, i.e., input intensities. This is confirmed by the mean field analysis of the dynamics and by comparison to structures present in randomized networks. Note that other mechanisms of cluster formation in sparsely connected networks have been also reported [60].

- Even though the synchronization patterns in the two hierarchical models correspond, the firing activity of the areas differs in these models, pointing out the nontriviality of the neural dynamics.

- In the case of chemical coupling, which occurs frequently in biological systems, the average firing frequency of ML neurons of one area reflects the strength of the areal connectivity to the other areas. The higher the areal intensity, the higher the firing frequency. The hierarchical model of FHN neurons shows the reverse relationship of areal intensity and firing activity. This probably happens because of the diffusive electrical coupling, which modifies the neuronal dynamics to the averaged global activity of the whole area.

Thus, one can conclude that a biologically realistic large-scale hierarchical model of the cortex succesfully reveals part of the complex relationship between functional connectivity and its underlying neural substrate.

Chapter 6

Neural mass model of cortical dynamics

The analysis of the multilevel model of cat cortex has revealed a close relationship between the underlying structure and system dynamics. The correlations of the mean field activity of sets of neurons representing cortical areas are in correspondence with the coupling between these areas. As an alternative for a small-world network of neurons representing a cortical area, we can use a population model. Such models are commonly used in the modeling of the EEG activity of a neuronal ensemble. Would such a model, implemented in the cat cortical network, generate a similar pattern of dynamics as the multilevel model? The main aim of this chapter is to study dynamics of a network of neural mass models (previously described in Section 4.2) and the structure-function relationship.

6.1 Dynamics of neural mass model

The neural mass model that we use is a set of pyramidal cells and excitatory and inhibitory interneurons [129]. The activity of such a model is expressed as a difference between the post-synaptic membrane potential of excitatory v^e and inhibitory v^i interneurons as $V = v^e - v^i$, see Fig. 6.1(a). In the model of the cat cortical network, each macroscopic neural mass oscillator represents a single area. The areas are linked according to the anatomical connectivity represented by the coupling matrix M^A_{IJ}, shown in Figure 3.2. The external input from other groups of neurons and noise are fed into the population of excitatory interneurons. The equations of the whole system take the form:

$$\ddot{v}^p_I = Aaf(v^e_I - v^i_I) - 2a\dot{v}^p_I - a^2 v^p_I, \tag{6.1}$$

$$\ddot{v}^i_I = BbC_4 f(C_3 v^p_I) - 2b\dot{v}^i_I - b^2 v^i_I, \tag{6.2}$$

$$\ddot{v}^e_I = Aa\Big[C_2 f(C_1 v^p_I) + p_I(t) + \frac{g}{\langle S\rangle}\sum_J^N M^A_{IJ} f(v^e_J - v^i_J)\Big] - 2a\dot{v}^e_I - a^2 v^e_I, \tag{6.3}$$

We normalize the coupling strength g by the mean incoming intensity $\langle S \rangle$ of areas represented in the matrix M^A_{IJ}. As in [129], in our simulations, we take $p_I(t) = p_0 + \xi_I(t)$, where $\xi_I(t)$ is Gaussian white noise with standard deviation $D = 2$. The main results do not show a sensitive dependence on D. We fix $p_0 = 180$ so that the system is in the periodic regime corresponding to alpha waves.

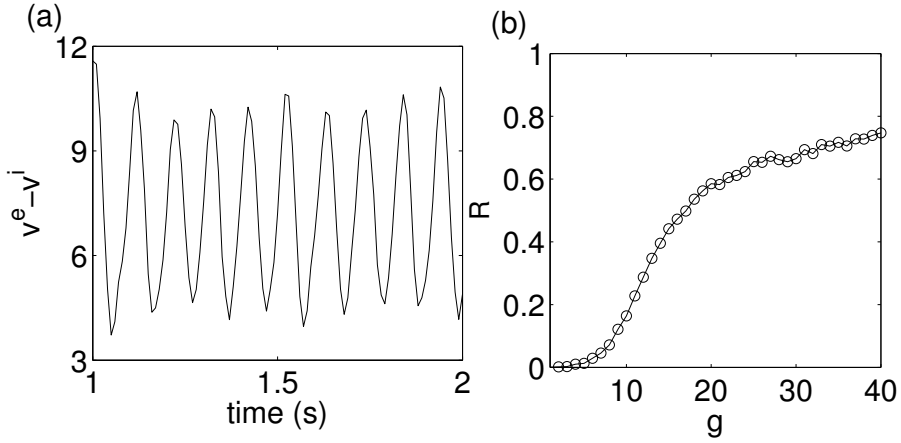

Figure 6.1: (a) Typical activity V of the uncoupled neural mass model. (b) The average correlation coefficient R vs. the coupling strength g in Eq. 6.3.

More sophisticated population models contain up to four subsets of neurons linked with various nonlinear functions, e.g., see Ursino et al. [124]. These models are able to exhibit a wide frequency spectrum of activity corresponding closely to the biological signals measured in human EEG.

We have observed the dependence of the oscillations of coupled populations on the strength of the coupling, see Fig. 6.1(b). Synchronization between the areas is measured by the linear correlation coefficient $r(I,J)$ between the population outputs V_I and V_J, already defined in Section 5.1.1 in Eq. 5.3. Other measures, like phase synchronization, would provide very similar information about the intercorrelation between the areas. The average correlation of all pairs of areas R (see Eqs. 5.3, 5.4), is shown in Fig. 6.1(b) as a function of the coupling strength g. The results indicate that no clear correlation occurs for weak coupling $g < 5$. For large coupling values, some nontrivial correlation seems to be expressed. This observation is in correspondence with the behavior of large-scale hierarchical model of the brain activity (see Fig. 5.3(b) for comparison).

In Fig. 6.2, the correlations for two different regimes are displayed. The dynamical pattern is not structured at very weak coupling, but at stronger couplings ($g \geq 5$), the system forms a large cluster including most of the areas from V, SM and FL. The auditory system A remains relatively independent. This is consistent with the intercommunity connectivity shown in Table 5.2.

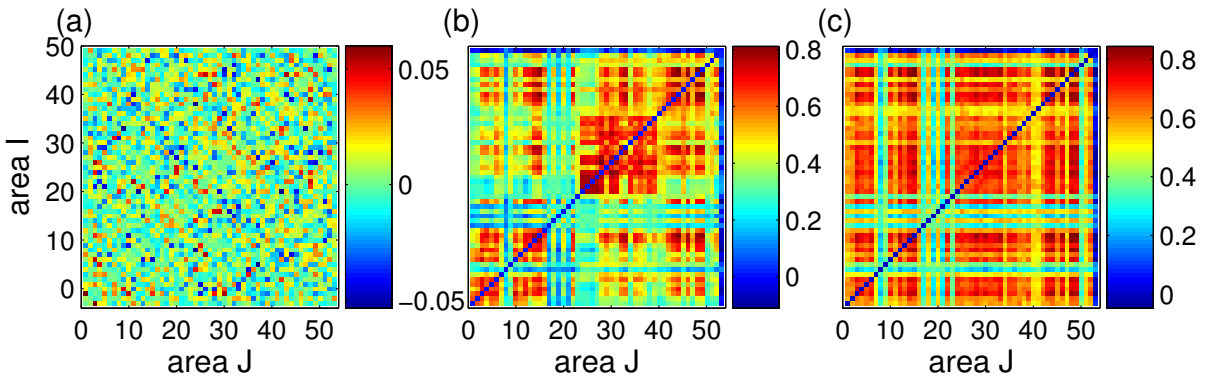

Figure 6.2: Correlation matrices $r(I,J)$ of the cat cortical network with (a) weak coupling $g = 2$ and (b) strong coupling $g = 15$. In (c), we see $r(I,J)$ for a randomized network with $g = 15$. Note the different scales in the colorbars.

6.2 Impact of node intensity on areal dynamics

As we have already discussed in Section 5.1.3.5, random networks of coupled oscillators (x_I) with a sufficiently strong coupling can achieve a high level of global synchronization [134, 136]. Such synchronization is expressed as a collective oscillation in the mean activity $X = (1/N)\sum_I^N x_I$. The cat cortical network exhibits an organization of communities, but it also possesses many random-like connections between the communities. Similar to the multilevel model, a mean field approximation might provide a relevant explanation of the dynamical organization in the strong coupling regime. The average input that a node I receives from its k_I direct neighbors can be replaced by the mean activity $f(X)$, i.e. $\sum_J^N M_{IJ}^A f(V_J) \approx S_I f(X)$ where $X = (1/N)\sum_J^N V_J$. The coupling term in Equation 4.16 can be written as

$$\frac{g}{\langle S\rangle}\sum_J^N M_{IJ}^A f(v_J^e - v_J^i) \approx \frac{gS_I}{\langle S\rangle} f(X). \tag{6.4}$$

In this first-order approximation, the nonlinearity of the original sigmoid function $f(v)$ is also neglected. It means that nodes with large intensities S are more strongly coupled to the global mean field X. These nodes usually synchronize with X and form an effective cluster. However, nodes with small intensities S are not significantly influenced by the activity of other nodes and preserve their own, rather independent, dynamics.

The above analysis has been again largely confirmed by our simulations (see also Section 5.1.3.5). We calculate the correlation coefficient R_X between the activity V_I of an area and the global mean field $X = (1/N)\sum_I^N V_I$. In Fig. 6.3, R_X is averaged for nodes with the same values of intensity S and plotted for various coupling strengths. It is roughly an increasing function of S. We have performed simulations on randomized cat cortical networks, maintaining both the input degree k_I and intensity S_I of all the nodes [80]. In this case, the results of R_X again shows a monotonous increase with the intensity S (Fig. 6.3). The fluctuation of R_X of the

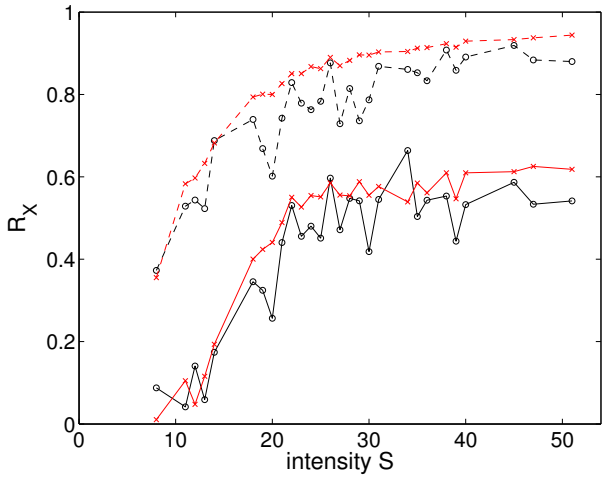

Figure 6.3: Correlation R_X between the activity of an area V_I and the global mean field X, as a function of the intensity S. Solid lines: $g = 10$, dashed lines: $g = 20$. Black points correspond to the original cat cortical network, while red points correspond to the randomized matrix.

original cortical network is mainly due to the clustered organization at various levels (Fig. 6.3). We also show a typical correlation pattern of these randomized networks; for a more detailed comparison see Fig. 6.2(c). The major dynamical organization is very similar for both the cat network and the randomized network. This correspondence points out that dynamics using a neural mass oscillator depend little on the detailed network topology, but largely on the input intensity of the nodes.

There is little direct relationship between the pairwise coupling M^A_{IJ} and the strength of synchronization $r_{I,J}$. To demonstrate this, we distinguish three cases for any pair of nodes in the network: reciprocal projections (P2), uni-directional couplings (P1) and non-connection (P0) (see also Section 5.1.2). We compute the distribution of the correlation $r_{I,J}$ for these cases separately. Figure 6.4(a) depicts the weak coupling (e.g., $g = 2$), where the distributions for P0, P1 and P2 pairs coincide and display a Gaussian shape centered at zero. Compared to the distribution obtained by computing the correlation for uncoupled nodes ($g = 0$) (Fig. 6.4), we can see that most of the correlations are insignificant. With increased coupling (e.g., $g = 5$), the correlation between P2 pairs is only slightly stronger than for P1 pairs. All three distributions still significantly overlap, what is also observed for strong couplings at $g = 20$ and comparable to the strong coupling regime at hierarchical model (Fig. 5.5(c)).

6.3 Summary of the chapter

We have described the dynamics of the cortical network modeled by a set of neural mass oscillators.

- In general, two dynamical regimes at the weak and strong coupling were detected.

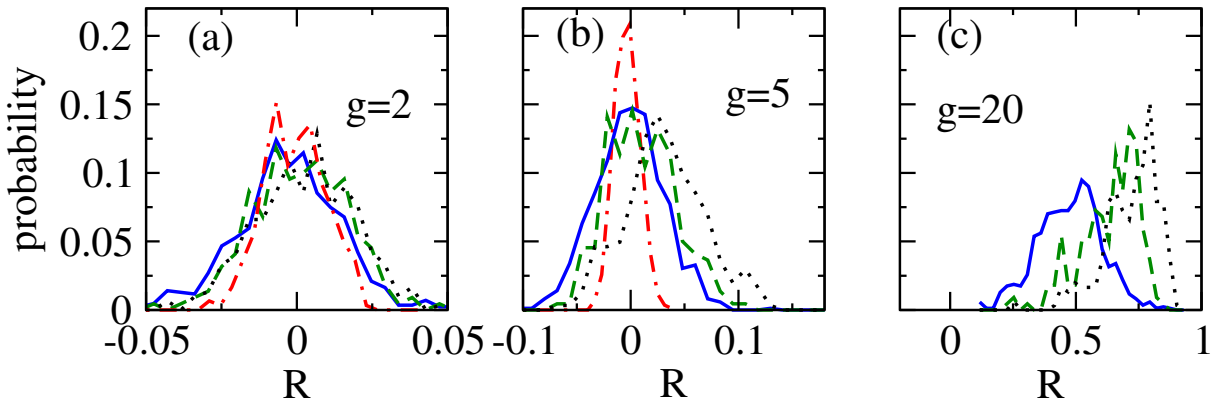

Figure 6.4: Distribution of the correlation $r(I,J)$ for P0 (solid blue line), P1 (dashed green line) and P2 (dotted black line) pairs with various values of the coupling strength g, (a) $g = 2$, (b) $g = 5$ and (c) $g = 20$. The dash-dotted red lines in (a) and (b) indicate the distribution between uncoupled areas ($g = 0$). The different shapes of the distributions in (a) and (b) are due to different bin sizes.

- Analysis of the correlation patterns of cortical areas for both regimes did not clearly detect the presence of hierarchical clusters in the dynamics, as was found in the case of the multilevel model.
- Results have also shown that the dynamics of the network of the generic oscillators (in our case neural mass oscillators) depend on single node characteristics, but the network topology is not very relevant. This is manifested in the well expressed, single-scale oscillations generated by the model.
- At a sufficiently strong coupling strength, the sustained oscillations propagate continuously from a node to its neighbors and next neighbors. As a result, the whole system oscillates collectively. In reality, continuous and large-scale spreading of neural activity in a strongly synchronized manner occurs only in pathological states like epileptic seizures [70].
- Other generic models of oscillators with noise (e.g., Van der Pol), models of excitable/spiking neurons, such as the simple integrate-and-fire model, or linear dynamical models based on Gaussian stochastic processes [110] would generate similar results, especially at the systems level.

The spontaneous EEG signal of healthy humans exhibits a broad range of timescales [87], which are not accounted for in this model. Thus, such a simplified model of EEG activity seems to be far less suitable to investigate the relationship between structural and functional connectivity when compared to the model of coupled excitable elements with structured connectivity presented previously. On the other hand, even if this model is not able to mimic resting state of the brain with background spontaneous activity, a set of coupled neural mass oscillators with forward, backward and lateral processes was recently used to model event-related responses in the brain [35]. Estimation of the coupling parameters of such models using empirical data can be used to assess causal (effective) connectivity between brain areas.

Chapter 7

Conclusion

In this dissertation, the relationship between topological structures and synchronization dynamics of neural networks was investigated by using a realistic network of cat corticocortical connectivity. The simulated system, a network of networks, represents a multilevel model which focuses on the organization of the highest network level, modeling each cortical area by a one-level SW subnetwork. The results obtained from this multilevel model are compared to the model where a population model stands for a single area.

7.1 Main results

The main finding is that the dynamics of the multilevel model show a hierarchical organization revealing different levels of modular organization in the anatomical connectivity of the corticocortical networks. The model of coupled neural populations does not reflect closely the modular structure of the dynamics. The most important results are summarized in the following part:

7.1.1 Hierarchical model of the cortex

- Three main dynamical regimes with weak, intermediate and strong synchronization have been observed depending on the coupling strength between the neurons and between the areas.
- In the biologically plausible regime of weak synchronization, the dynamical clusters unveil the topological communities of the anatomical network.
- Several areas bridge different anatomical communities and functional clusters in the weak coupling regime.
- In the functional networks extracted from the model, a hierarchical structure of dynamics is manifested.

- Large coupling leads to a strong synchronization of areal activity with similar dynamical behavior as observed, for example, by epileptic seizures.
- The dynamics at strong coupling are mainly determined by local structural properties of the areas (input intensities).

7.1.2 Population model of the cortex

- The weak coupling regime of this model does not reveal dynamical patterns which would reflect the underlying topology.
- Whenever the coupling becomes significant, the oscillatory model displays a prominent two-cluster behavior, as in the strong coupling regime of the hierarchical model.
- At stronger coupling, dynamical patterns are largely determined by the total input strength (intensity) of nodes, but not by the detailed network topology.

We stress again that the striking relationship between the dynamical organization and the network topology in the weak coupling regime results from our biologically plausible modeling of the cortical areas as subnetworks of excitable neurons. Due to the nature of localized signal propagation, such a hierarchical network of excitable elements appears to be more efficient in the detection of hierarchical communities in a broad range of complex systems than schemes based on self-sustained oscillator models [7] (especially when the community structures are not very clear).

Our findings are also interesting from the general perspective of network dynamics. Previous analysis of synchronization dynamics has mainly focused on the stability of the ideal case of the complete synchronization state as a function of the global statistics of the networks, such as the mean degree, or the ratio of maximal and minimal eigenvalues, etc. [9, 15, 27, 82, 83, 88, 121, 134, 136]. Here, we have shown that the detailed dynamical organization varies in different dynamical regimes, determined by different underlying topological structures of the same network (e.g., more local features of communities, or more global measures of intensity). This study reveals both the possibilities and the limitations of the complex network approach for the understanding of complex systems based on the interaction topology. The results also provide an additional motivation to characterize complex network systems beyond global statistics, since more local or detailed connection structures can be the most important determinants for the dynamical behavior of the system.

7.2 Further work

The presented analysis of the dynamical clusters provides a meaningful bridge that mediates the gap between the topology (communities) and function (functional subdivision) of the brain

cortex, even when the model subnetworks are strongly simplified and the dynamics do not reflect specific information processing. In the future, the model should be extended and improved in several ways to capture more realistic information processing in the brain:

1. Biologically, a system of 10^5 neurons with around 10^4 synapses per neuron corresponding to a cubic millimeter of cortex is the minimal system size at which the complexity of the cortex can be represented [21, 81]. Supplementary levels of clustered network organization representing minicolumns, columns and cellular circuits within each cortical area would better model the realistic connectivity. The organization of neurons into the horizontal cortical layers could be considered, eventually. In addition, the obtained significant functional correlations are relatively low (max. $0.1 - 0.2$) in the biologically plausible regime. Such an extended hierarchical representation of the cortex could significantly broaden these regimes, with a corresponding increase of correlation strength, as observed experimentally [38, 98, 115, 117]. Besides this, the thalamo-cortical connectivity [100] can be taken into account.

2. Cortical neurons exhibit rich dynamics, e.g., tonic spiking and burst firing, which would require more subtle neural models. These different firing modes have significant effects on the synchronization of coupled neurons [91], which may affect global functional connectivity. Moreover, in reality, both classes of excitability and also both types of coupling (electrical and chemical) are present in the global neuronal population. A biologically more realistic coupling could be achieved with the addition of synaptic plasticity and time delay in the transmission of the signal. Another possibility would be to model each node of the subnetwork by another population of neurons (three-level hierarchy) and to employ neural mass models [34] for the node dynamics. Biologically based population models, such as the neural mass oscillator, can reproduce all frequency ranges observed in brain dynamics under different physiological states [34].

3. In the future the proposed framework could be used to investigate the relative contributions of network topology and task-related network activations to functional brain connectivity and information processing. The model dynamics could be compared to the observed activity spread in the cortex [69, 75, 102] and to the functional connectivity [4, 12, 38, 98, 115, 117] at suitable spatio-temporal scales. However, this achievement would require significant developments in neurophysics, in the theory of dynamical complex networks, in algorithms of parallel computing [14, 81] as well as in the high-resolution neurological recordings.

These more realistic implementations would allow localized and strong synchronization in some low-level clusters and naturally organized dynamics at higher levels. Thus, the biologically plausible regimes would be significantly broadened.

However, this ‘bottom-up’ approach faces a huge gap of information regarding the details of the structures of the anatomical and functional connectivities crossing various hierarchies. Due to the invasive nature of neuroanatomical techniques (mainly by tracer injection), the topological properties of human connectome remain largely unclear [29, 111]. The most complete data about the anatomical connectivity are available only from animal brains. For this reason,

a direct comparison with the large-scale functional networks from human fMRI seems to be infeasible within foreseeable time. In spite of the progress made in revealing the general principles of structural and functional networks, the relationship between these two parts is still an open problem requiring significant development in various fields ranging from neurobiology to complex system theory.

Acknowledgments

I would like to thank all the people who helped me in every way to make this work possible. First of all, my thanks goes to Prof. Dr. Kurths for offering me the opportunity to come and work in his group and for all his encouragement and advises during my study.

As the second, I would like to thank to Changsong Zhou, for his immense help, patience and endless stimuli and discussions. Without his help I would probably get lost in the jungle of the theoretical physics. Together with Gorka Zamora they motivated and supported me strongly in my work. Thanks for all these hours spent at work together at different places and at different time!

I should not forget about the close co-worker Prof. Dr. Claus Hilgetag. I thank him for bringing more biological background and inspiration to our work. My thanks goes also to the people from AGNLD and Helmholtz Center for Mind and Brain Dynamics, for the warm atmosphere of the meetings and fruitfull discussions.

I am very gratefull to Birgit and Tessi, both for their friendliness and help in the administration, for technical support, and for the help in the daily 'German' life.

I specially thank to for my closest friends here: Natalia, Priya, Aneta, James and Ellen, Mamen and Marco, and Nicoleta and Cosmin. To all of you I owe a lot, for your endless support in scientific and also private area, for nice moments we had together but mainly for your great friendship. Thank you!

I wish to thank also to numerous friends from different countries across the world, but mainly for my friends at home in Slovakia. I cannot forget about the family Makuch and Halámek, for their helping hand at the beginning of my stay in Potsdam, but also for the big support during the whole time I spent here.

Veľká vďaka patrí mojim rodičom a bratom za ich neustálu pomoc, lásku a morálnu podporu. Taktiež ďakujem aj rodine Kriványekovej, ktorá ma prijala za svoju ako i Tinke Lukáčovej za jej priateľstvo.

Moja najväčšia vďaka patrí Rolandovi. Roli, ďakujem, že si pri mne stál v jednom z mojich najnamáhavejších období v doterajšom živote a bol mi vždy oporou, utešovateľom i povzbudzovateľom, a hlavne vynikajúcim priateľom.

Ďakujem! Vďaka, Bože!

Appendix A

Appendix: Source code

The subroutine `Matrices3Dnetwork` creates a two-level model of a network. The upper level is represented by the 'mcat' network, and the structure of the lower level, an individual area, is of small-world character.

```
SUBROUTINE Matrices3Dnetwork(mcat,Ninh)

IMPLICIT NONE
INTEGER(KIND=4), PARAMETER :: m=53, n=200, ka=int(n*0.1)
INTEGER(KIND=4) :: i1, i2, j1, j2, jn, ab, l2, c
REAL(KIND=8) :: ran1, a1, b, a2
INTEGER(KIND=4), INTENT(IN) :: mcat(m,m)
INTEGER(KIND=4), INTENT(OUT) :: Ninh(m,n)
INTEGER(KIND=4), DIMENSION(m,n,n) :: m1(m,n,n), m2(m,n,n),
                                     mlocal(m,n,n), NN(m,n,0:n)


! m1, m2 - basic regular matrix (1 and 0), ka nearest neighbours
DO i1=1,m,1
   DO j1=1,n,1
      DO j2=1,(ka+1),1
         c=mod((n+(j1-1)+(j2-1)-ka/2),n)+1
         if (j1/=c) m1(i1,j1,c)=1
         m2(i1,j1,c)=m1(i1,j1,c)
      END DO
   END DO
END DO

! generation of the small-world network - rewired m2 matrix
! if a>p, connection stays = 1, weaker connection, rewiring,
! finding the new 2.node and avoid selfconnetion and
! doubleconnection
```

```
DO i1=1,m,1
   DO j2=1,n-1,1
      DO j1=1+j2,n,1
         IF ((m1(i1,j1,j2).EQ.1)) THEN
            a1= ran1(idum)
            IF (a1.GT.p) THEN
               m2(i1,j1,j2)=1
               m2(i1,j2,j1)=1
            ELSE IF (a1.LE.p) THEN
               b = ran1(idum)
               jn=INT(b*n)+1
               IF ((jn.NE.j1).AND.(m2(i1,j1,jn).NE.1)) THEN
                  m2(i1,jn,j1)=1
                  m2(i1,j1,jn)=1
                  m2(i1,j2,j1)=0
                  m2(i1,j1,j2)=0
               ELSE IF ((jn.EQ.j1).OR.(m2(i1,j1,jn).EQ.1)) THEN
                  DO WHILE ((jn.EQ.j1).OR.(m2(i1,j1,jn).EQ.1))
                     b = ran1(idum)
                     jn=INT(b*n)+1
                  END DO
                  m2(i1,jn,j1)=1
                  m2(i1,j1,jn)=1
                  m2(i1,j2,j1)=0
                  m2(i1,j1,j2)=0
               END IF
            END IF
         END IF
      END DO
   END DO
END DO

! include excitatory and inhibitory connections -  mlocal
DO i1=1,m,1
   DO j2=1,n,1
      a2=ran1(idum)
      IF (a2.LT.p2) THEN
         ab = -1
         Ninh(i1,j2)=1
      ELSE
         ab = 1
      END IF
      DO j1=1,n,1
         mlocal(i1,j1,j2)=ab*m2(i1,j1,j2)
      END DO
      a2=ran1(idum)
   END DO
END DO
```

```
! matrix for faster computation - indices of localy connected
! neurons NN
DO i1=1,m,1
   DO j1=1,n,1
      NN(i1,j1,0)=0
      DO j2=1,n,1
         IF (mlocal(i1,j1,j2).ne.0) THEN
            NN(i1,j1,0)=NN(i1,j1,0) + 1
            l2=NN(i1,j1,0)
            NN(i1,j1,l2)= j2*mlocal(i1,j1,j2)
         END IF
      END DO
   END DO
END DO


RETURN
END SUBROUTINE Matrices3Dnetwork
```

The subroutine `Matrices3Dmeanfield` creates a network of networks, with 5% of neurons of an area receiving the mean field signals from connected areas.

```
SUBROUTINE Matrices3Dmeanfield(Labelnn,Label_gl)

IMPLICIT NONE
INTEGER(KIND=4), PARAMETER :: m=53, n=200, num1=20
REAL(KIND=8), PARAMETER :: p3=0.05
REAL(KIND=8) :: ran1, a3
INTEGER(KIND=4) :: i1, i2, j1, j2, NN2,
INTEGER(KIND=4) :: Label(m,m,n)
INTEGER(KIND=4), INTENT(OUT) :: Labelnn(m,n,0:num1)

! inicialization to 0
Label(1:m,1:m,1:n)=0
Labelnn(1:m,1:n,1:num1)=0

! selecting neurons getting extra-areal input
DO i1=1,m,1
      DO i2=1,m,1
         DO j1=1,n,1
            a3=ran1(idum)
            IF (a3.LE.p3) THEN
               Label(i1,i2,j1)=1
            ELSE
               Label(i1,i2,j1)=0
            END IF
         END DO
      END DO
```

```
END DO

! for each neuron j1 from each area  i1 saving number
! and indices of connected areas i2 sending input
DO i1=1,m,1
      DO j1=1,n,1
            NN2=0
            DO i2=1,m,1
                  IF (Label(i1,i2,j1).eq.1) THEN
                        NN2=NN2 + 1
                        Labelnn(i1,j1,NN2)=i2
                  END IF
            END DO
            Labelnn(i1,j1,0)=NN2
      END DO
END DO

RETURN
END SUBROUTINE Matrices3Dmeanfield
```

The subroutine `Matrices3Dchemsynap` generates long-range connections between cortical area, where the *Mt* links are established of neuron-to-neuron character. Multiple links between two neurons from two areas are avoided.

```
SUBROUTINE Matrices3Dchemsynap(mcat,Ninh,Label_neur,Labelnn,Label_gl)

IMPLICIT NONE
INTEGER(KIND=4), PARAMETER :: m=53, n=200, ka=int(n*0.1),
                              num1=20, num2=20
REAL(KIND=8), PARAMETER :: p3=0.05
INTEGER(KIND=4) :: i1, i2, j1, j2, NN2, NN3, Ml, Mt
REAL(KIND=8) :: ran1, x1, x2
INTEGER(KIND=4), INTENT(IN) :: mcat(m,m), Ninh(m,n)
INTEGER(KIND=4) :: NN_area(m,n), NN_neuron(m,n,0:m), numbe(n)
INTEGER(KIND=4), INTENT(OUT) :: Labelnn(m,n,0:num1),
                                Label_neur(m,n,m,n),
                                Label_gl(m,n,0:num1,0:num2)


! Labelnn(i1,j1,NN2) - save indices of areas i2 sending to i1, j1
! Label_gl(i1,j1,NN2,NN3) - save the index of neuron j2 from i2
! Label_neur(i1,j1,i2,j2) - save all established connection
! NN_neuron(i1,j1,NN2) - count # of neurons getting from i2
! NN_area(i1,j1) - count # of areas sending to i1,j1

! initialization to 0
Labelnn(1:m,1:n,0:num1)=0
```

```
Label_gl(1:m,1:n,0:num1,0:num2)=0
NN_area(1:m,1:n)=0
NN_neuron(1:m,1:n,1:m)=0

Mt=int(n*ka*p3)

CALL Matrices3D_network

! for each connected areas (i2->i1) a specific number Mt of
! connections is established, where we generate j1 (from i1)
! getting connection from i2 and also generate connection j2
! (from i2) sending to j1 (from i1)

DO i1=1,m,1
      NN2=0
      DO i2=1,m,1
            IF (mcat(i1,i2)/=0) THEN
                Ml=0
                numbe(1:n)=0
                DO WHILE (Ml<Mt)
                     x1=ran1(idum)
                     j1=int(x1*N) + 1
                     x2=ran1(idum)
                     j2=int(x2*N) + 1

                     ! if j2 is excitatory neuron and if
                     ! connection j1, j2 do not exist,
                     ! establish connection
                     IF ((Ninh(i2,j2)==0).and.(Label_neur(i1,j1,i2,j2)==0)) THEN
                          Label_neur(i1,j1,i2,j2)=1

                          ! save index of i2, ONLY ONCE
                          ! if neuron j1 appears for the first time then
                          ! count number of areas sending to i1,j1
                          IF (numbe(j1)==0) THEN
                               NN_area(i1,j1)=NN_area(i1,j1)+1
                               numbe(j1)=1
                          ELSE
                               NN_area(i1,j1)=NN_area(i1,j1)
                          END IF

                          NN2=NN_area(i1,j1)
                          Labelnn(i1,j1,NN2) = i2
                          Ml=Ml+1
                          NN_neuron(i1,j1,NN2)=NN_neuron(i1,j1,NN2) + 1
                          NN3=NN_neuron(i1,j1,NN2)
                          Label_gl(i1,j1,NN2,NN3)=j2
                     END IF
                END DO
```

```
            END IF
        END DO
        DO j1=1,n
                Labelnn(i1,j1,0)=NN_area(i1,j1)
                DO i2=1,NN_area(i1,j1)
                        Label_gl(i1,j1,i2,0)=NN_neuron(i1,j1,i2)
                END DO
        END DO
END DO


RETURN
END SUBROUTINE Matrices3Dchemsynap
```

Bibliography

[1] Brain maps. *http://brainmaps.org/*, 2005–2006. copyright UC Regents Davis campus.

[2] Cortical connectivity in macaque. *http://cocomac.org/*, 2006.

[3] Neocortical microcircuit database. *http://microcircuit.epfl.ch/*, 2006. copyright 2003 Brain & Mind Institute, EPFL, Lausanne, Switzerland.

[4] S. Achard, R. Salvador, B. Whitcher, J. Suckling, and E. Bullmore. A resilient, low-frequency, small-world human brain functional network with highly connected association cortical hubs. *J. Neurosci.*, 26(1):63–72, 2006.

[5] R. Albert and A. L. Barabási. Statistical mechanics of complex networks. *Rev. Mod. Phys.*, 74:47–97, 2002.

[6] Z. F. Altun and D. H. Hall. Wormatlas. *http://www.wormatlas.org/*, 2002–2006.

[7] A. Arenas, A. Díaz-Guilera, and C. J. Pérez-Vicente. Synchronization reveals topological scales in complex networks. *Phys. Rev. Lett.*, 96:114102, 2006.

[8] P. Balenzuela and J. García-Ojalvo. Role of chemical synapses in coupled neurons with noise. *Phys. Rev. E*, 72:021901, 2005.

[9] M. Barahona and L.M. Pecora. Synchronization in small-world systems. *Phys. Rev. Lett.*, 89:054101, 2002.

[10] M. Barbosa, K. Dockendorf, M. Escalona, B. Ibarz, A. Miliotis, I. Sendi na Nadal, G. Zamora, and L. Zemanová. *Lectures in Supercomputational Neuroscience:Dynamics in Complex Brain Networks*, chapter Parallel computation of large neuronal networks with structured connectivity. Springer, Berlin, 1st edition, 2008.

[11] D. S. Bassett and E. Bullmore. Small-world brain networks. *Neuroscientist*, 12(6):512–523, 2006.

[12] D. S. Bassett, A. Meyer-Lindenberg, S. Achard, T. Duke, and E. Bullmore. Adaptive reconfiguration of fractal small-world human brain functional networks. *Proc. Nat. Acad. Sci. USA*, 103:19518–19523, 2006.

[13] M. Bazhenov, N. Rulkov, J. Fellous, and I. Timofeev. Role of network dynamics in shaping spike timing reliability. *Phys. Rev. E*, 72:041903, 2005.

[14] P. beim Graben, J. Kurths, M. Thiel, and C. S. Zhou, editors. *Lectures in Supercomputational Neuroscience:Dynamics in Complex Brain Networks*. Springer, Berlin, 1st edition, 2008.

[15] I. Belykh, E. de Lange, and M. Hasler. Synchronization of bursting neurons: What matters in the network topology. *Phys. Rev. Lett.*, 94:188101, 2005.

[16] B.H.Jansen and V.G. Rit. Electroencephalogram and visual evoked potential generation in a mathematical model of coupled cortical columns. *Biol. Cybern.*, 73(4):357–366, 1995.

[17] G.-Q. Bi and M.-M. Poo. Synaptic modification by correlated activity: Hebb's postulate revisited. *Annu. Rev. Neurosci.*, 24:139–166, 2001.

[18] T. Binzegger, R. J. Douglas, and K. A. C. Martin. A quantitative map of the circuit of cat primary visual cortex. *J. Neurosci.*, 24(39):8441–8453, 2004.

[19] S. Boccaletti, J. Kurths, G. Osipov, D. L. Valladares, and C.S. Zhou. The synchronization of chaotic systems. *Phys. Rep.*, 366:1–101, 2002.

[20] S. Boccaletti, V. Latora, Y. Moreno, M. Chavez, and D.-U. Hwang. Complex networks: structure and dynamics. *Phys. Rep.*, 424:175–308, 2006.

[21] V. Braitenberg and A. Schüz. *Anatomy of the cortex: statistics and geometry*. Springer, Berlin, 1991.

[22] M. Breakspear and C.J. Stam. Dynamics of a neural system with a multiscale architecture. *Phil. Trans. R. Soc. B*, 360:1051–1074, 2005.

[23] N. Brunel. Dynamics of sparsely connected networks of excitatory and inhibitory spiking neurons. *J. Comput. Neurosci.*, 8:183–208, 2000.

[24] G. A. P. C. Burns and M. P. Young. Analysis of the connectional organization of neural systems associated with the hippocampus in rats. *Phil. Trans. R. Soc. Lond. B*, 355:55–70, 2000.

[25] D. Buxhoeveden and M. F. Casanova. The minicolumn hypothesis in neuroscience. *Brain*, 125:935–951, 2002.

[26] G. Buzsáki, C. Geisler, D. A. Henze, and X.-J. Wang. Interneuron diversity series: Circuit complexity and axon wiring economy of cortical interneurons. *Trends Neurosci.*, 27:186–193, 2004.

[27] M. Chavez, D.-U. Hwang, A. Amann, H. G. E.Hentschel, and S. Boccaletti. Synchronization is enhanced in weighted complex networks. *Phys. Rev. Lett.*, 94:218701, 2005.

[28] D. Chorvát. *Biofyzika*. Vydavatelstvo Univerzity Komenského, Bratislava, 1998.

[29] F. Crick and E. Jones. Backwardness of human neuroanatomy. *Nature*, 361:109–110, 1993.

[30] L. da F. Costa, M. Kaiser, and C. C. Hilgetag. Predicting the connectivity of primate cortical networks from topological and spatial node properties. *BMC Systems Biology*, 1(16), 2007.

[31] L. da F. Costa and O. Sporns. Hierarchical features of large-scale cortical connectivity. *BMC Systems Biology*, 1(16), 2007.

[32] F. H. Lopes da Silva, A. Hoeks, H. Smits, and L. H. Zetterberg. Model of brain rhythmic activity – the alpha-rhythm of the thalamus. *Kybernetik*, 15:27–37, 1974.

[33] O. David, D. Cosmelli, and K. J. Friston. Evalution of different measures of functional connectivity using a neural mass model. *NeuroImage*, 21:659–673, 2004.

[34] O. David and K. J. Friston. A neural mass model for MEG/EEG: coupling and neuronal dynamics. *NeuroImage*, 20:1743–1755, 2003.

[35] O. David, L. Harrison, and K. J. Friston. Modelling event-related responses in the brain. *NeuroImage*, 25:756–770, 2005.

[36] A. Destexhe, Z. F. Mainen, and T. J. Sejnowski. An efficient method for computing synaptic conductances based on a kinetic model of receptor binding. *Neural Comput.*, 6:14–18, 1994.

[37] Z. Ding, J. C. Gore, and A. W. Anderson. Classification and quantification of neuronal fiber pathways using diffusion tensor MRI. *Magn. Reson. Med.*, 49:716–721, 2003.

[38] V.M. Eguíluz, D.R. Chialvo, G. Cecchi, M. Baliki, and A. Vania Apkarian. Scale-free brain functional networks. *Phys. Rev. Lett.*, 94:018102, 2005.

[39] A. K. Engel, P. Fries, and W. Singer. Dynamic predictions: oscillations and synchrony in top-down processing. *Nature*, 2:704–716, 2001.

[40] C. W. Eurich, K. Pawelzik, U. Ernst, J. D. Cowan, and J. G. Milton. Dynamics of self-organized delay adaptation. *Phys. Rev. Lett.*, 82(7):1594–1597, 1999.

[41] D. J. Felleman and D. C. Van Essen. Distributed hierarchical processing in the primate cerebral cortex. *Cereb. Cortex*, 1:1–47, 1991.

[42] R. FitzHugh. Impulses and physiological states in theoretical models of nerve membrane. *Biophys. J.*, 1:445–466, 1961.

[43] W. J. Freeman. Models of the dynamics of neural populations. *Electroencephalogr Clin Neurophysiol Suppl.*, 34:9–18, 1978.

[44] W. J. Freeman. Characteristics of the synchronization of brain activity imposed by finite conduction velocities of axons. *Int. J. Bifur. Chaos*, 10:2307–2322, 2000.

[45] P. Fries. A mechamism for cognitive dynamics: neuronal communication through neuronal coherence. *Trends Cogn. Sci.*, 9:474–480, 2005.

[46] K. J. Friston. Functional and effective connectivity in neuroimaging: a synthesis. *Hum. Brain Mapp.*, 2:56–78, 1994.

[47] X. Guardiola, A. Diaz-Guilera, M. Llas, and C.J. Perez. Synchronization, diversity, and topology of networks of integrate and fire oscillators. *Phys. Rev. E*, 62:5565–5570, 2000.

[48] D. Hansel and G. Mato. Existence and stability of persistent states in large neural networks. *Phys. Rev. Lett.*, 86:4175–4178, 2001.

[49] C.C. Hilgetag, G.A.P.C. Burns, M.A. O'Neill, J.W. Scannell, and M.P. Young. Anatomical connectivity defines the organization of clusters of cortical areas in macaque monkey and cat. *Phil. Trans. R. Soc. Lond. B*, 355:91–110, 2000.

[50] C.C. Hilgetag and M. Kaiser. Clustered organization of cortical connectivity. *Neuroinformatics*, 2:353–360, 2004.

[51] C.C. Hilgetag, R. Kötter, K.E. Stephan, and O. Sporns. *Computational Neuroanatomy*. Humana Press, Totowa, NJ, 2002.

[52] B. Hu and C. S. Zhou. Phase synchronization in coupled nonidentical excitable systems and array-enhanced coherence resonance. *Phys. Rev. E*, 61(2):1001–1004, 2000.

[53] J. Ito and K. Kaneko. Spontaneous structure formation in a network of chaotic units with variable connection strengths. *Phys. Rev. Lett.*, 88:028701, 2001.

[54] M. V. Ivanchenko, G. V. Osipov, V. D. Shalfeev, and J. Kurths. Synchronized bursts following instability of synchronous spiking in chaotic neural networks. *arXiv.org:nlin/0601023*, 2006.

[55] E. M. Izhikevich. Which model to use for cortical spiking neurons? *IEEE Trans. Neural Netw.*, 15(5):1063–1070, 2004.

[56] E. M. Izhikevich. Polychronization: Computation with spikes. *Neural Comput.*, 18:245–282, 2006.

[57] E. M. Izhikevich. *Dynamical Systems in Neuroscience: The Geometry of Excitability and Bursting*. The MIT Press, 2007.

[58] E. M. Izhikevich and R. FitzHugh. Fitzhugh-Nagumo model. *Scholarpedia*, 1:3193/5642, 2006. http://www.scholarpedia.org/article/FitzHugh-Nagumo_Model.

[59] E. M. Izhikevich, J. A. Gally, and G. M. Edelman. Spike-timing dynamics of neuronal groups. *Cereb. Cortex*, 14:933–944, 2004.

[60] S. Jalan and R. E. Amritkar. Self-organised and driven phase synchronization in coupled maps. *Phys. Rev. Lett.*, 90:014101, 2003.

[61] M. Kaiser, M. Görner, and C.C. Hilgetag. Criticality of spreading dynamics in hierarchical cluster networks without inhibition. *New J. Phys.*, 9(110), 2007.

[62] M. Kaiser and C.C. Hilgetag. Spatial growth of real-world networks. *Phys. Rev. E*, 69:036103, 2004.

[63] M. Kaiser, R. Martin, P. Andras, and M.P. Young. Simulation of robustness against lesions of cortical networks. *Eur. J. Neurosci.*, 25:3185–3192, 2007.

[64] E. R. Kandel, J. H. Schwartz, and T. M. Jessell, editors. *Principles of Neural Science*. McGraw Hill, 4th edition, 2000.

[65] K. Kaneko. *Life: An Introduction to Complex Systems Biology*, chapter How Should Living Systems Be Studied?, pages 1–36. Springer, Heidelberg, 2006.

[66] T. Kiss and P. Erdi. Mesoscopic neurodynamics. *Biosystems*, 64(1):119–126(8), 2002.

[67] A. Knoblauch and F. T. Sommer. Synaptic plasticity, conduction delays, and inter-areal phase relations of spike activity in a model of reciprocally connected areas. *Neurocomp.*, 52-54:301–306, 2003.

[68] N. Kopell, G. B. Ermentrout, M. A. Whittington, and R. D. Traub. Gamma rhythms and beta rhythms have different synchronization properties. *Proc. Natl. Acad. Sci. USA*, 2000.

[69] R. Kötter and F. T. Sommer. Global relationshhip between anatomical connectivity and activity propagation in the cerebral cortex. *Phil. Trans. R. Soc. Lond. B*, 355:127–134, 2000.

[70] P. Kudela, P. J. Franaszczuk, and G. K. Bergey. Changing excitation and inhibition in simulated neural networks: effects on induced bursting behavior. *Biol. Cybern.*, 88:276–285, 2003.

[71] L. F. Lago-Fernández, F. J. Corbacho, and R. Huerta. Connection topology dependence of synchronization of neural assemblies on class 1 and 2 excitability. *Neural Networks*, 14:687–696, 2001.

[72] L. F. Lago-Fernández, R. Huerta, F. Corbacho, and J. A. Sigüenza. Fast response and temporal coherent oscillations in small-world networks. *Phys. Rev. Lett.*, 84(12):2758–2761, 2000.

[73] L. Lee, L. M. Harrison, and A. Mechelli. A report of the functional connectivity workshop, Düsseldorf 2002. *NeuroImage*, 19:457–465, 2003.

[74] K. Lehnertz and C. E. Elger. Can epileptic seizures be predicted? evidence from nonlinear time series analysis of brain electrical activity. *Phys. Rev. Lett.*, 80:5019–5022, 1998.

[75] P. D. MacLean and K. H. Pribram. Neuronographic analysis of medial and basal cerebral cortex I. cat. *J. Neurophysiol.*, 16:312–323, 1953.

[76] K.V. Mardia, J.T. Kent, and J.M. Bibby. *Multivariate Analysis*. Academic Press Limited, London, 1989.

[77] H. Markram. The Blue Brain Project. *Nat. Rev. Neurosci.*, 7:153–160, 2006. Perspectives.

[78] H. Markram, M. Toledo-Rodriguez, Y. Wang, A. Gupta, G. Silberberg, and C. Wu. Interneurons of the neocortical inhibitory system. *Nat. Rev. Neurosci.*, 5:793–807, 2004.

[79] N. Masuda and K. Aihara. Global and local synchrony of coupled neurons in small-world networks. *Biol. Cybern.*, 90:302–309, 2004.

[80] R. Milo, S. Shen-Orr, S. Itzkovitz, N. Kashtan, D. Chlkovskii, and U. Alon. Network motifs: Simple building blocks of complex networks. *Science*, 298:824–827, 2002.

[81] A. Morrison, C. Mehring, T. Geisel, A. Aersten, and M. Diesmann. Advacing the boundaries of high-connectivity network simulation with distributed computing. *Neural Computation*, 17:1776–1801, 2005.

[82] A. E. Motter, C. S. Zhou, and J. Kurths. Enhancing complex-network synchronization. *Europhys. Lett.*, 69:334–341, 2005.

[83] A. E. Motter, C. S. Zhou, and J. Kurths. Network synchronization, diffusion, and the paradox of heterogeneity. *Phys. Rev. E*, 71:016116, 2005.

[84] M. E. J. Newman. The structure and function of complex networks. *arXiv:cond-math/0303516*, 2003.

[85] M. E. J. Newman. Detecting community structure in networks. *Eur. Phys. J B*, 38:321–330, 2004.

[86] M. E. J. Newman and M. Girvan. Finding and evaluating community structure in networks. *Phys. Rev. E*, 69:026113, 2004.

[87] E. Niedermeyer and F. Lopes da Silva, editors. *Electroencephalography: Basic principles, clinical applications, and related fields*. Williams & Wilkins, Baltimore, 1993.

[88] T. Nishikawa, A. E. Motter, Y.-C. Lai, and F. C. Hoppensteadt. Heterogeneity in oscillator networks: are smaller world easier to synchronize? *Phys. Rev. Lett.*, 91:014101, 2003.

[89] A. S. Pikovsky and J. Kurths. Coherence resonance in a noise-driven excitable system. *Phys. Rev. Lett.*, 78(5):775–778, 1997.

[90] A. S. Pikovsky, M. Rosenblum, and J. Kurths. *Synchronization — A unified approach to nonlinear science*. Cambridge University Press, 2001.

[91] S. Postnova, B. Wollweber, K. Voigt, and H. Braun. Impulse pattern in bi-directionally coupled model neurons of different dynamics. *Biosystems*, 189(1–3):135–142, 2007.

[92] M. I. Rabinovich, P. Varona, A. I. Selverston, and H. D. I. Abarbanel. Dynamical principles in neuroscience. *Rev. Mod. Phys.*, 78:1213–1265, 2006.

[93] J. Rinzel and G. B. Ermentrout. *Methods in Neuronal Modeling: from Synapses to Networks*, chapter Analysis of neural excitability and oscillations, pages 135–169. The MIT Press, Cambridge, MA, 1989.

[94] K. S. Rockland and N. Ichinohe. Some thoughts on cortical minicolumns. *Exp Brain Res*, 158:265–277, 2004.

[95] D. Rodney and M. Kevan. *The Synaptic Organization of the Brain*, chapter Neocortex, pages 459–509. Springer, New York, 1991.

[96] N. Rulkov, I. Timofeev, and M. Bazhenov. Oscillations in large-scale cortical networks: map-based model. *J. Comput. Neurosci.*, 17(2):203–223, 2004.

[97] E. Salinas and T.J. Sejnowski. Correlated neuronal activity and the flow of neural information. *Nat. Rev. Neurosci.*, 2:539–550, 2001.

[98] R. Salvador, J. Suckling, M.R. Coleman, J.D. Pickard, D. Menon, and E. Bullmore. Neurophysiological architecture of functional magnetic resonance images of human brain. *Cereb. Cortex*, 15:1332–1342, 2005.

[99] J. W. Scannell, C. Blakemore, and M. P. Young. Analysis of connectivity in the cat cerebral cortex. *J. Neurosci*, 15(2):1463–1483, 1995.

[100] J. W. Scannell, G. A. P. C. Burns, C. C. Hilgetag, M. A. O'Neil, and M. P. Young. The connectional organization of the cortico-thalamic system of the cat. *Cereb. Cortex*, 9:277–299, 1999.

[101] L. Schimansky-Geier, V.S. Anishchenko, and A. Neiman. *Neuro-Informatics and Neural Modelling*, chapter Phase Synchronization: From Periodic to Chaotic and Noisy, pages 23–82. Elsevier, Amsterdam, The Netherlands, 2001.

[102] V. Schmitt, R. Kötter, and F. T. Sommer. The impact of thalamo-cortical projections on activity spread in cortex. *Neurocomputing*, 52-54:919–924, 2003.

[103] A. Schnitzler and J. Gross. Normal and pathological oscillatory communication in the brain. *Nat. Rev. Neurosci.*, 6:285–296, 2005.

[104] D. Schubert, R. Kötter, H. J. Luhmann, and J. F. Staiger. Morphology, Electrophysiology and Functional Input Connectivity of Pyramidal Neurons Characterizes a Genuine Layer Va in the Primary Somatosensory Cortex. *Cereb. Cortex*, 16:223–236, 2006.

[105] C. Song, S. Havlin, and H.E. Makse. Self-similarity of complex networks. *Nature (London)*, 433:392–395, 2005.

[106] S. Song, K. D. Miller, and L. F. Abbot. Competitive Hebbian learning through spike-timing-dependent synaptic plasticity. *Nat. Neurosc*, 3(9):919–926, 2000.

[107] O. Sporns. Network analysis, complexity and brain function. *Complexity*, 8:56–60, 2003.

[108] O. Sporns, D. R. Chialvo, M. Kaiser, and C. C. Hilgetag. Organization, development and function of complex brain networks. *Trends Cogn. Sci.*, 8:418–425, 2004.

[109] O. Sporns, J. A. Gally, G. N. Reeke Jr., and G. M. Edelman. Reentrant signaling among simulated neuronal groups leads to coherency in their oscillatory activity. *Proc. Natl. Acad. Sci. USA*, 86:7265–7269, 1989.

[110] O. Sporns, G. Tononi, and G. M. Edelman. Theoretical neuroanatomy: relating anatomical and functional connectivity in graphs and cortical connection matrices. *Cereb. Cortex*, 10:127–141, 2000.

[111] O. Sporns, G. Tononi, and R. Kötter. The human connectome: a structural description of the human brain. *PLoS Comput. Biol.*, 1(4):0245–0251, 2005.

[112] O. Sporns and J. D. Zwi. The small world of the cerebral cortex. *Neuroinformatics*, 2:145–162, 2004.

[113] M. St-Hilaire and A. Longtin. Comparison of coding capabilities of type I and type II neurons. *J. Comput. Neurosci*, 16:299–313, 2004.

[114] C. J. Stam and E. A. de Bruin. Scale-free dynamics of global functional connectivity in the human brain. *Hum. Brain Mapp.*, 22:97–109, 2004.

[115] C. J. Stam, B. F. Jones, G. Nolte, M. Breaskpear, and P. Scheltens. Small-world networks and functional connectivity in Alzheimer's disease. *Cereb. Cortex*, 26(1):63–72, 2006.

[116] C.J. Stam. Synchronization likelihood: an unbiased measure of generalized synchronization in multivariate data sets. *Physica D*, 163:226–251, 2002.

[117] C.J. Stam. Functional connectivity patterns of human magnetoencephalographic recordings: a 'small-world' network? *Neurosci. Lett.*, 355:25–28, 2004.

[118] K. E. Stephan, C.C. Hilgetag, G. A. P. C. Burns, M. A. O'Neill, M. P. Young, and R. Kötter. Computational analysis of functional connectivity between areas of primate cerebral cortex. *Phil. Trans. R. Soc. Lond. B*, 355:111–126, 2000.

[119] S. H. Strogatz. Exploring complex networks. *Nature*, 410:268–276, 2001.

[120] M.-A. Tagamets and B. Horwitz. Integrating electrophysiological and anatomical exerimental data to create a large-scale model that simulates a delayed match-to-sample human brain imaging study. *Cereb. Cortex*, 8:310–320, 1998.

[121] M. Timme, F. Wolf, and T. Geisel. Coexistence of regular and irregular dynamics in complex networks of pulse-coupled oscillators. *Phys. Rev. Lett.*, 89:258701, 2002.

[122] G. Tononi and G. M. Edelman. Consciousness and complexity. *Science*, 282:1846–1851, 1998.

[123] K. Tsumoto, T. Yoshinaga, K. Aihara, and H. Kawakami. Bifurcations in Morris-Lecar neuron model. In *Int. Symp. on Nonlin. Theory and its Appl.*, 2002.

[124] M. Ursino, M. Zavaglia, L. Astolfi, and F. Babiloni. Use of a neural mass model for the analysis of effective connectivity among cortical regions based on high resolution EEG recordings. *Biol. Cybern.*, 96:351–365, 2007.

[125] C. van Vreeswijk and H. Sompolinsky. Chaos in neuronal networks with balanced excitatory and inhibitory activity. *Science*, 274:1724–1726, 1996.

[126] X. F. Wang and G. Chen. Complex networks: Small-world, scale-free and beyond. *ICEE Circuits 6 Systems Magazine*, first quarter:6–20, 2003.

[127] D. J. Watts and S. H. Strogatz. Collective dynamics of 'small world' networks. *Nature*, 393:441–442, 1998.

[128] F. Wendling, F. Bartolomei, J. J. Bellanger, and P. Chauvel. Epileptic fast activity can be explained by a model of impaired GABAergic dendritic inhibition. *Europ. J. Neurosci.*, 15:1499–1508, 2002.

[129] F. Wendling, J. J. Bellanger, F. Bartolomei, and P. Chauvel. Relevance of nonlinear lumped-parameter models in the analysis of depth-EEG epileptic signals. *Biol. Cybern.*, 83:367–378, 2000.

[130] J. J. Wright, C. J. Rennie, G. J. Lees, P. A. Robinson, P. D. Bourke, C. L. Chapman, E. Gordon, and D. L. Rowe. Simulated electrocortical activity at microscopic, mesoscopic and global scales. *Neuropsychopharmacol*, 14(2):80–93, 2003.

[131] M. P. Young. The architecture of visual cortex and inferential processes in vision. *Spatial Vis.*, 13(2,3):137–146, 2000.

[132] L. Zemanová, C. S. Zhou, and J. Kurths. Structural and functional clusters of complex brain networks. *Physica D*, 224:202–212, 2006.

[133] L. Zemanová, C. S. Zhou, and J. Kurths. *Lectures in Supercomputational Neuroscience:Dynamics in Complex Brain Networks*, chapter Building a large-scale computational model of a cortical neuronal network. Springer, Berlin, 1st edition, 2008.

[134] C. S. Zhou and J. Kurths. Dynamical weights and enhanced synchronization in adaptive complex networks. *Phys. Rev. Lett.*, 96:164102, 2006.

[135] C. S. Zhou, J. Kurths, and B. Hu. Array-enhanced coherence resonance: nontrivial effects of heterogeneity and spatial independence of noise. *Phys. Rev. Lett.*, 87(9):098101, 2001.

[136] C. S. Zhou, A. E. Motter, and J. Kurths. Universality in the synchronization of weighted random networks. *Phys. Rev. Lett.*, 96:034101, 2006.

[137] C. S. Zhou, L. Zemanová, and J. Kurths. *Lectures in Supercomputational Neuroscience:Dynamics in Complex Brain Networks*, chapter Synchronization dynamics in complex networks. Springer, Berlin, 1st edition, 2008.

[138] C. S. Zhou, L. Zemanová, G. Zamora, C. C. Hilgetag, and J. Kurths. Hierarchical organization unveiled by functional connectivity in complex brain networks. *Phys. Rev. Lett.*, 97:238103, 2006.

[139] C. S. Zhou, L. Zemanová, G. Zamora-López, C. C. Hilgetag, and J. Kurths. Structure-function relationship in complex brain networks expressed by hierarchical synchronization. *New J. Phys.*, 9(178), 2007.

[140] C.S. Zhou, J. Kurths, and B. Hu. Frequency and phase locking of noise-sustained oscillations in coupled excitable systems: array-enhanced resonances. *Phys. Rev. E*, 67:030101, 2003.